Supporting Information

Achieving short ignition delay and high specific impulse with cyanoborohydride-based hypergolic ionic liquids

Amélie Pialat,[a] Alexandros A. Kitos,[a] Tomasz G. Witkowski,[a,b] Cyril Cook,[a] Shiliang Wang,[c] Anguang Hu*[c] and Muralee Murugesu*[a]

[a] Department of Chemistry, University of Ottawa,10 Marie Curie, Ottawa, Ontario, Canada, K1N 6N5

[b] Present affiliation: Federal Institute for Materials Research and Testing (BAM), Division 2.6 Testing and Evaluation of Explosives and Pyrotechnics, Unter den Eichen 87, D-12205 Berlin, Germany

[c] Defense R&D Canada-Suffield Research Centre, PO Box 4000 Station Main Medicine Hat, AB, Canada, T1A 8K6

Table of Contents

X-Ray crystallographic studies

X-ray crystallographic data for compound **20** were collected on a single crystal mounted on a loop fibre. Data were collected using a Bruker Venture diffractometer equipped with a Photon 100 CMOS Detector, a Helios MX optics (Ga *K*α radiation, λ = 1.34139 Å) and a Kappa goniometer. The crystal-to-detector distance was 4.0 cm, and the data collection was carried out in 1024 x 1024 pixel mode. SADABS2014/5 (Bruker, 2014/5) was used for absorption correction. H atoms were treated by a mixture of independent and constrained refinement. Crystallographic data for the structure reported in this paper have been deposited with the Cambridge Crystallographic Centre (CCDC) as supplementary publication no. 1549198.

Table 1. Selected crystallographic data for **20**.

	20
Empirical formula	$[C_{28}H_{60}N][CH_3BN]$
Formula weight/ gmol^{-1}	450.62
T/ K	105
Crystal system	Triclinic
Space group	*P*-1
a/Å	9.5425 (6)
b/Å	11.4283 (7)
c/Å	14.5168 (9)
α/ °	89.121 (4)
β/ °	78.840 (3)
γ/ °	88.990 (3)
V/ Å^3	1552.83 (17)
Z	2
Radiation type	Ga Kα, λ = 1.34139 Å
Crystal size/ mm	0.36 x 0.18 x 0.1
μ/ mm^{-1}	0.25
Reflections collected	6484
Independent reflns [R_{int}]	6484 [0.094]
Goodness-of-fit on F^2	1.031
R[F^2 > 2s(F^2)]	0.086
wR(F^2)	0.251

Table S2. Selected geometric parameters (Å, º)

N1—C1	1.522 (4)	C15—H15B	0.9900
N1—C8	1.519 (3)	C15—C16	1.506 (4)
N1—C15	1.520 (3)	C16—H16A	0.9900
N1—C22	1.518 (3)	C16—H16B	0.9900
C1—H1A	0.9900	C16—C17	1.527 (4)
C1—H1B	0.9900	C17—H17A	0.9900
C1—C2	1.515 (4)	C17—H17B	0.9900
C2—H2A	0.9900	C17—C18	1.521 (4)
C2—H2B	0.9900	C18—H18A	0.9900

C2—C3	1.520 (4)	C18—H18B	0.9900
C3—H3A	0.9900	C18—C19	1.525 (4)
C3—H3B	0.9900	C19—H19A	0.9900
C3—C4	1.514 (4)	C19—H19B	0.9900
C4—H4A	0.9900	C19—C20	1.510 (4)
C4—H4B	0.9900	C20—H20A	0.9900
C4—C5	1.519 (4)	C20—H20B	0.9900
C5—H5A	0.9900	C20—C21	1.522 (4)
C5—H5B	0.9900	C21—H21A	0.9800
C5—C6	1.510 (4)	C21—H21B	0.9800
C6—H6A	0.9900	C21—H21C	0.9800
C6—H6B	0.9900	C22—H22A	0.9900
C6—C7	1.513 (4)	C22—H22B	0.9900
C7—H7A	0.9800	C22—C23	1.513 (4)
C7—H7B	0.9800	C23—H23A	0.9900
C7—H7C	0.9800	C23—H23B	0.9900
C8—H8A	0.9900	C23—C24	1.525 (4)
C8—H8B	0.9900	C24—H24A	0.9900
C8—C9	1.507 (4)	C24—H24B	0.9900
C9—H9A	0.9900	C24—C25	1.510 (4)
C9—H9B	0.9900	C25—H25A	0.9900
C9—C10	1.530 (4)	C25—H25B	0.9900
C10—H10A	0.9900	C25—C26	1.534 (4)
C10—H10B	0.9900	C26—H26A	0.9900
C10—C11	1.508 (4)	C26—H26B	0.9900
C11—H11A	0.9900	C26—C27	1.508 (4)
C11—H11B	0.9900	C27—H27A	0.9900
C11—C12	1.526 (4)	C27—H27B	0.9900
C12—H12A	0.9900	C27—C28	1.521 (4)
C12—H12B	0.9900	C28—H28A	0.9800
C12—C13	1.504 (4)	C28—H28B	0.9800

C13—H13A	0.9900	C28—H28C	0.9800
C13—H13B	0.9900	N2—C29	1.093 (5)
C13—C14	1.524 (4)	C29—B1	1.611 (7)
C14—H14A	0.9800	B1—H1C	1.11 (4)
C14—H14B	0.9800	B1—H1D	0.97 (4)
C14—H14C	0.9800	B1—H1E	1.10 (4)
C15—H15A	0.9900		
C8—N1—C1	105.8 (2)	N1—C15—H15B	108.2
C8—N1—C15	110.8 (2)	H15A—C15—H15B	107.3
C15—N1—C1	111.6 (2)	C16—C15—N1	116.4 (2)
C22—N1—C1	111.0 (2)	C16—C15—H15A	108.2
C22—N1—C8	111.5 (2)	C16—C15—H15B	108.2
C22—N1—C15	106.3 (2)	C15—C16—H16A	109.6
N1—C1—H1A	108.1	C15—C16—H16B	109.6
N1—C1—H1B	108.1	C15—C16—C17	110.4 (2)
H1A—C1—H1B	107.3	H16A—C16—H16B	108.1
C2—C1—N1	117.0 (2)	C17—C16—H16A	109.6
C2—C1—H1A	108.1	C17—C16—H16B	109.6
C2—C1—H1B	108.1	C16—C17—H17A	109.2
C1—C2—H2A	109.5	C16—C17—H17B	109.2
C1—C2—H2B	109.5	H17A—C17—H17B	107.9
C1—C2—C3	110.5 (2)	C18—C17—C16	112.0 (2)
H2A—C2—H2B	108.1	C18—C17—H17A	109.2
C3—C2—H2A	109.5	C18—C17—H17B	109.2
C3—C2—H2B	109.5	C17—C18—H18A	108.7
C2—C3—H3A	109.1	C17—C18—H18B	108.7
C2—C3—H3B	109.1	C17—C18—C19	114.3 (3)
H3A—C3—H3B	107.9	H18A—C18—H18B	107.6
C4—C3—C2	112.4 (2)	C19—C18—H18A	108.7
C4—C3—H3A	109.1	C19—C18—H18B	108.7

C4—C3—H3B	109.1	C18—C19—H19A	108.6
C3—C4—H4A	108.3	C18—C19—H19B	108.6
C3—C4—H4B	108.3	H19A—C19—H19B	107.6
C3—C4—C5	115.8 (2)	C20—C19—C18	114.6 (3)
H4A—C4—H4B	107.4	C20—C19—H19A	108.6
C5—C4—H4A	108.3	C20—C19—H19B	108.6
C5—C4—H4B	108.3	C19—C20—H20A	108.9
C4—C5—H5A	109.1	C19—C20—H20B	108.9
C4—C5—H5B	109.1	C19—C20—C21	113.2 (3)
H5A—C5—H5B	107.8	H20A—C20—H20B	107.8
C6—C5—C4	112.7 (2)	C21—C20—H20A	108.9
C6—C5—H5A	109.1	C21—C20—H20B	108.9
C6—C5—H5B	109.1	C20—C21—H21A	109.5
C5—C6—H6A	108.5	C20—C21—H21B	109.5
C5—C6—H6B	108.5	C20—C21—H21C	109.5
C5—C6—C7	114.9 (2)	H21A—C21—H21B	109.5
H6A—C6—H6B	107.5	H21A—C21—H21C	109.5
C7—C6—H6A	108.5	H21B—C21—H21C	109.5
C7—C6—H6B	108.5	N1—C22—H22A	108.1
C6—C7—H7A	109.5	N1—C22—H22B	108.1
C6—C7—H7B	109.5	H22A—C22—H22B	107.3
C6—C7—H7C	109.5	C23—C22—N1	116.7 (2)
H7A—C7—H7B	109.5	C23—C22—H22A	108.1
H7A—C7—H7C	109.5	C23—C22—H22B	108.1
H7B—C7—H7C	109.5	C22—C23—H23A	109.7
N1—C8—H8A	108.3	C22—C23—H23B	109.7
N1—C8—H8B	108.3	C22—C23—C24	109.8 (2)
H8A—C8—H8B	107.4	H23A—C23—H23B	108.2
C9—C8—N1	116.0 (2)	C24—C23—H23A	109.7
C9—C8—H8A	108.3	C24—C23—H23B	109.7
C9—C8—H8B	108.3	C23—C24—H24A	108.9

C8—C9—H9A	109.7	C23—C24—H24B	108.9
C8—C9—H9B	109.7	H24A—C24—H24B	107.7
C8—C9—C10	110.0 (2)	C25—C24—C23	113.3 (2)
H9A—C9—H9B	108.2	C25—C24—H24A	108.9
C10—C9—H9A	109.7	C25—C24—H24B	108.9
C10—C9—H9B	109.7	C24—C25—H25A	108.8
C9—C10—H10A	109.1	C24—C25—H25B	108.8
C9—C10—H10B	109.1	C24—C25—C26	113.9 (2)
H10A—C10—H10B	107.8	H25A—C25—H25B	107.7
C11—C10—C9	112.7 (2)	C26—C25—H25A	108.8
C11—C10—H10A	109.1	C26—C25—H25B	108.8
C11—C10—H10B	109.1	C25—C26—H26A	108.3
C10—C11—H11A	108.7	C25—C26—H26B	108.3
C10—C11—H11B	108.7	H26A—C26—H26B	107.4
C10—C11—C12	114.2 (3)	C27—C26—C25	115.8 (3)
H11A—C11—H11B	107.6	C27—C26—H26A	108.3
C12—C11—H11A	108.7	C27—C26—H26B	108.3
C12—C11—H11B	108.7	C26—C27—H27A	109.2
C11—C12—H12A	109.0	C26—C27—H27B	109.2
C11—C12—H12B	109.0	C26—C27—C28	112.2 (3)
H12A—C12—H12B	107.8	H27A—C27—H27B	107.9
C13—C12—C11	113.1 (3)	C28—C27—H27A	109.2
C13—C12—H12A	109.0	C28—C27—H27B	109.2
C13—C12—H12B	109.0	C27—C28—H28A	109.5
C12—C13—H13A	108.9	C27—C28—H28B	109.5
C12—C13—H13B	108.9	C27—C28—H28C	109.5
C12—C13—C14	113.6 (3)	H28A—C28—H28B	109.5
H13A—C13—H13B	107.7	H28A—C28—H28C	109.5
C14—C13—H13A	108.9	H28B—C28—H28C	109.5
C14—C13—H13B	108.9	N2—C29—B1	179.1 (5)
C13—C14—H14A	109.5	C29—B1—H1C	113 (2)

C13—C14—H14B	109.5	C29—B1—H1D	113 (2)
C13—C14—H14C	109.5	C29—B1—H1E	111 (2)
H14A—C14—H14B	109.5	H1C—B1—H1D	108 (3)
H14A—C14—H14C	109.5	H1C—B1—H1E	106 (3)
H14B—C14—H14C	109.5	H1D—B1—H1E	105 (3)
N1—C15—H15A	108.2		
N1—C1—C2—C3	-177.8 (2)	C10—C11—C12—C13	-169.5 (3)
N1—C8—C9—C10	-174.4 (2)	C11—C12—C13—C14	-177.9 (2)
N1—C15—C16—C17	-179.6 (2)	C15—N1—C1—C2	-49.4 (3)
N1—C22—C23—C24	176.9 (2)	C15—N1—C8—C9	67.9 (3)
C1—N1—C8—C9	-171.0 (2)	C15—N1—C22—C23	-174.6 (3)
C1—N1—C15—C16	-54.9 (3)	C15—C16—C17—C18	-178.9 (3)
C1—N1—C22—C23	63.9 (3)	C16—C17—C18—C19	178.9 (3)
C1—C2—C3—C4	-167.3 (2)	C17—C18—C19—C20	67.9 (4)
C2—C3—C4—C5	-173.5 (3)	C18—C19—C20—C21	-178.6 (3)
C3—C4—C5—C6	-176.9 (2)	C22—N1—C1—C2	69.0 (3)
C4—C5—C6—C7	-175.8 (3)	C22—N1—C8—C9	-50.2 (3)
C8—N1—C1—C2	-169.9 (2)	C22—N1—C15—C16	-176.1 (3)
C8—N1—C15—C16	62.7 (3)	C22—C23—C24—C25	176.8 (3)
C8—N1—C22—C23	-53.9 (3)	C23—C24—C25—C26	-176.9 (3)
C8—C9—C10—C11	-166.0 (2)	C24—C25—C26—C27	-69.6 (4)
C9—C10—C11—C12	178.7 (2)	C25—C26—C27—C28	177.7 (2)

Table S3. Selected hydrogen-bond parameters.

D—H···*A*	*D*—H (Å)	H···*A* (Å)	*D*···*A* (Å)	*D*—H···*A* (°)
C23—H23B···N2	0.99	2.58	3.380 (5)	137.7

Characterization of the starting materials 2-9, 16 and 18

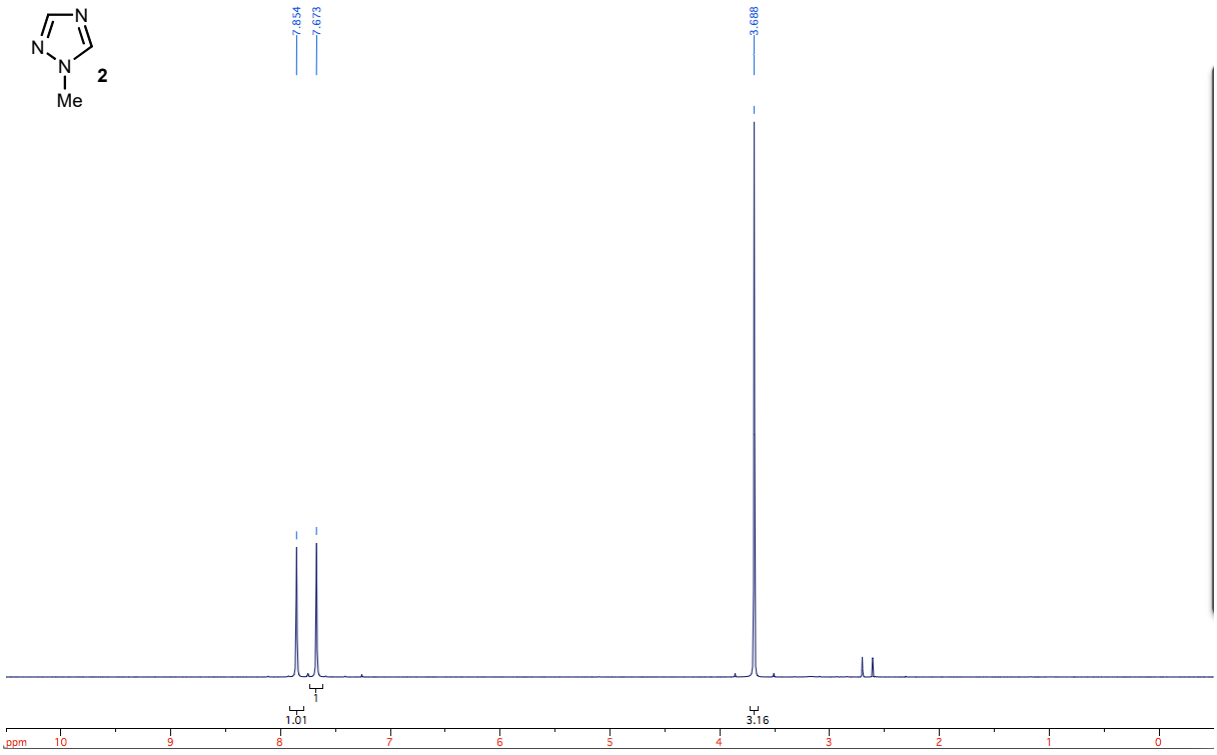

Fig. S1. ^{1}H NMR of 1-Methyl-1*H*-1,2,4-triazole (**2**).

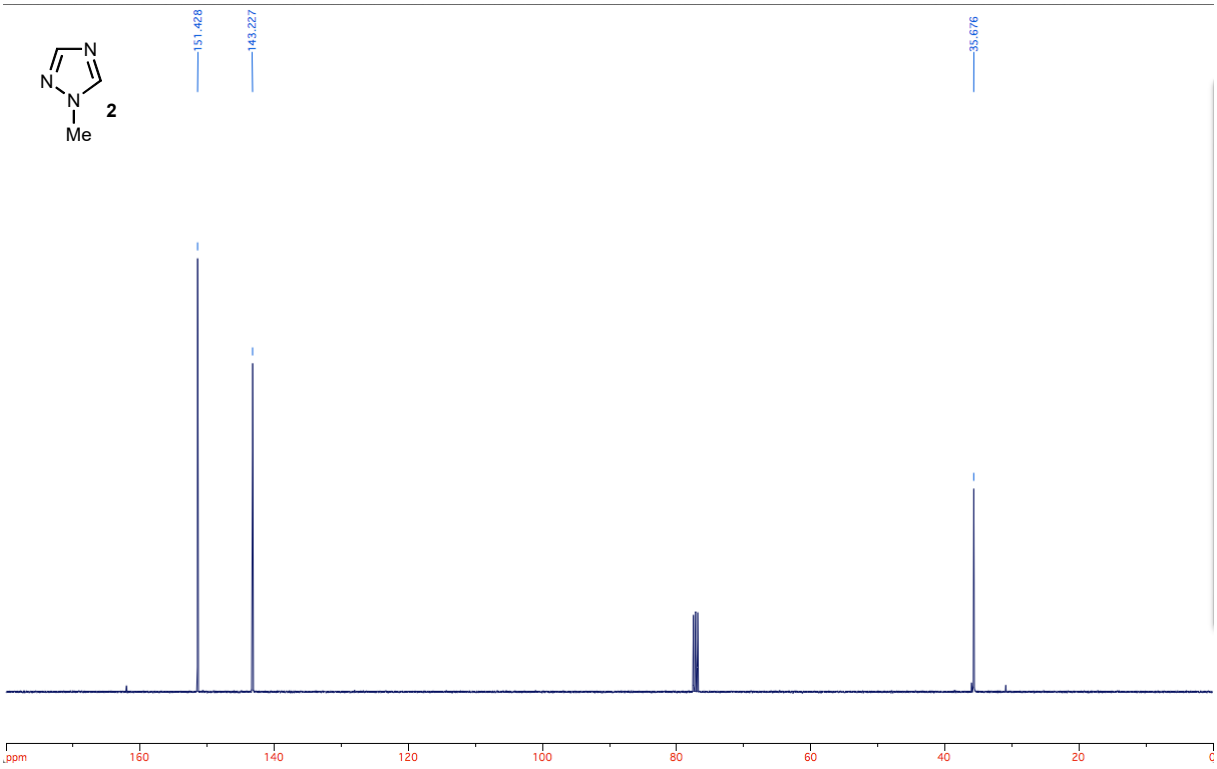

Fig. S2. ^{13}C NMR of 1-Methyl-1*H*-1,2,4-triazole (**2**).

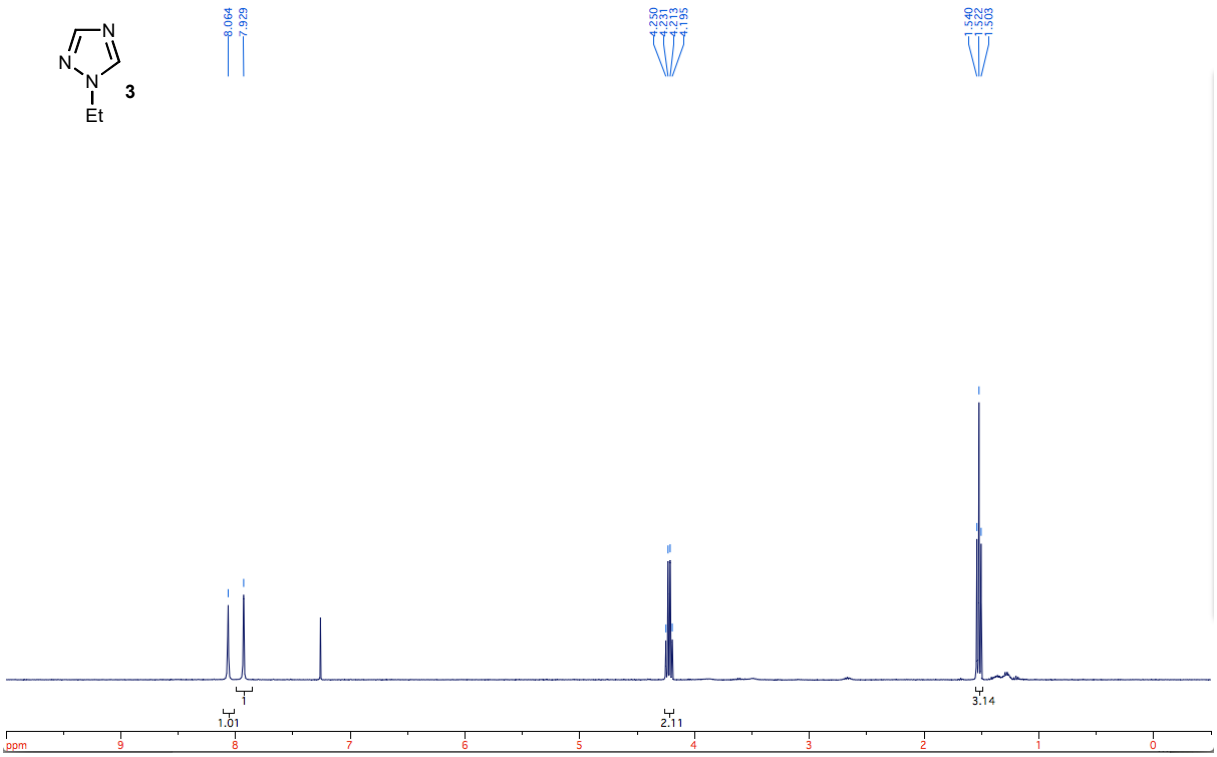

Fig. S3. ^{1}H NMR of 1-Ethyl-1*H*-1,2,4-triazole (**3**).

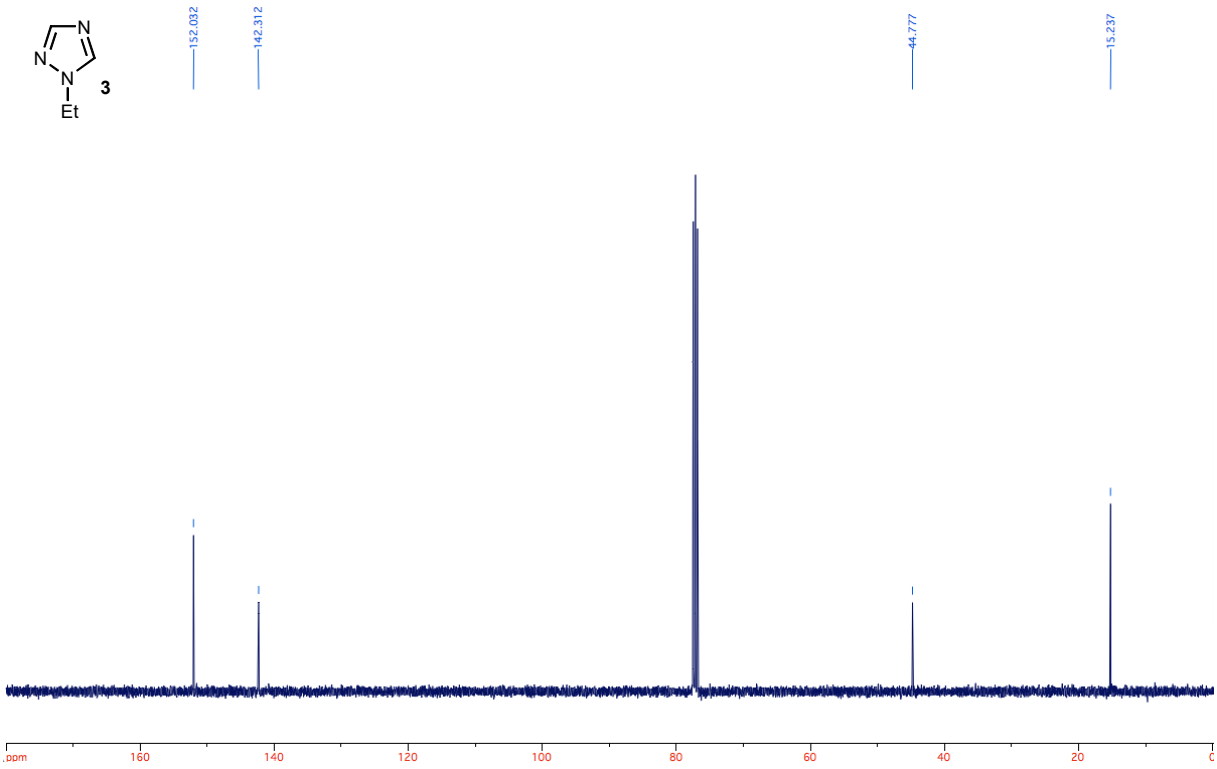

Fig. S4. ^{13}C NMR of 1-Ethyl-1*H*-1,2,4-triazole (**3**).

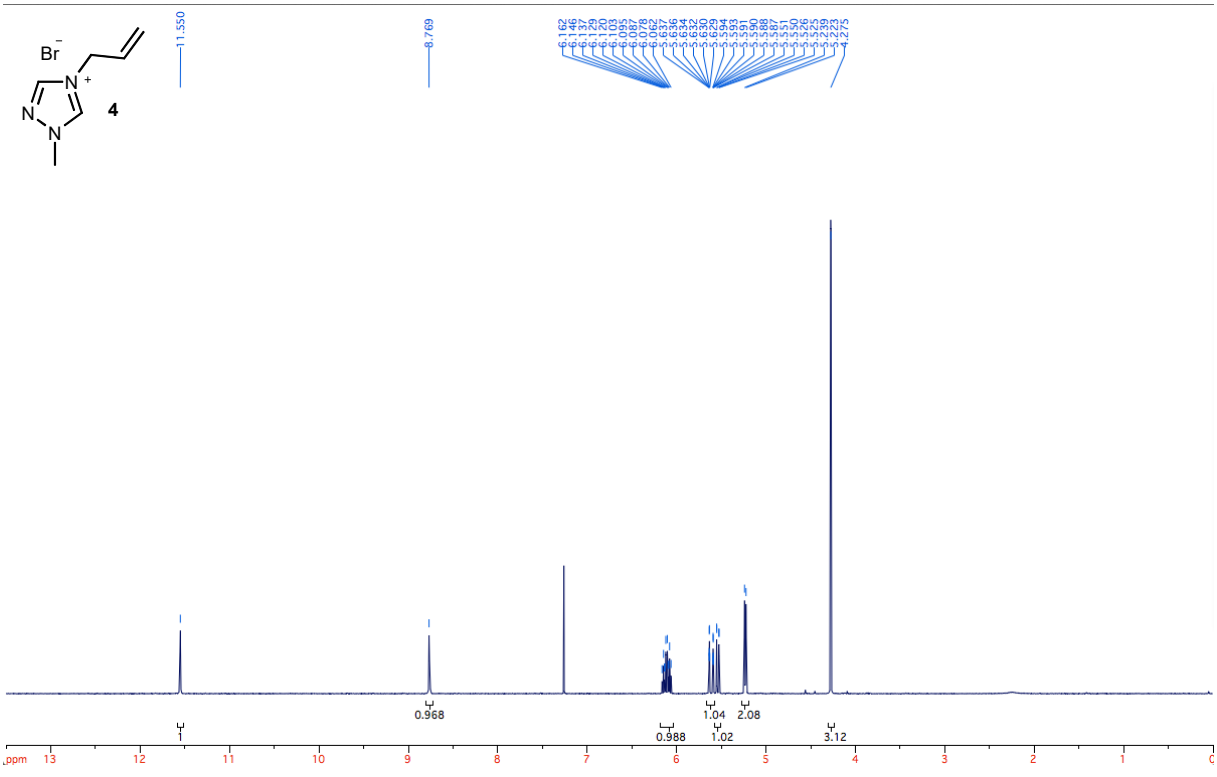

Fig. S5. ^{1}H NMR of 4-Allyl-1-methyl-1*H*-1,2,4-triazol-4-ium (**4**).

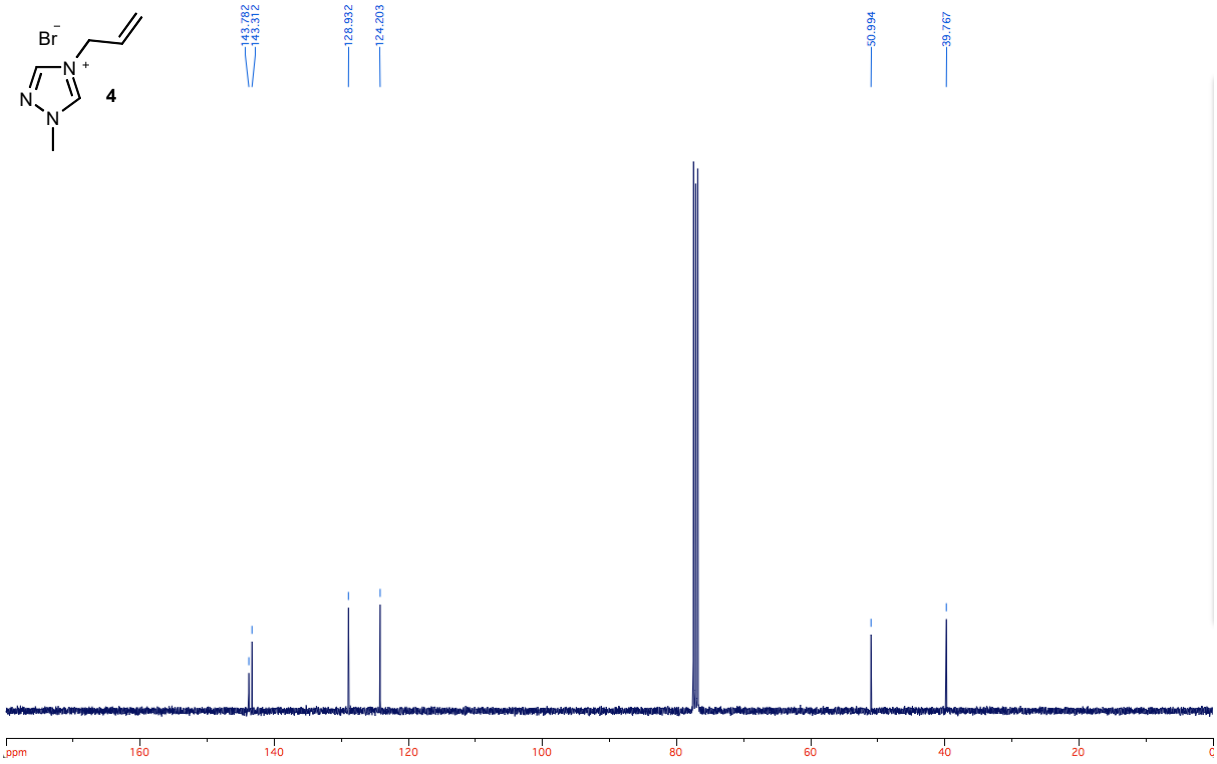

Fig. S6. ^{13}C NMR of 4-Allyl-1-methyl-1*H*-1,2,4-triazol-4-ium (**4**).

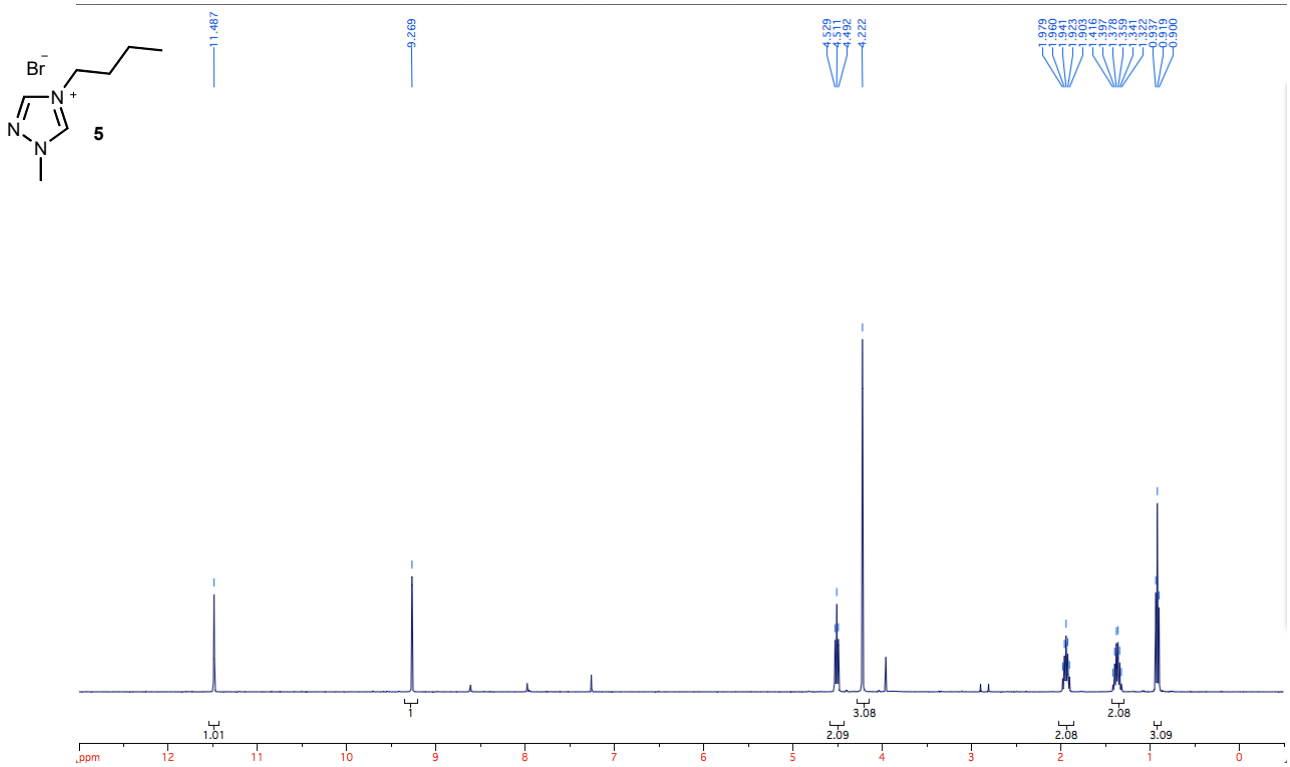

Fig. S7. ^{1}H NMR of 4-Butyl-1-methyl-1*H*-1,2,4-triazol-4-ium bromide (**5**).

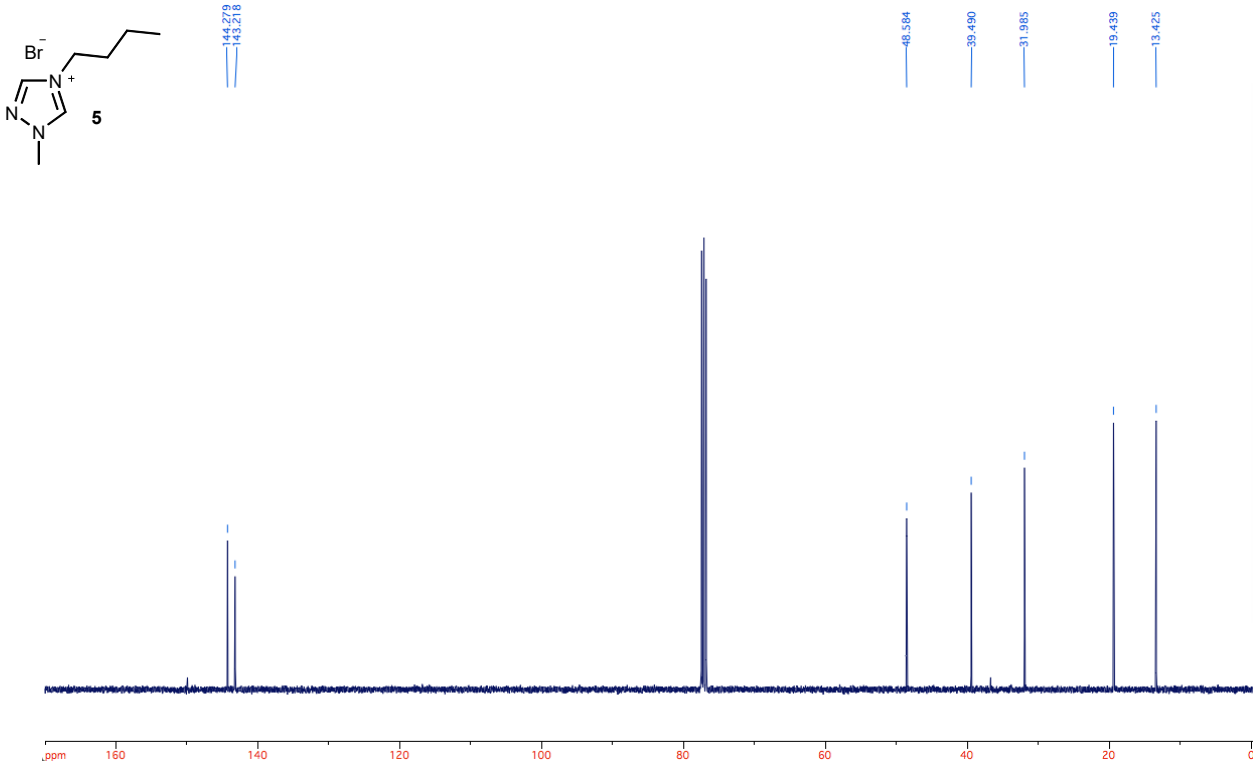

Fig. S8. ^{13}C NMR of 4-Butyl-1-methyl-1*H*-1,2,4-triazol-4-ium bromide (**5**).

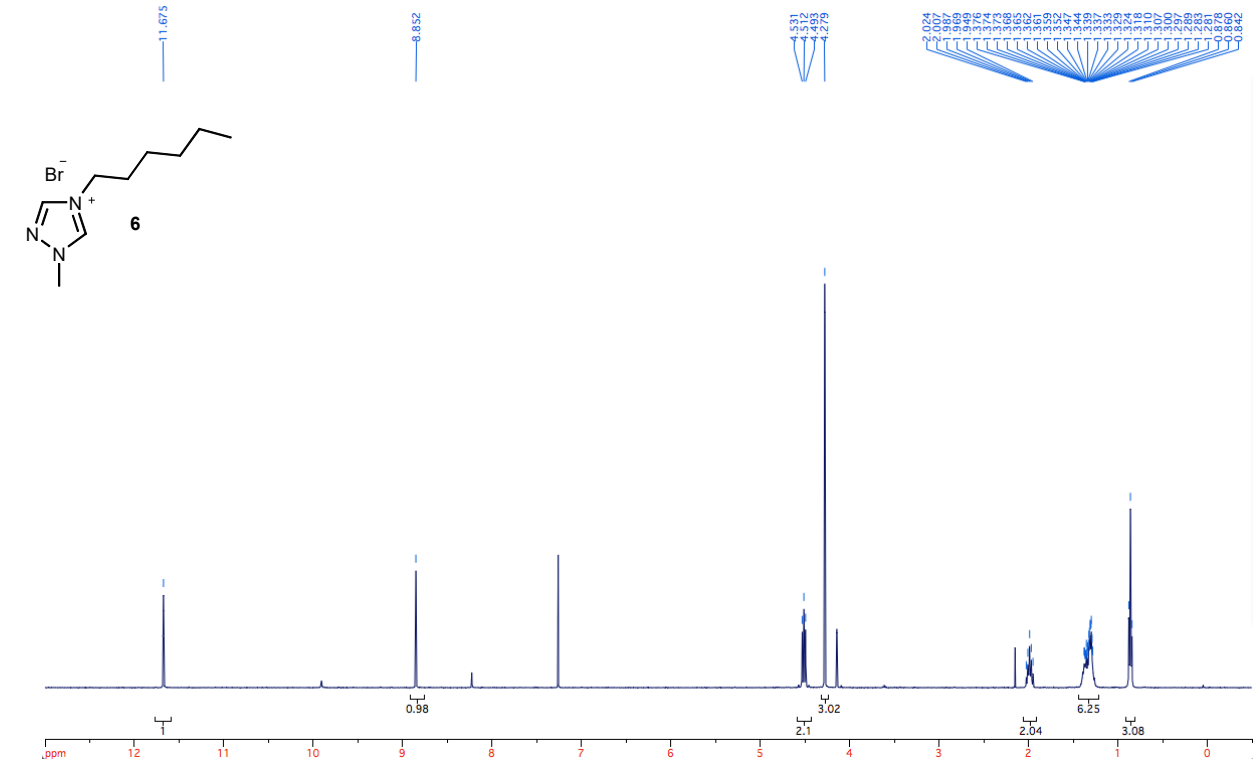

Fig. S9. ^{1}H NMR of 4-Hexyl-1-methyl-1*H*-1,2,4-triazol-4-ium (**6**).

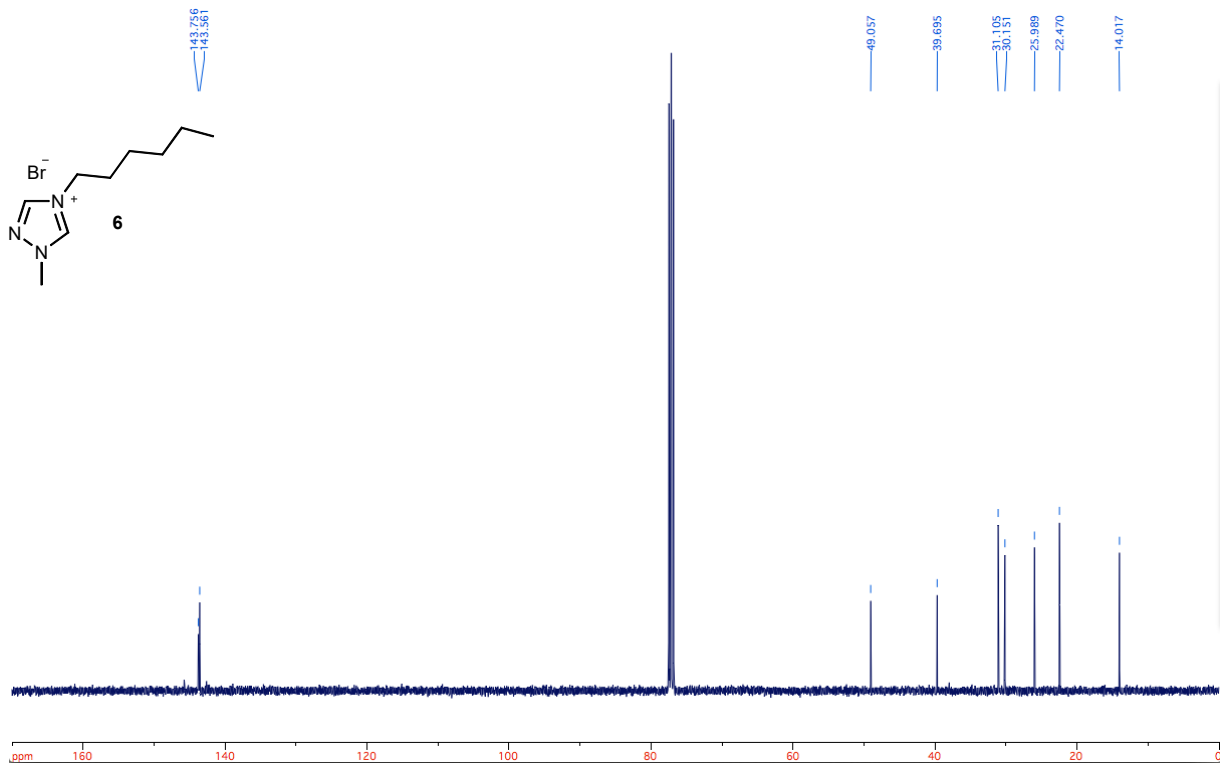

Fig. S10. ^{13}C NMR of 4-Hexyl-1-methyl-1*H*-1,2,4-triazol-4-ium (**6**).

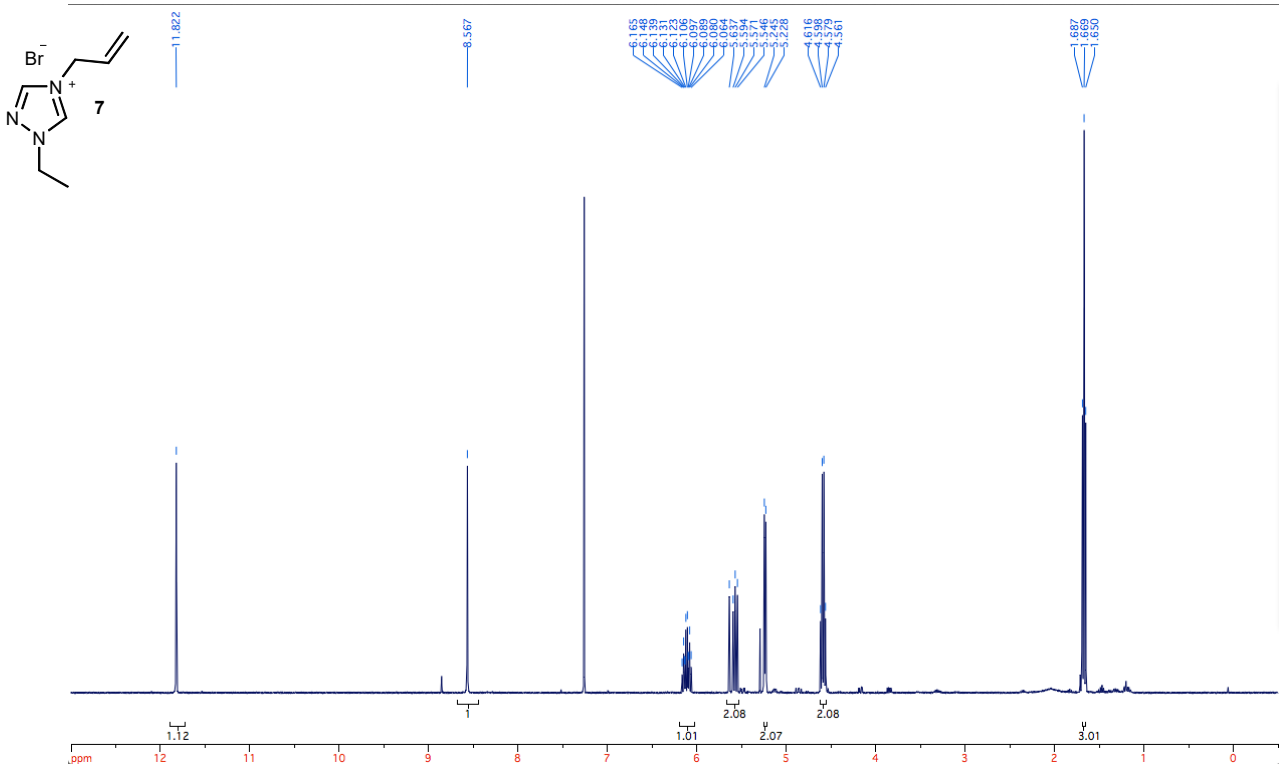

Fig. S11. ^{1}H NMR of 4-Allyl-1-ethyl-1*H*-1,2,4-triazol-4-ium bromide (**7**).

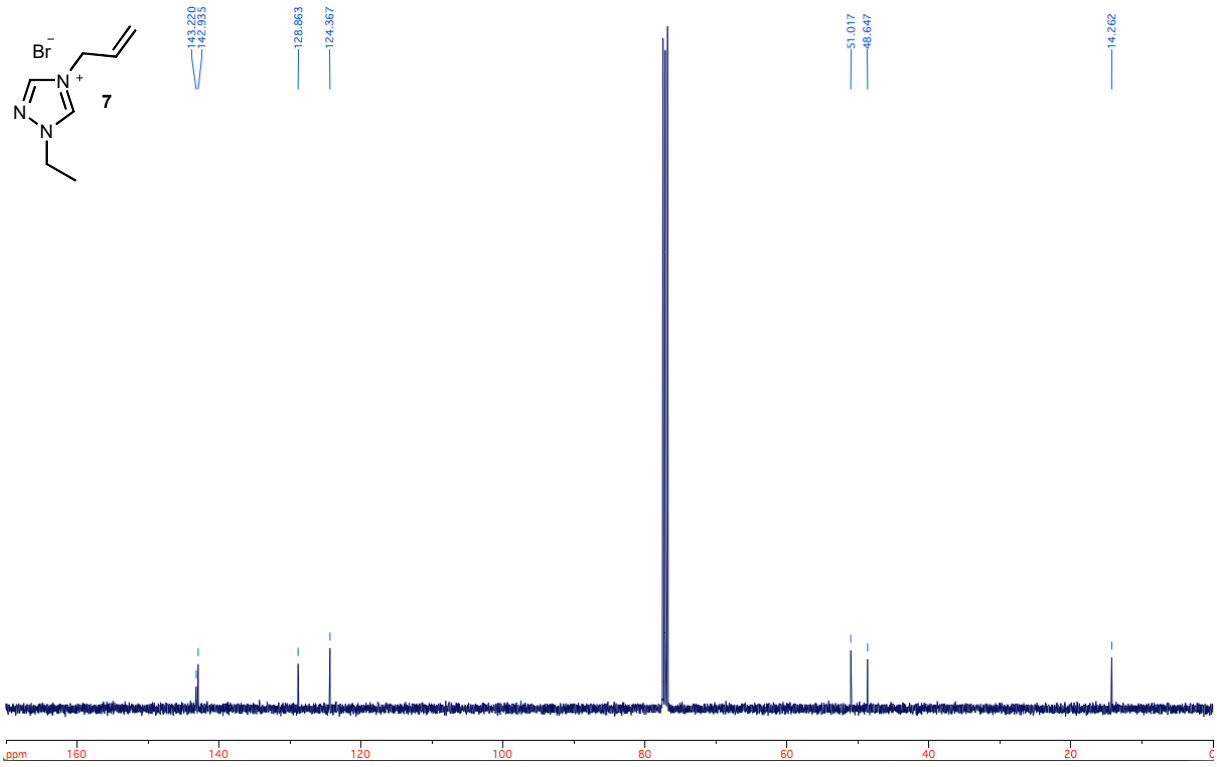

Fig. S12. ^{13}C NMR of 4-Allyl-1-ethyl-1*H*-1,2,4-triazol-4-ium bromide (**7**).

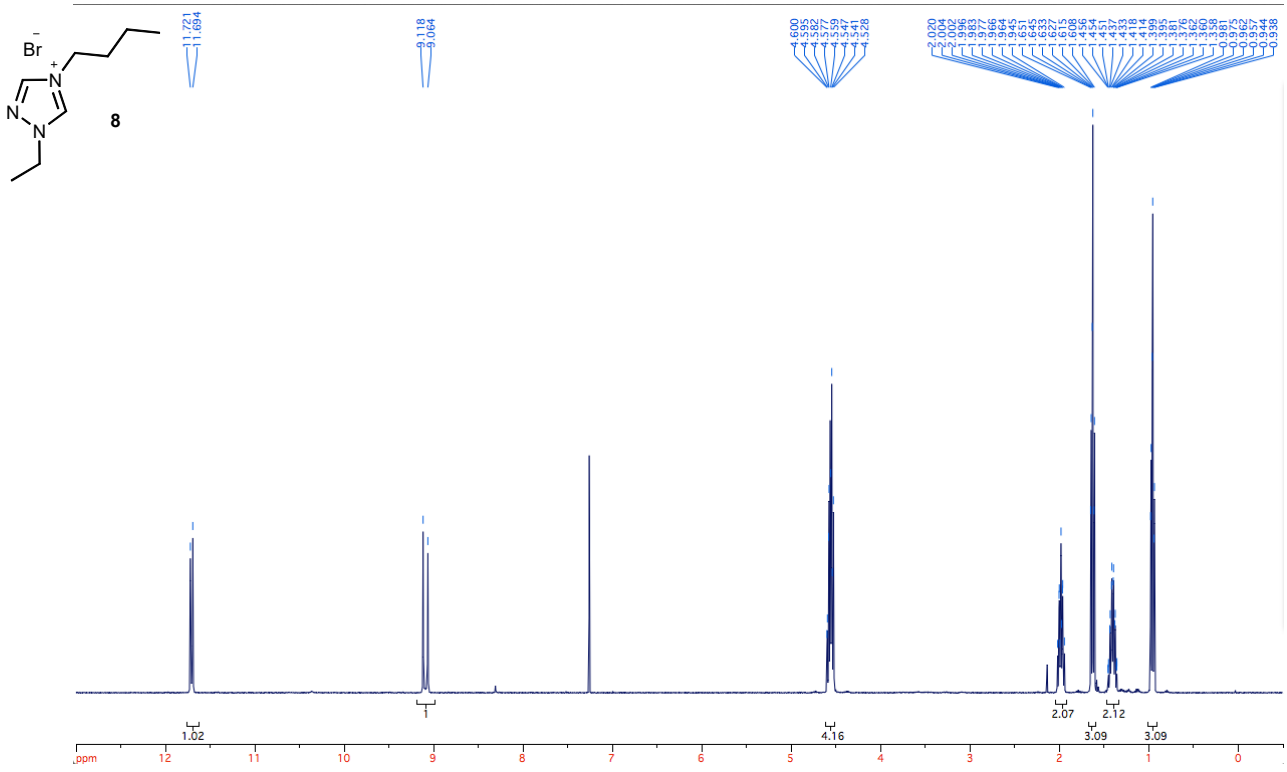

Fig. S13. ^{1}H NMR of 4-Butyl-1-ethyl-1*H*-1,2,4-triazol-4-ium bromide (**8**).

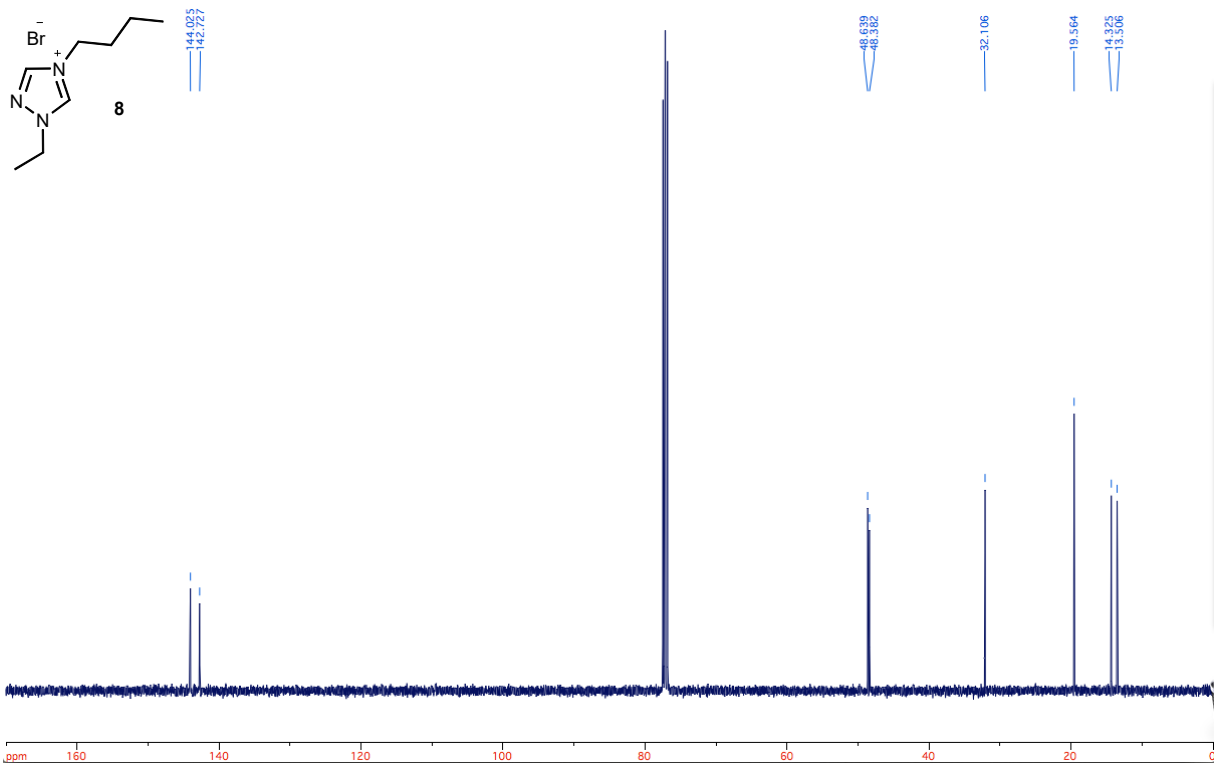

Fig. S14. ^{13}C NMR of 4-Butyl-1-ethyl-1*H*-1,2,4-triazol-4-ium bromide (**8**).

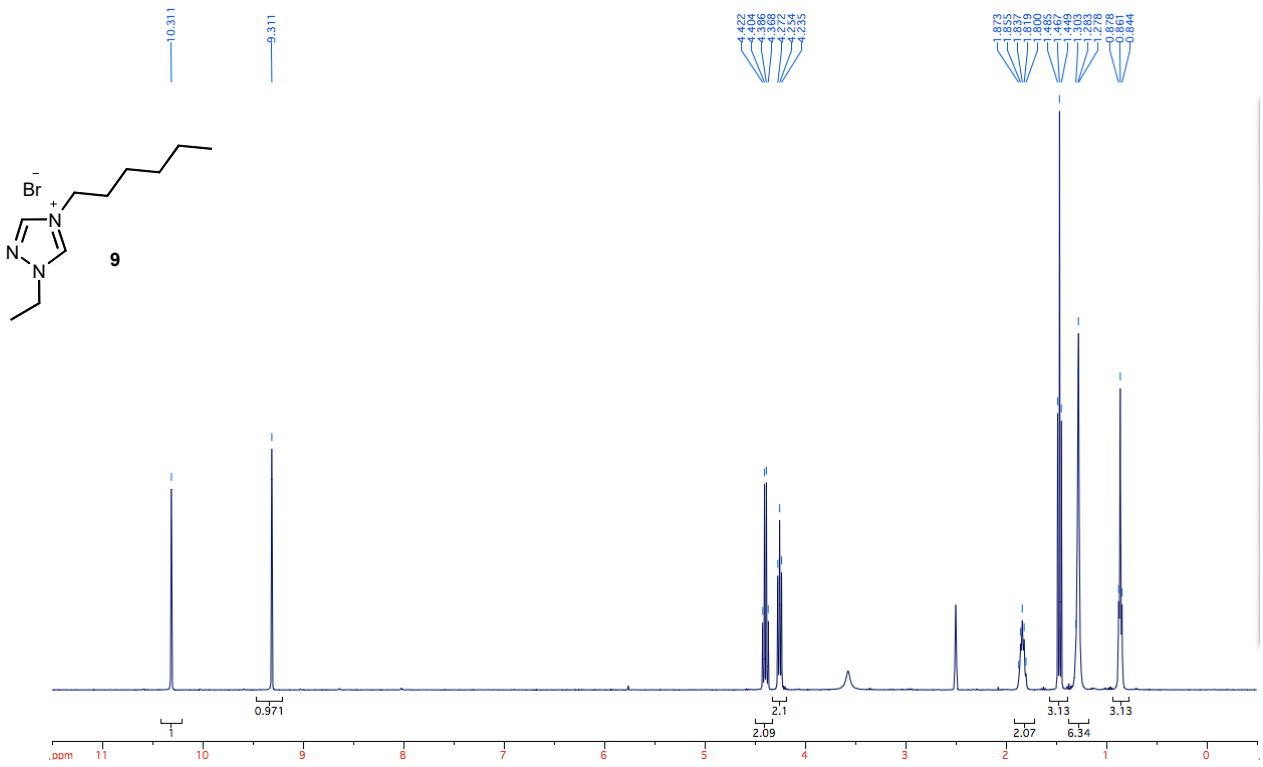

Fig. S15. ^{1}H NMR of 1-Ethyl-4-hexyl-1H-1,2,4-triazol-4-ium bromide (**9**).

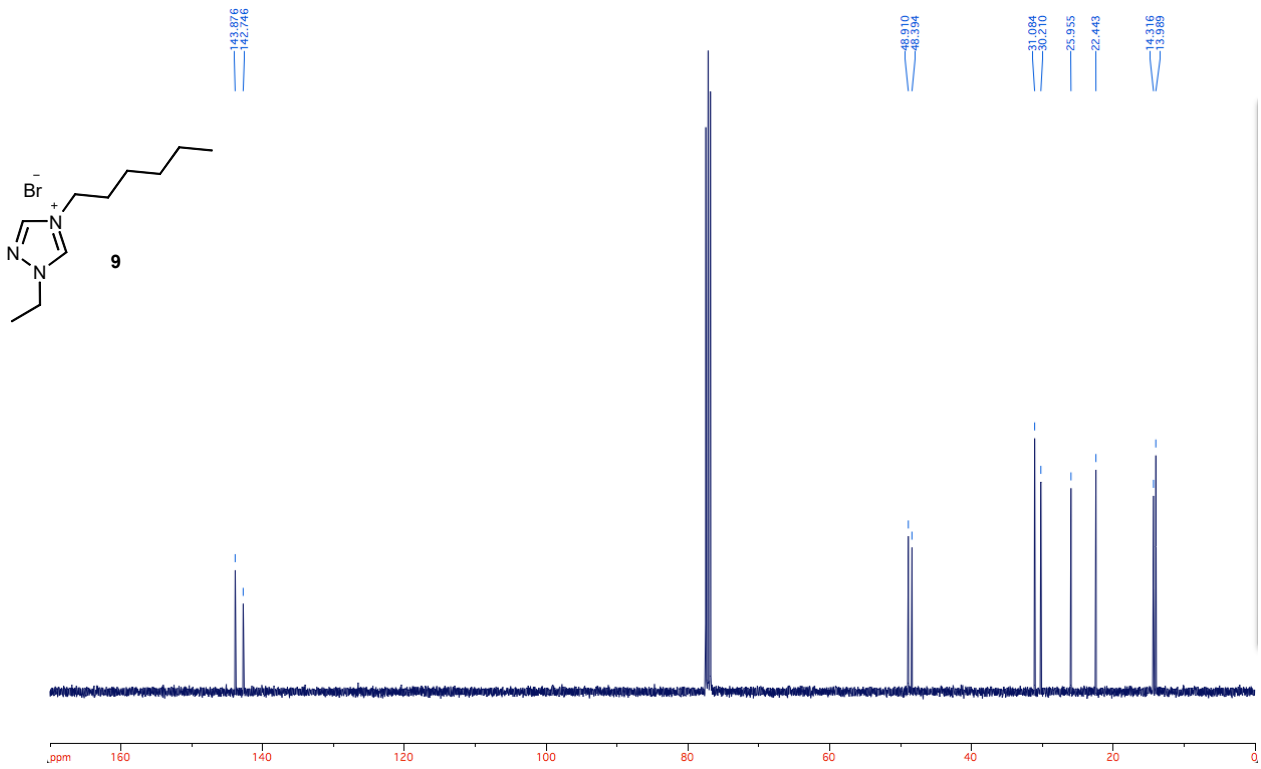

Fig. S16. ^{13}C NMR of 1-Ethyl-4-hexyl-1H-1,2,4-triazol-4-ium bromide (**9**).

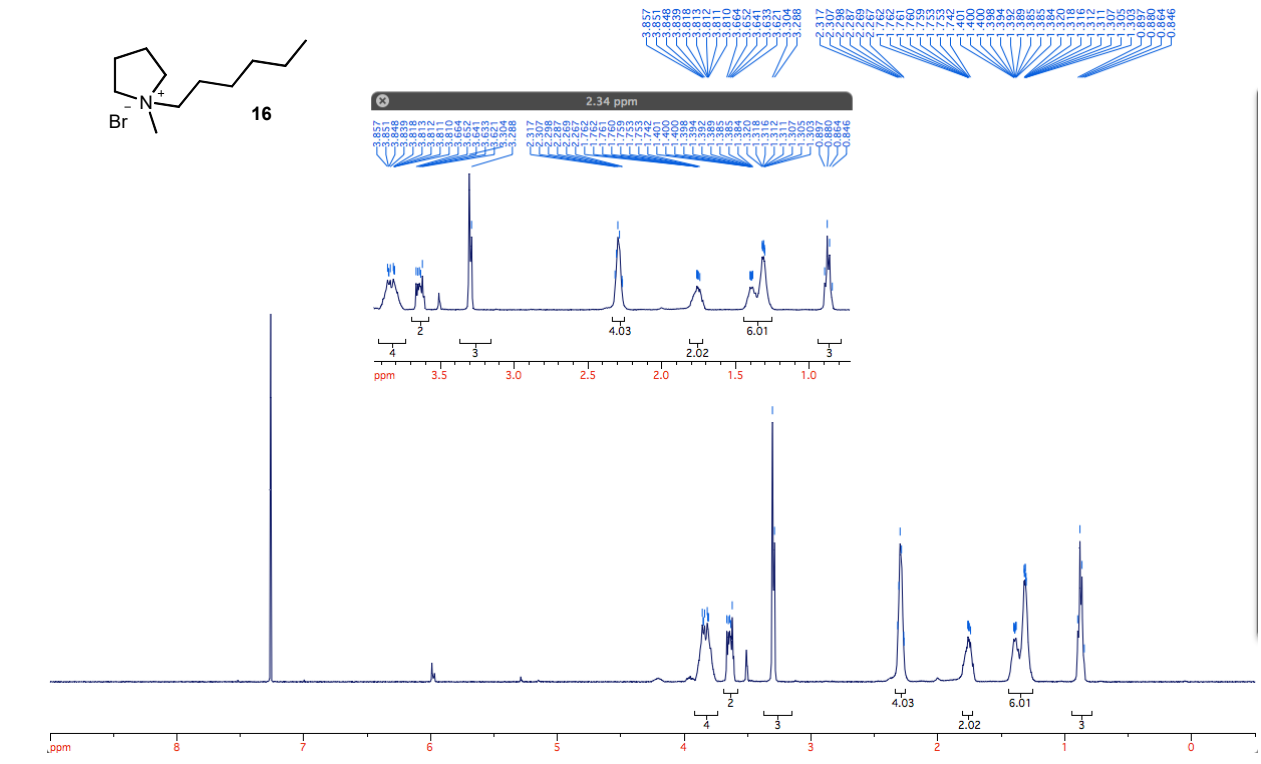

Fig. S17. ^{1}H NMR of 1-Hexyl-1-methylpyrrolidin-1-ium bromide (**16**).

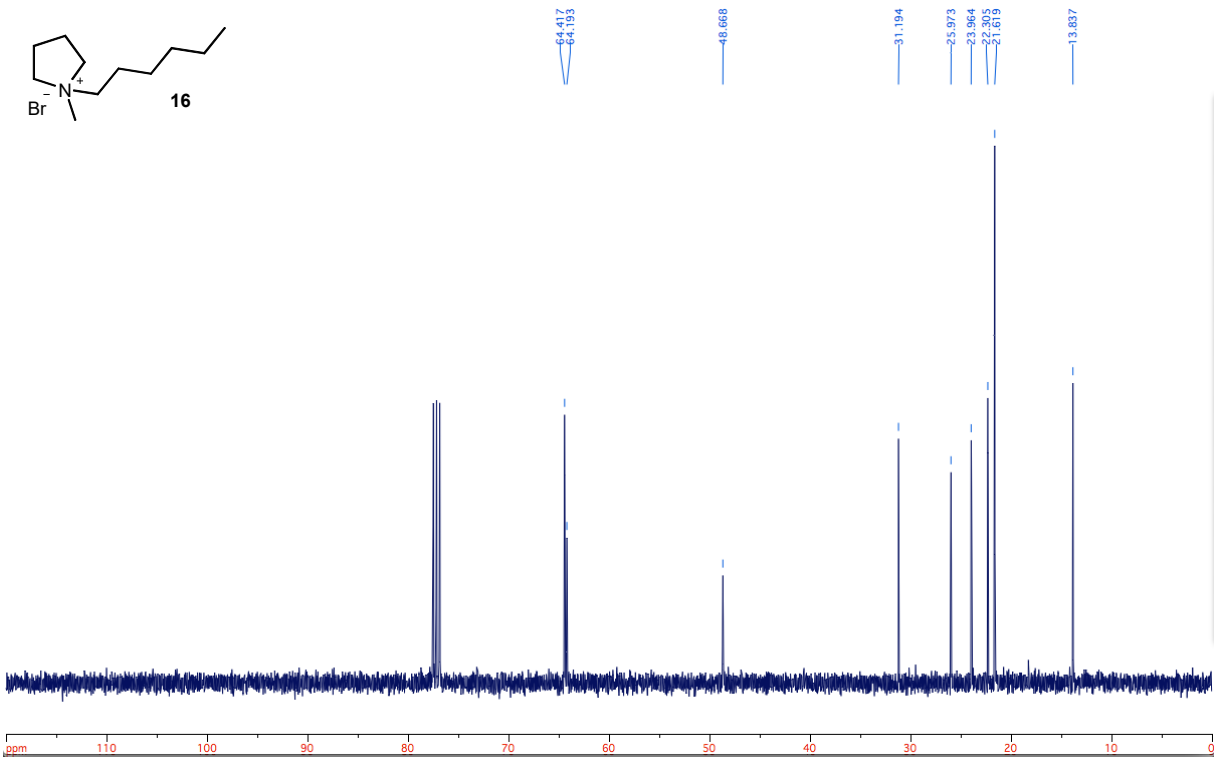

Fig. S18. ^{13}C NMR of 1-Hexyl-1-methylpyrrolidin-1-ium bromide (**16**).

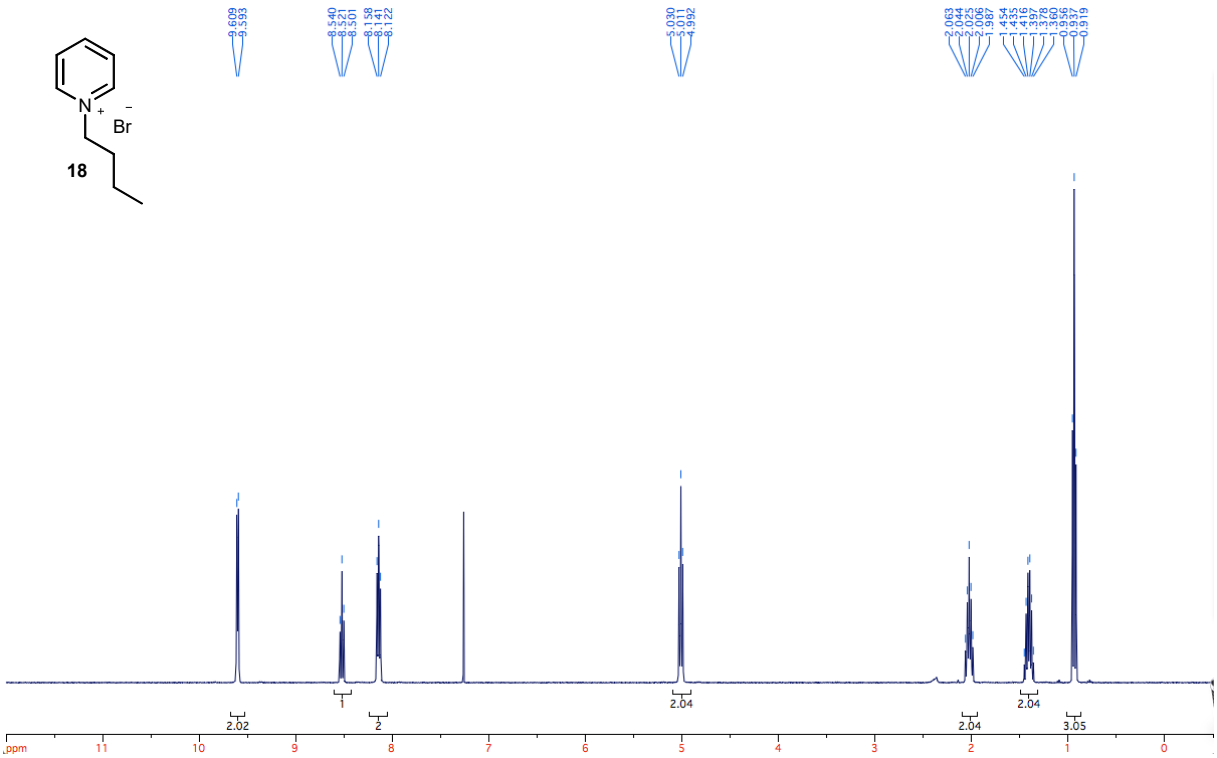

Fig. S19. ^{1}H NMR of 1-Butylpyridin-1-ium bromide (**18**).

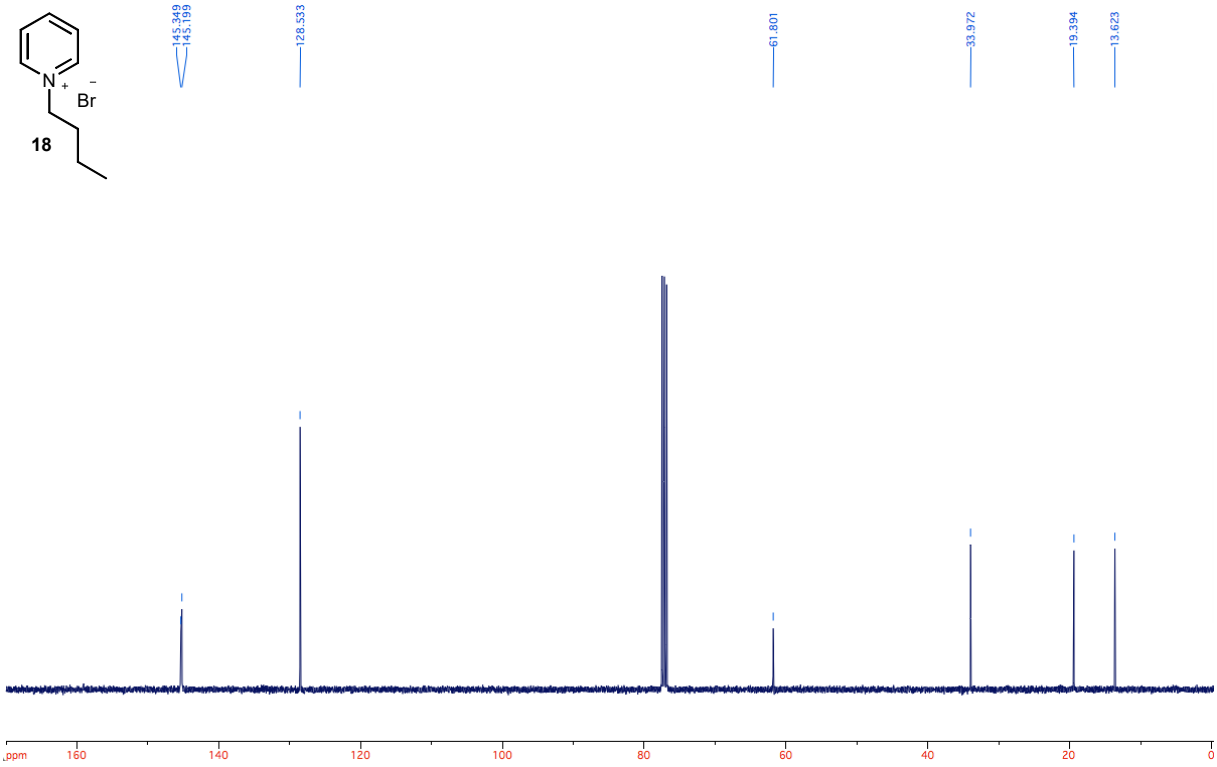

Fig. S20. ^{13}C NMR of 1-Butylpyridin-1-ium bromide (**18**).

Characterization of the ionic liquids 10-15, 17, 19 and 20

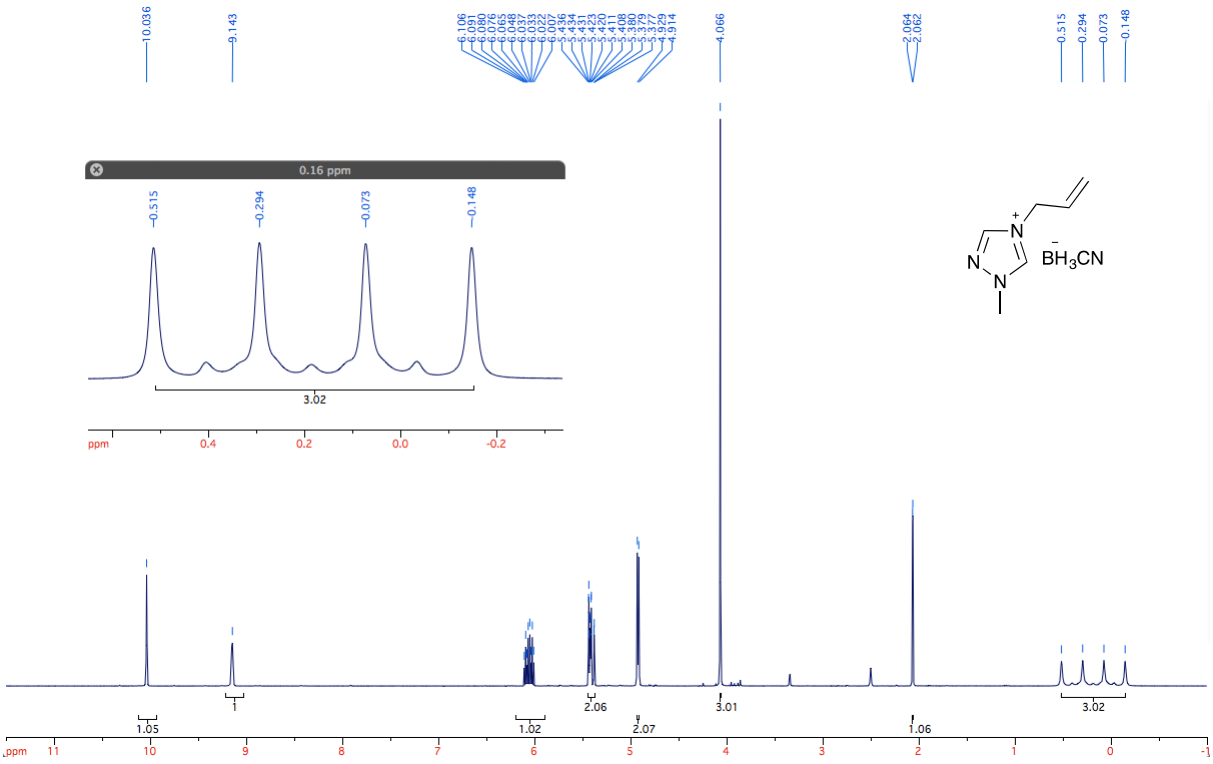

Fig. S21. ^{1}H NMR of 4-Allyl-1-methyl-1*H*-1,2,4-triazol-4-ium cyanotrihydroborate (**10**).

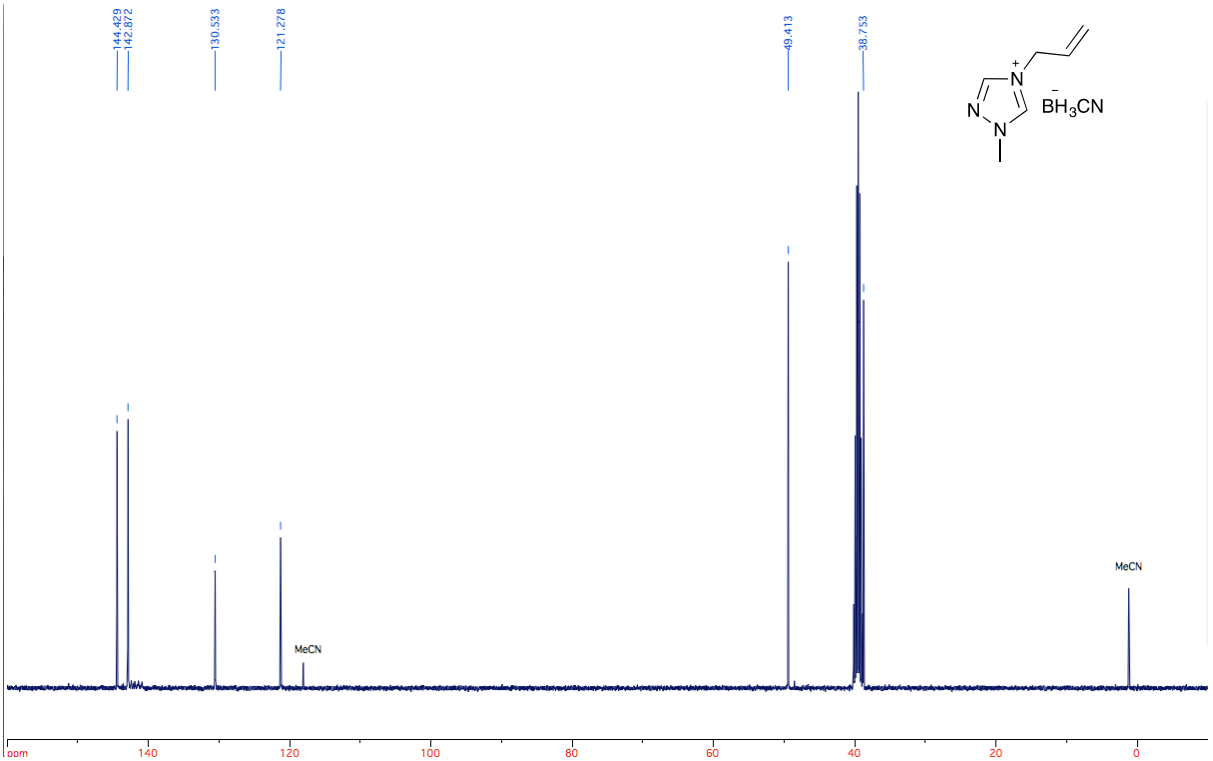

Fig. S22. ^{13}C NMR of 4-Allyl-1-methyl-1*H*-1,2,4-triazol-4-ium cyanotrihydroborate (**10**).

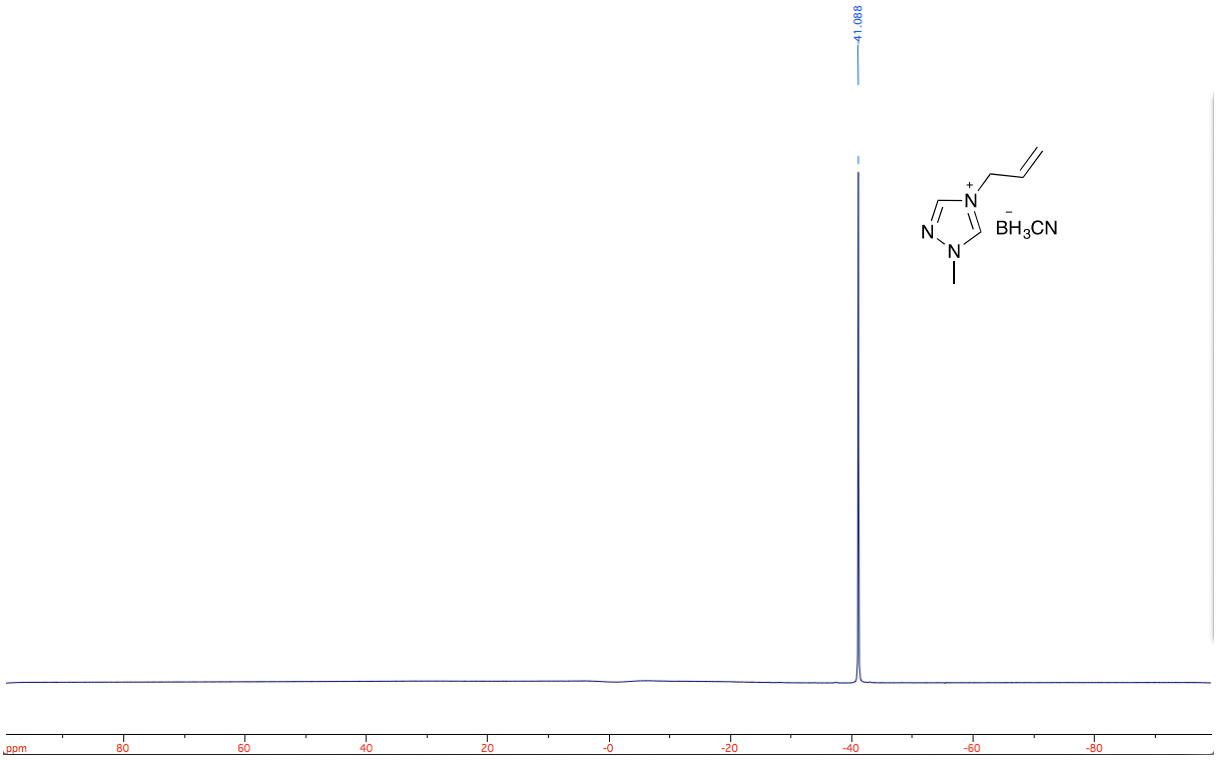

Fig. S23. ^{11}B NMR of 4-Allyl-1-methyl-1*H*-1,2,4-triazol-4-ium cyanotrihydroborate (**10**).

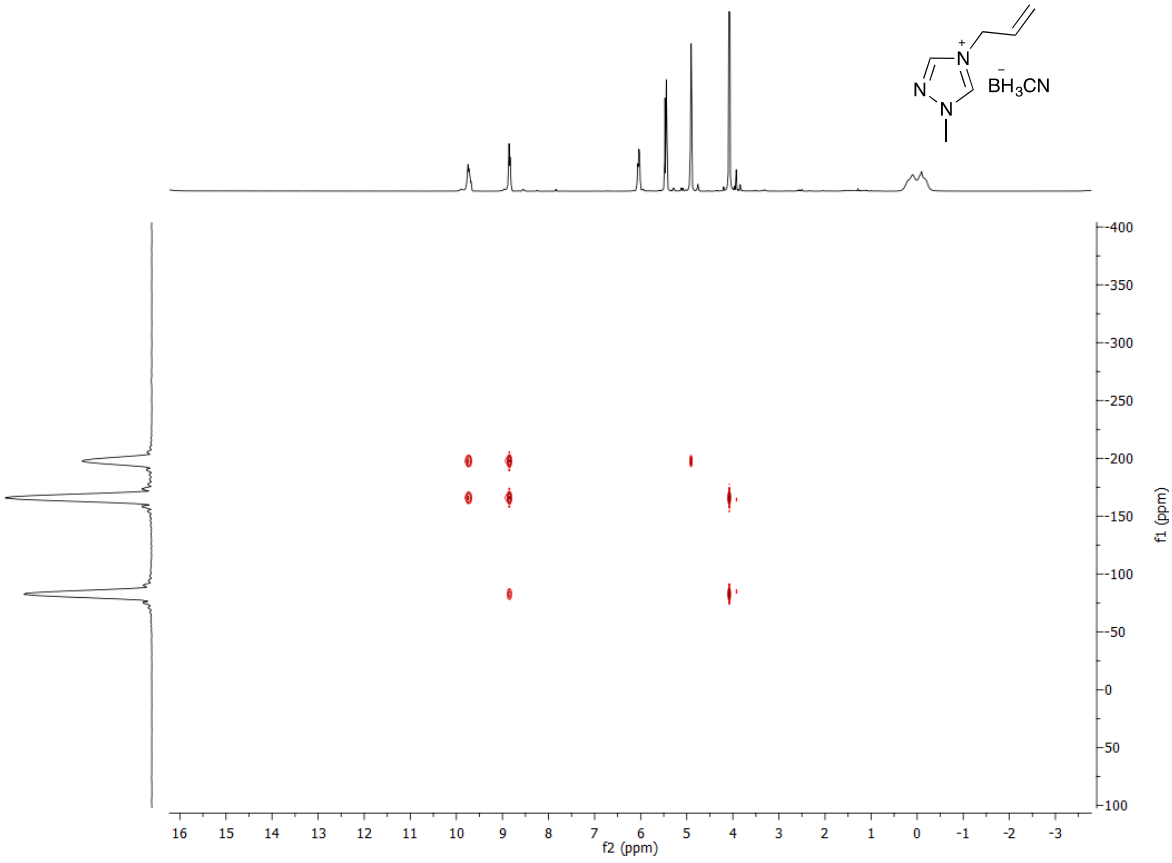

Fig. S24. ^{1}H-^{15}N HSQC of 4-Allyl-1-methyl-1*H*-1,2,4-triazol-4-ium cyanotrihydroborate (**10**).

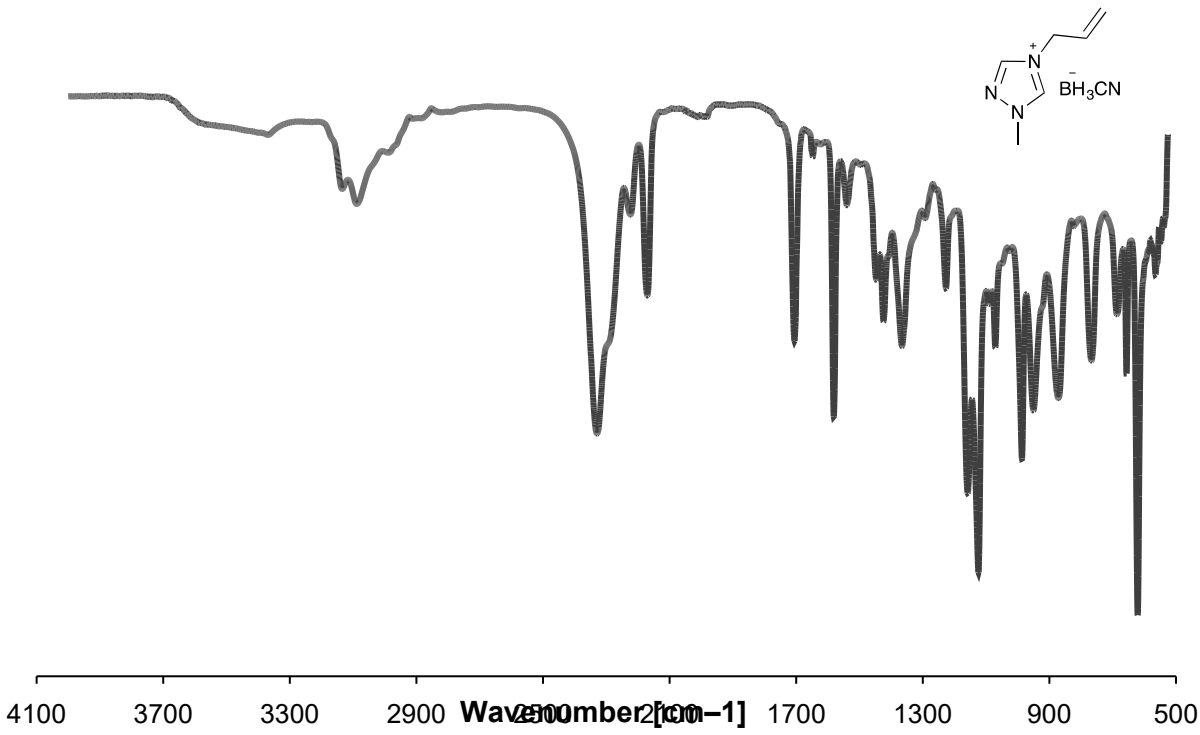

Fig. S25. IR Spectrum of 4-Allyl-1-methyl-1*H*-1,2,4-triazol-4-ium cyanotrihydroborate (**10**).

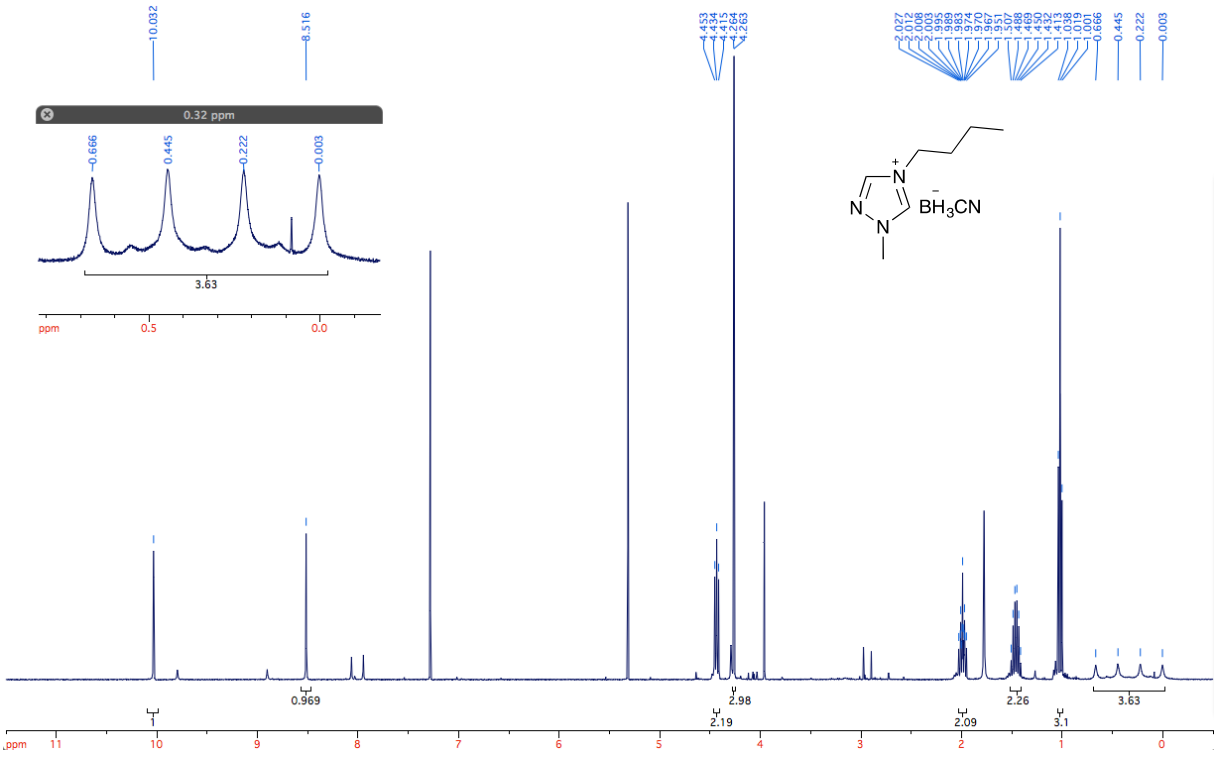

Fig. S26. ^{1}H NMR of 4-Butyl-1-methyl-1*H*-1,2,4-triazol-4-ium cyanotrihydroborate (**11**).

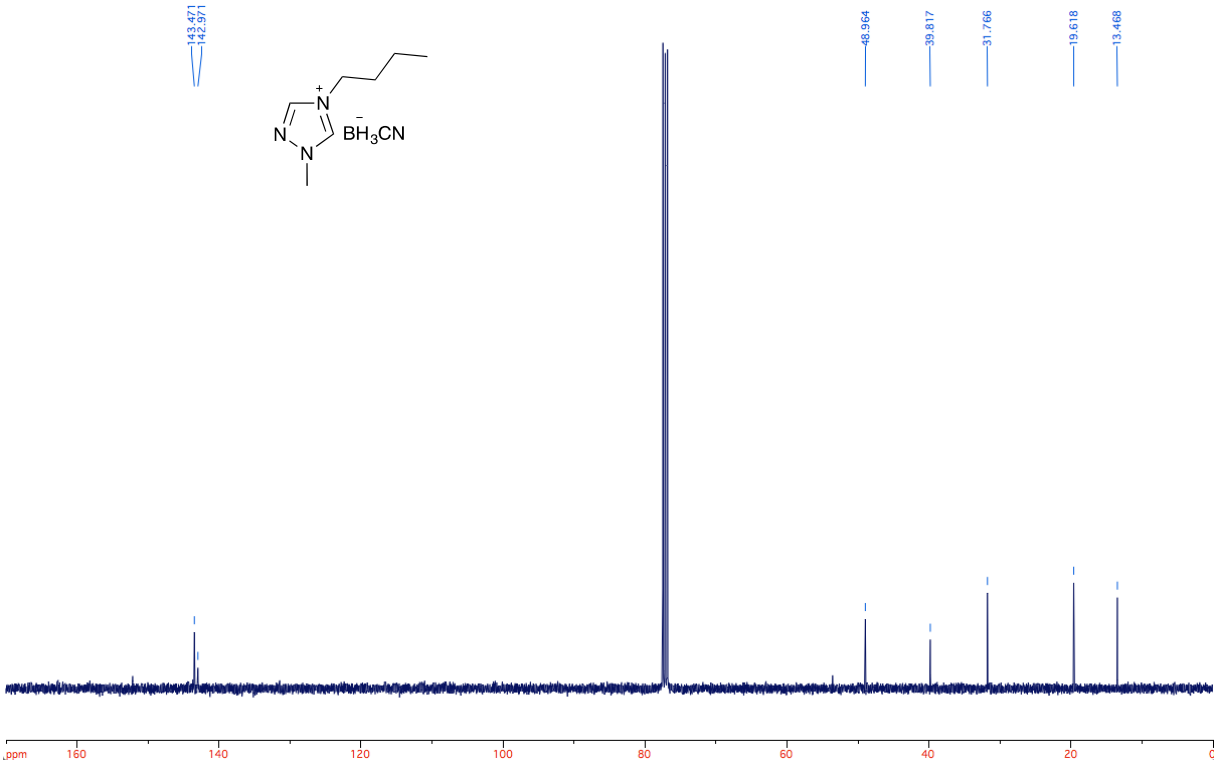

Fig. S27. ^{13}C NMR of 4-Butyl-1-methyl-1*H*-1,2,4-triazol-4-ium cyanotrihydroborate (**11**)

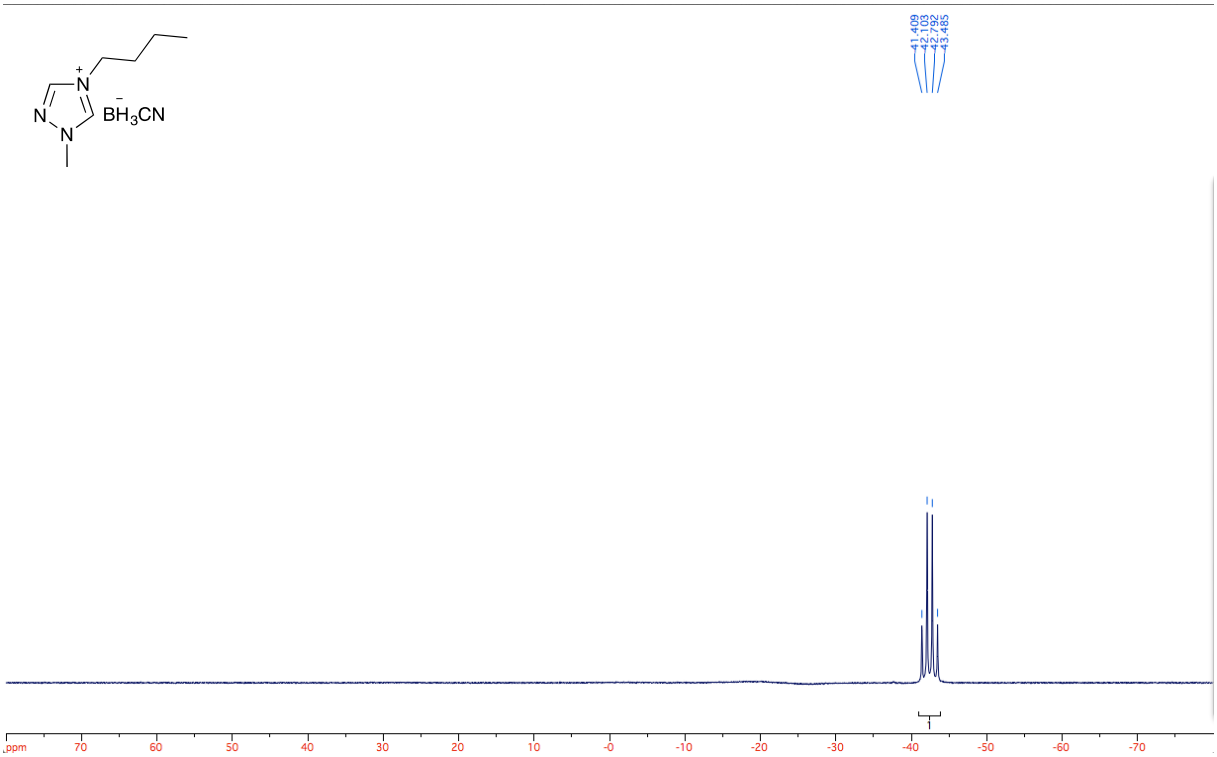

Fig. S28. ^{11}B NMR of 4-Butyl-1-methyl-1*H*-1,2,4-triazol-4-ium cyanotrihydroborate (**11**)

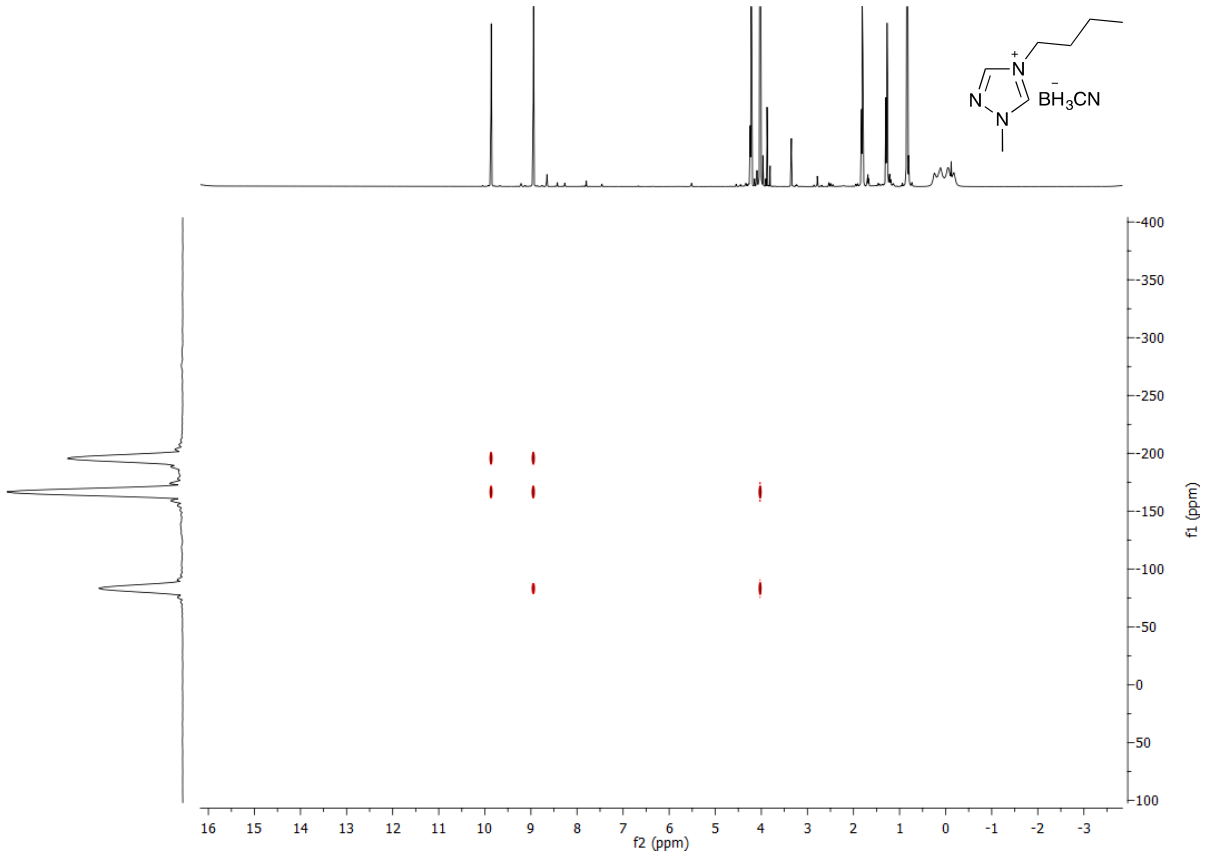

Fig. S29. ^{1}H-^{15}N HSQC of 4-Butyl-1-methyl-1*H*-1,2,4-triazol-4-ium cyanotrihydroborate (**11**).

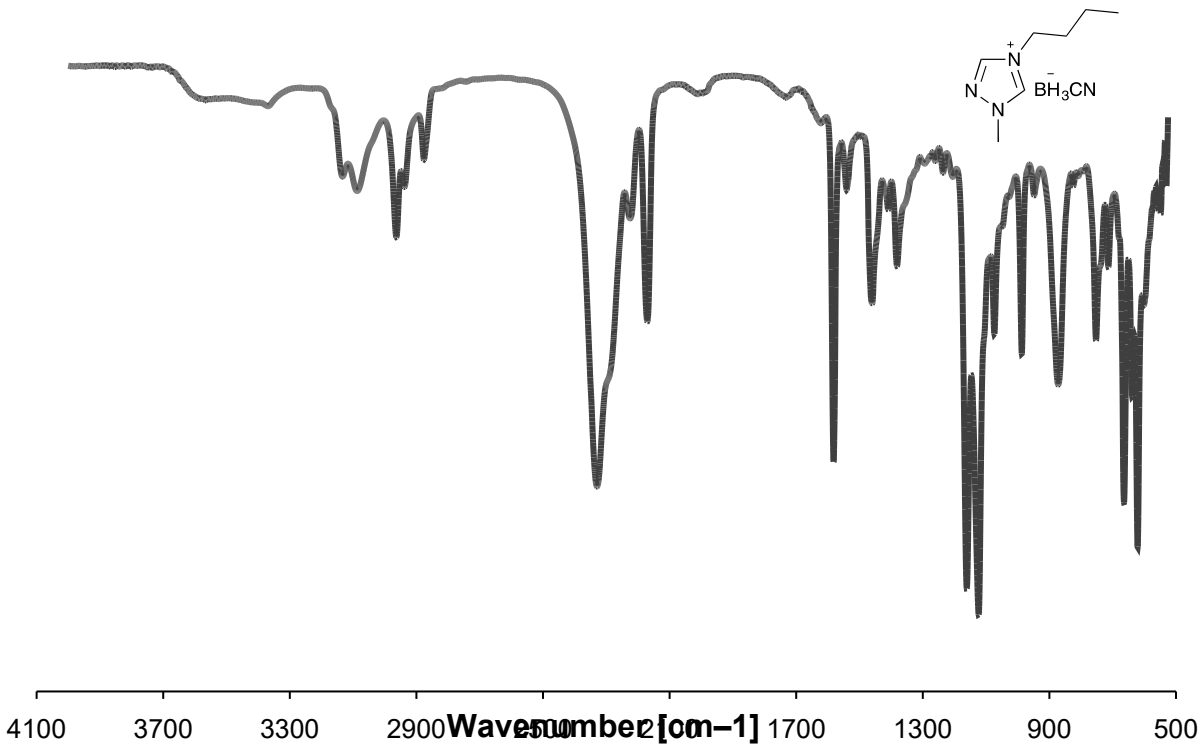

Fig. S30. IR Spectrum of 4-Butyl-1-methyl-1*H*-1,2,4-triazol-4-ium cyanotrihydroborate (**11**).

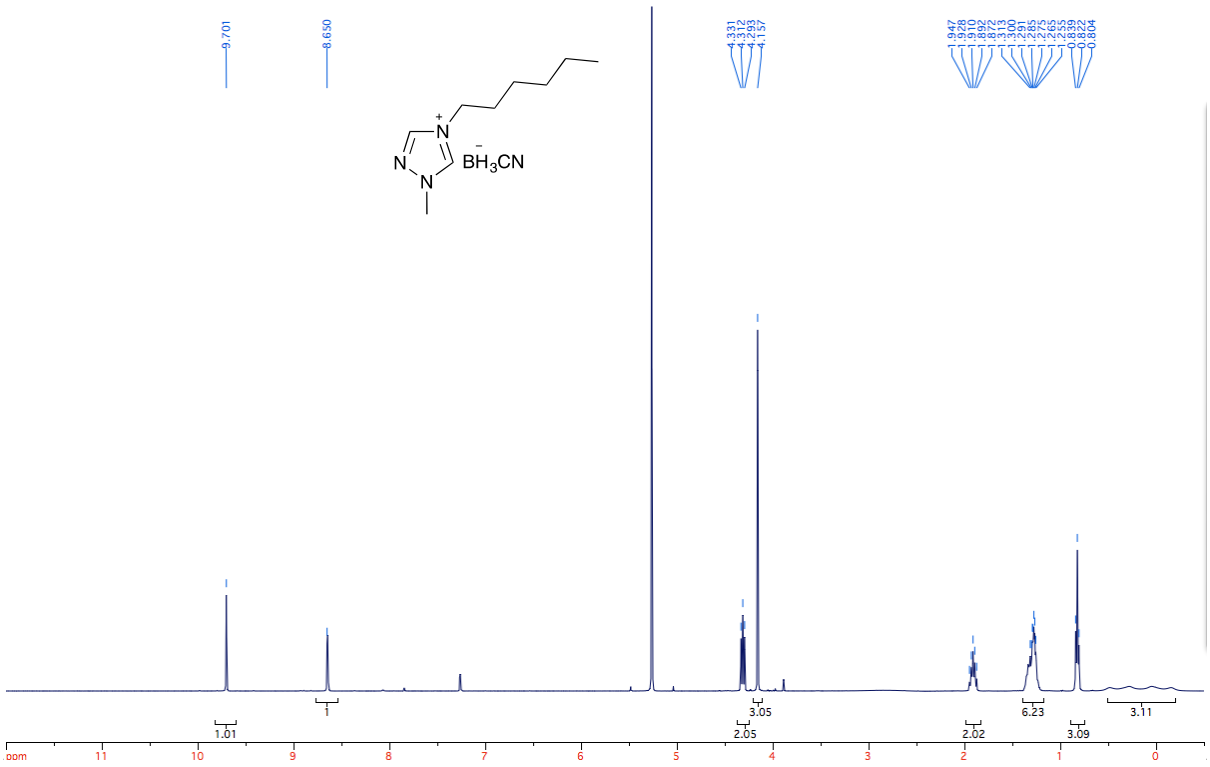

Fig. S31. ^{1}H NMR of 4-Hexyl-1-methyl-1*H*-1,2,4-triazol-4-ium cyanotrihydroborate (**12**).

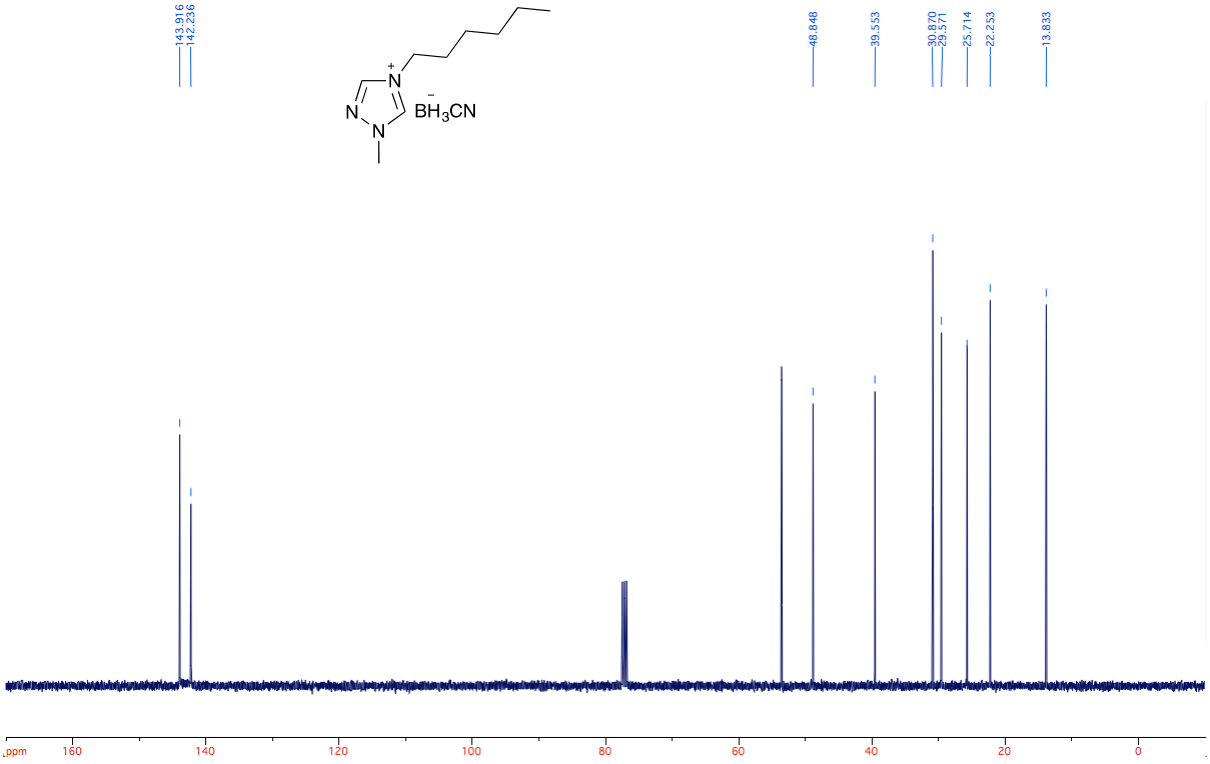

Fig. S32. ^{13}C NMR of 4-Hexyl-1-methyl-1*H*-1,2,4-triazol-4-ium cyanotrihydroborate (**12**).

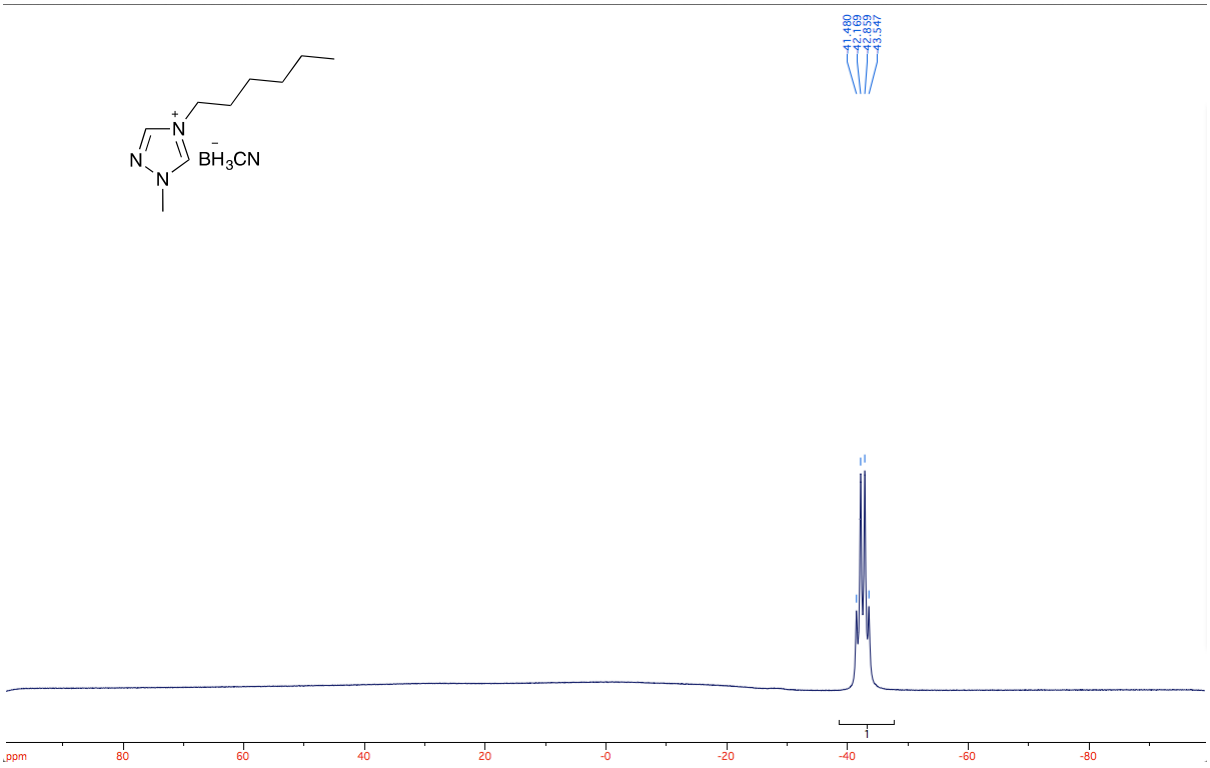

Fig. S33. ^{11}B NMR of 4-Hexyl-1-methyl-1*H*-1,2,4-triazol-4-ium cyanotrihydroborate (**12**).

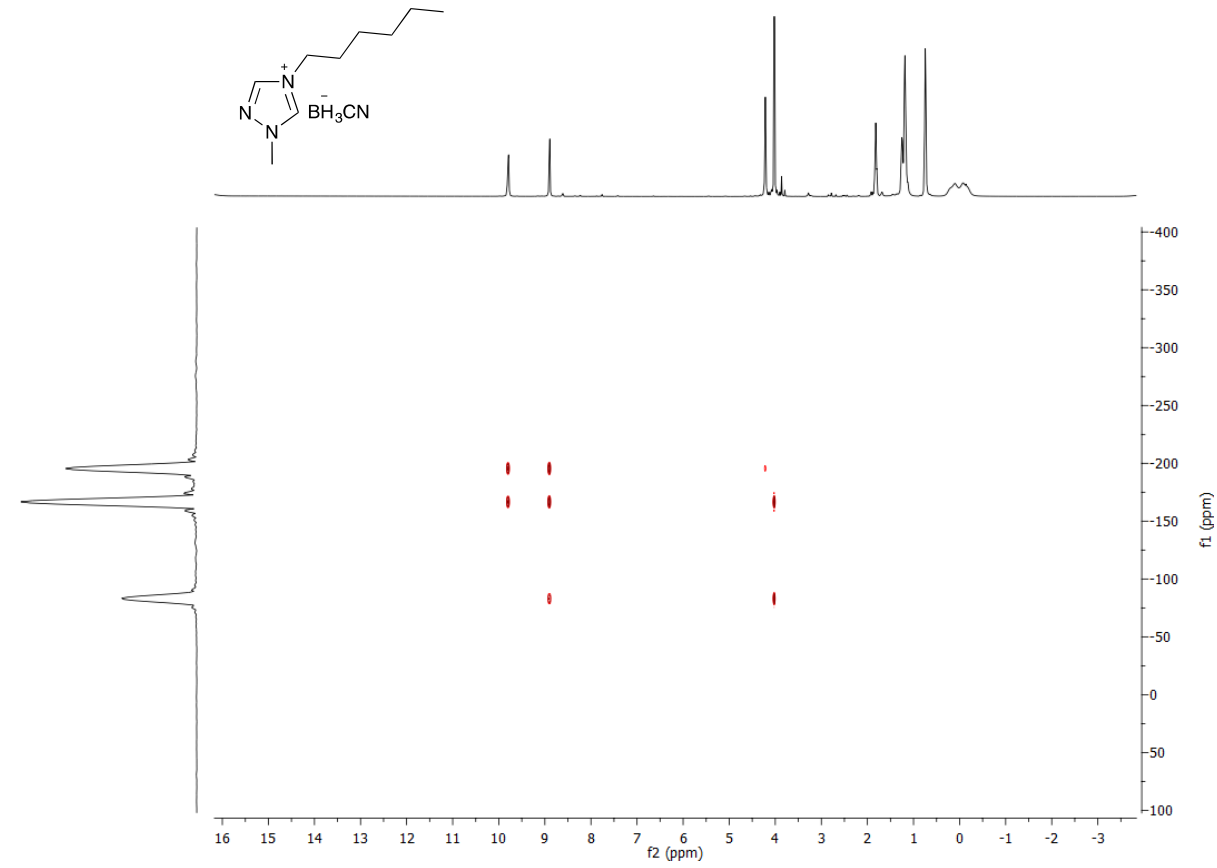

Fig. S34. ^{1}H-^{15}N HSQC of 4-Hexyl-1-methyl-1*H*-1,2,4-triazol-4-ium cyanotrihydroborate (**12**).

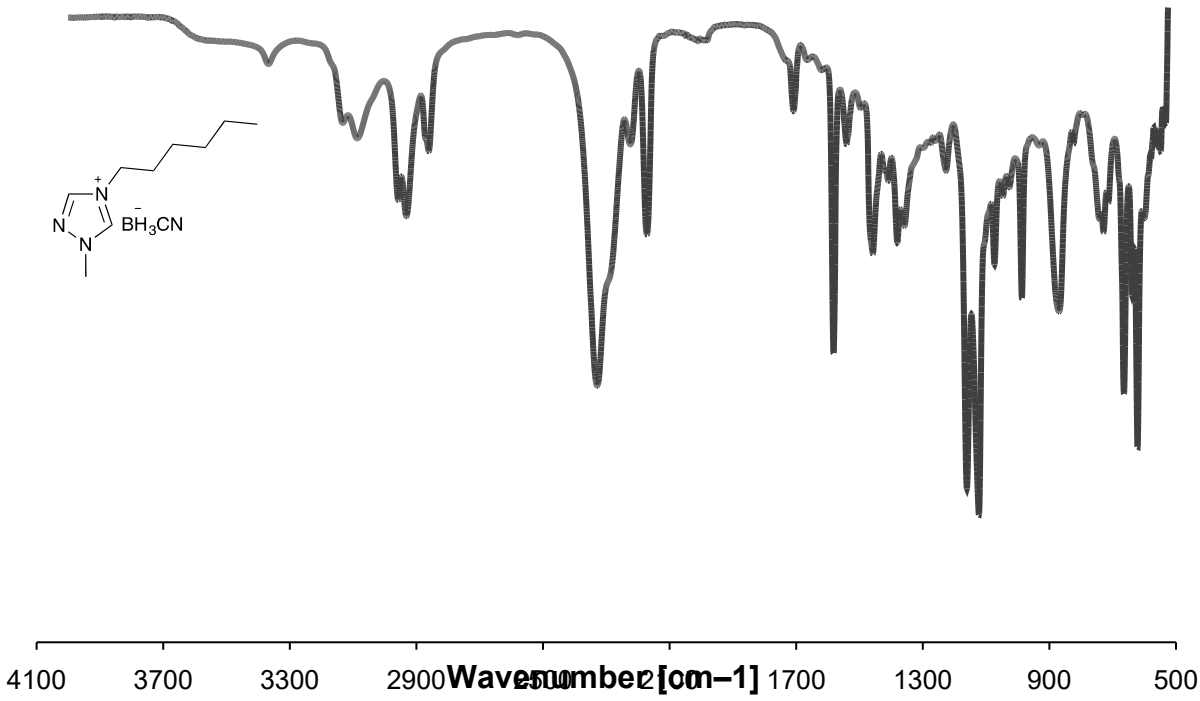

Fig. S35. IR Spectrum of 4-hexyl-1-methyl-1*H*-1,2,4-triazol-4-ium cyanotrihydroborate (**12**).

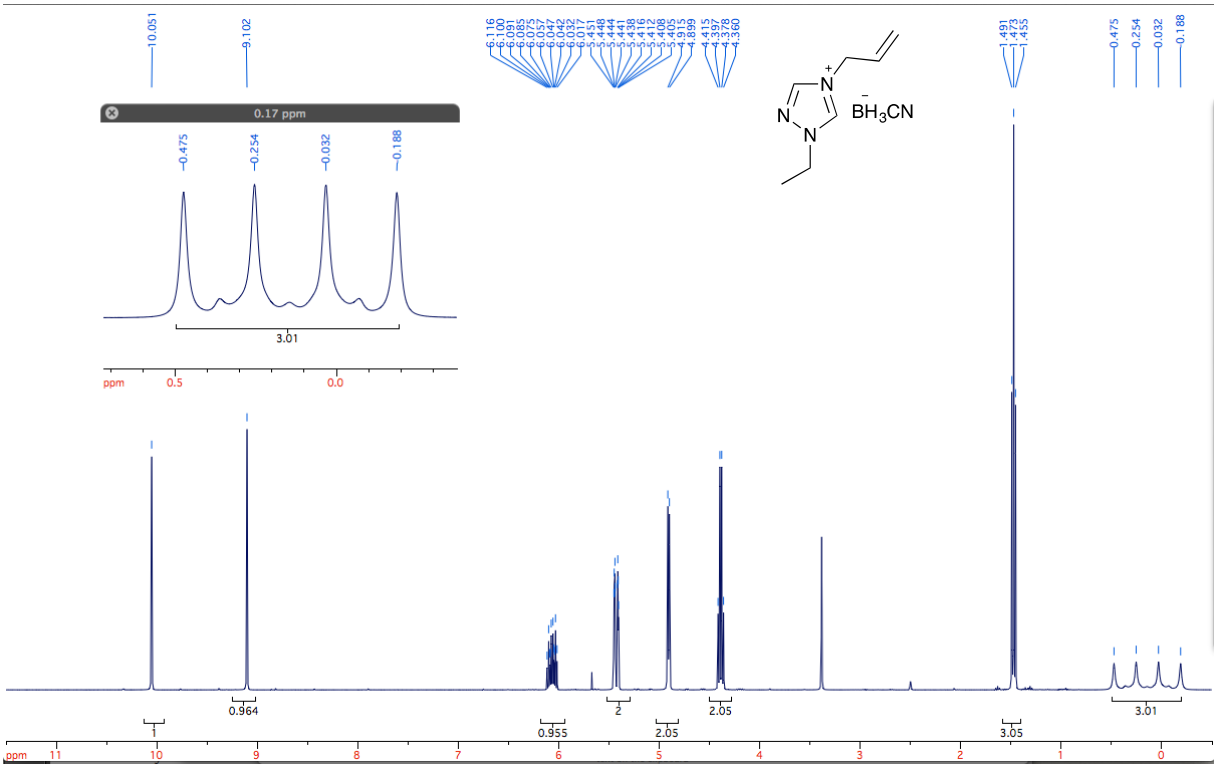

Fig. S36. ^{1}H NMR of 4-Allyl-1-ethyl-1*H*-1,2,4-triazol-4-ium cyanotrihydroborate (**13**).

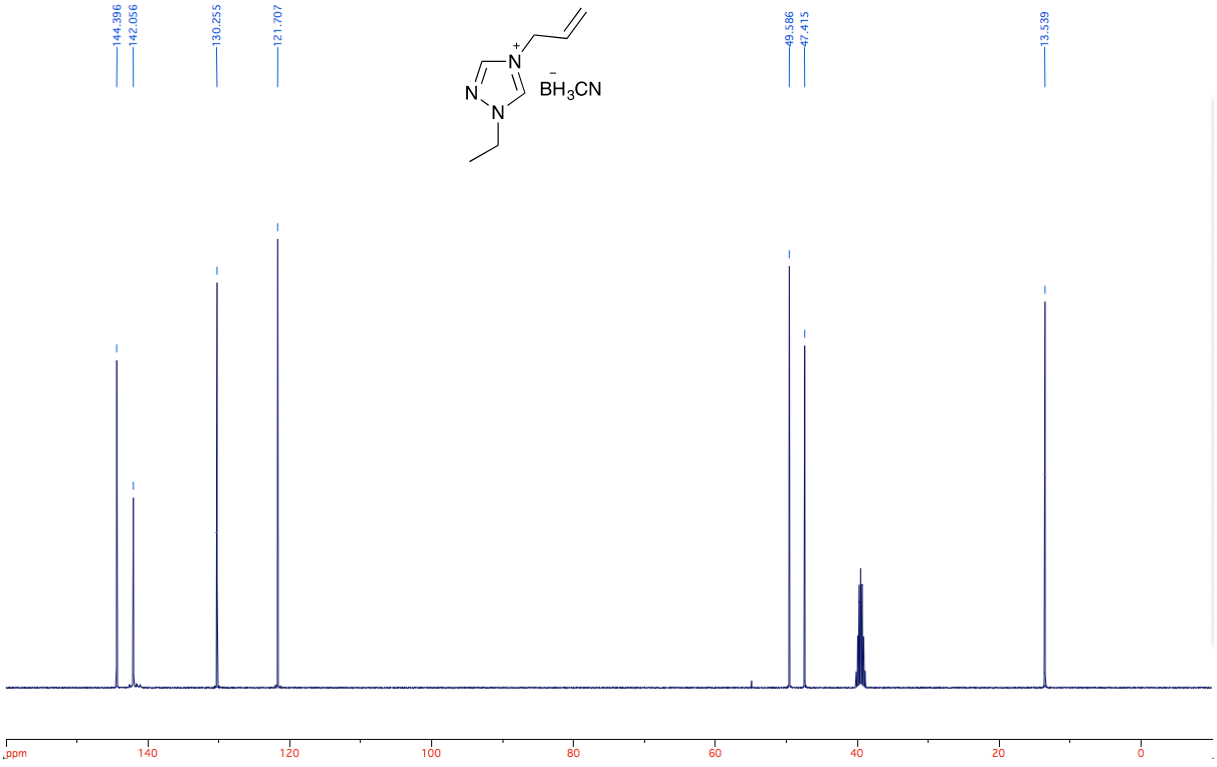

Fig. S37. ^{13}C NMR of 4-Allyl-1-ethyl-1*H*-1,2,4-triazol-4-ium cyanotrihydroborate (**13**).

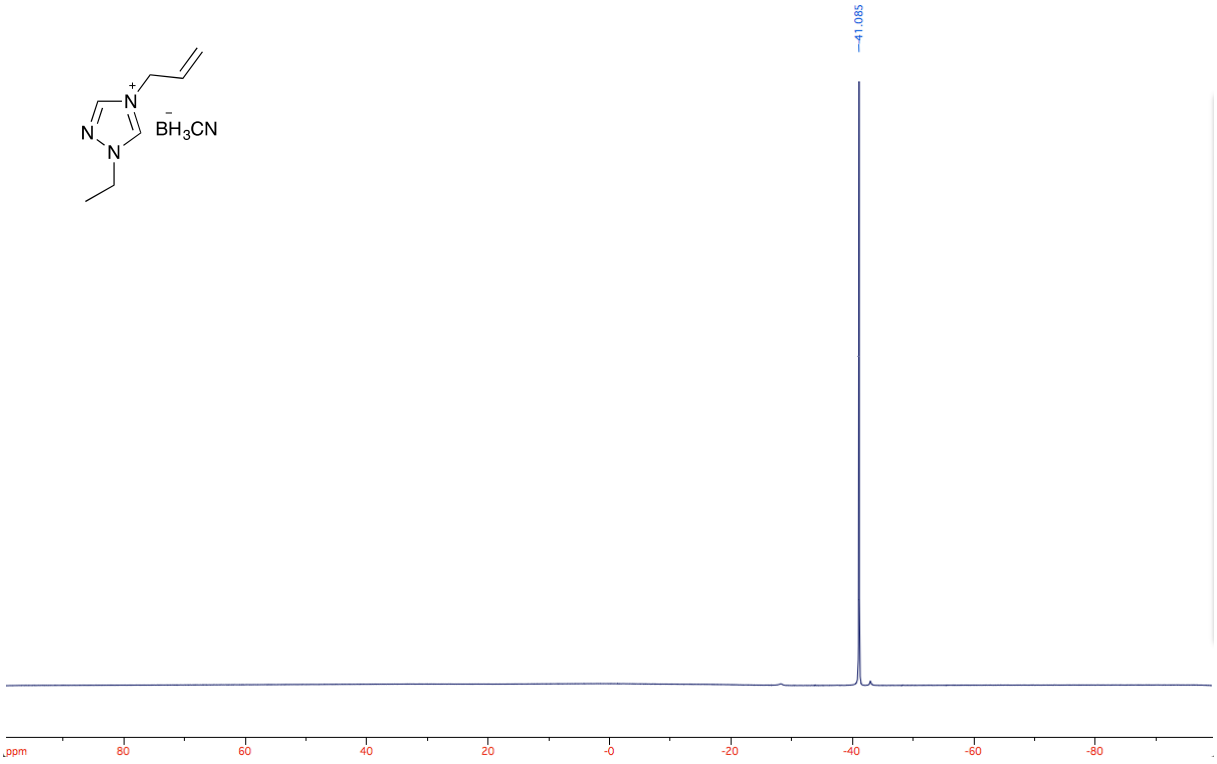

Fig. S38. ^{11}B NMR of 4-Allyl-1-ethyl-1*H*-1,2,4-triazol-4-ium cyanotrihydroborate (**13**).

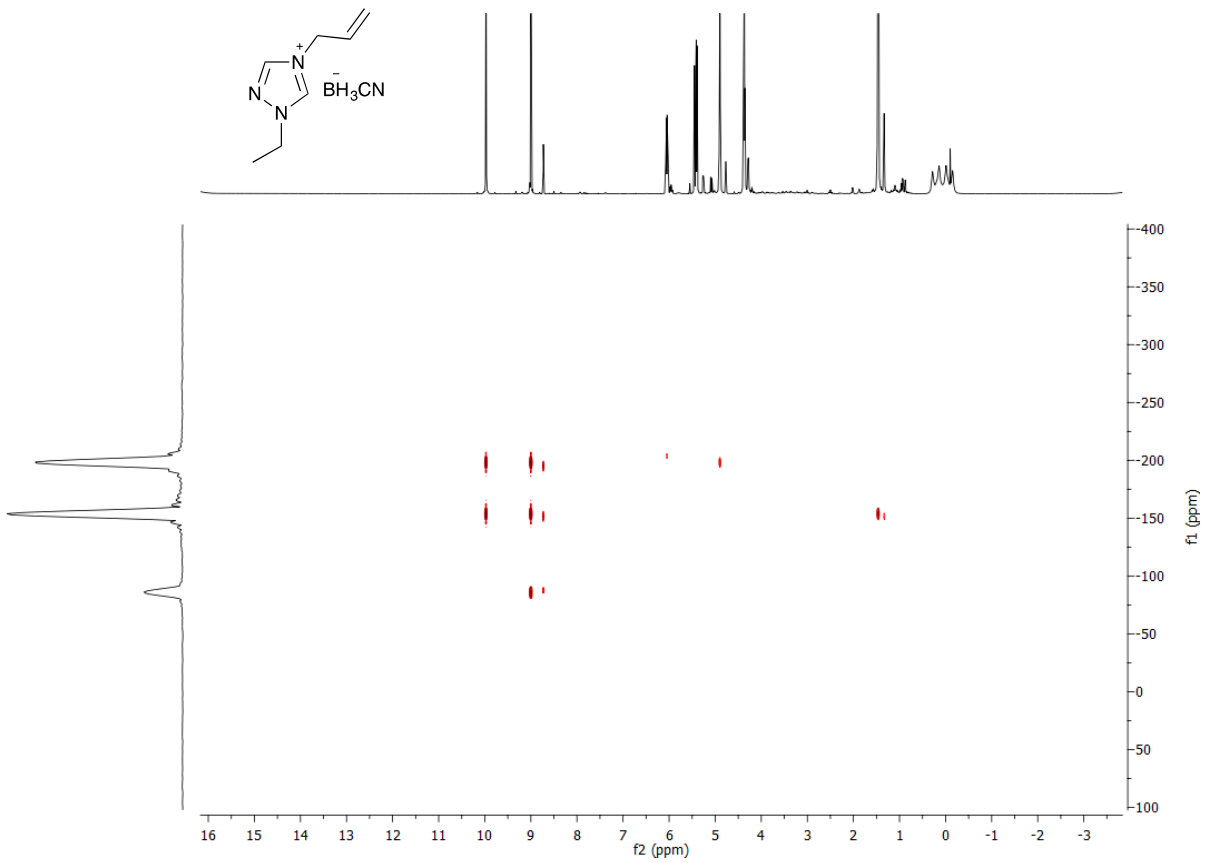

Fig. S39. ^{1}H-^{15}N HSQC of 4-Allyl-1-ethyl-1*H*-1,2,4-triazol-4-ium cyanotrihydroborate (**13**).

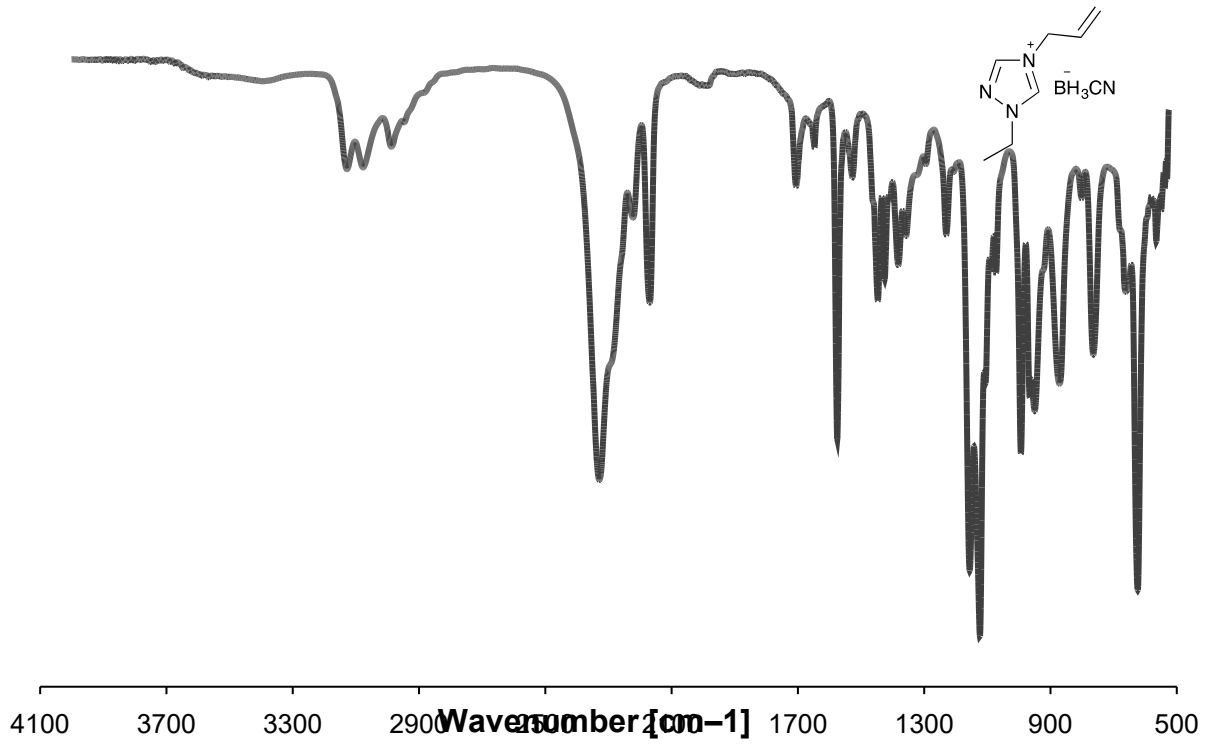

Fig. S40. IR spectrum of 4-Allyl-1-ethyl-1*H*-1,2,4-triazol-4-ium cyanotrihydroborate (**13**).

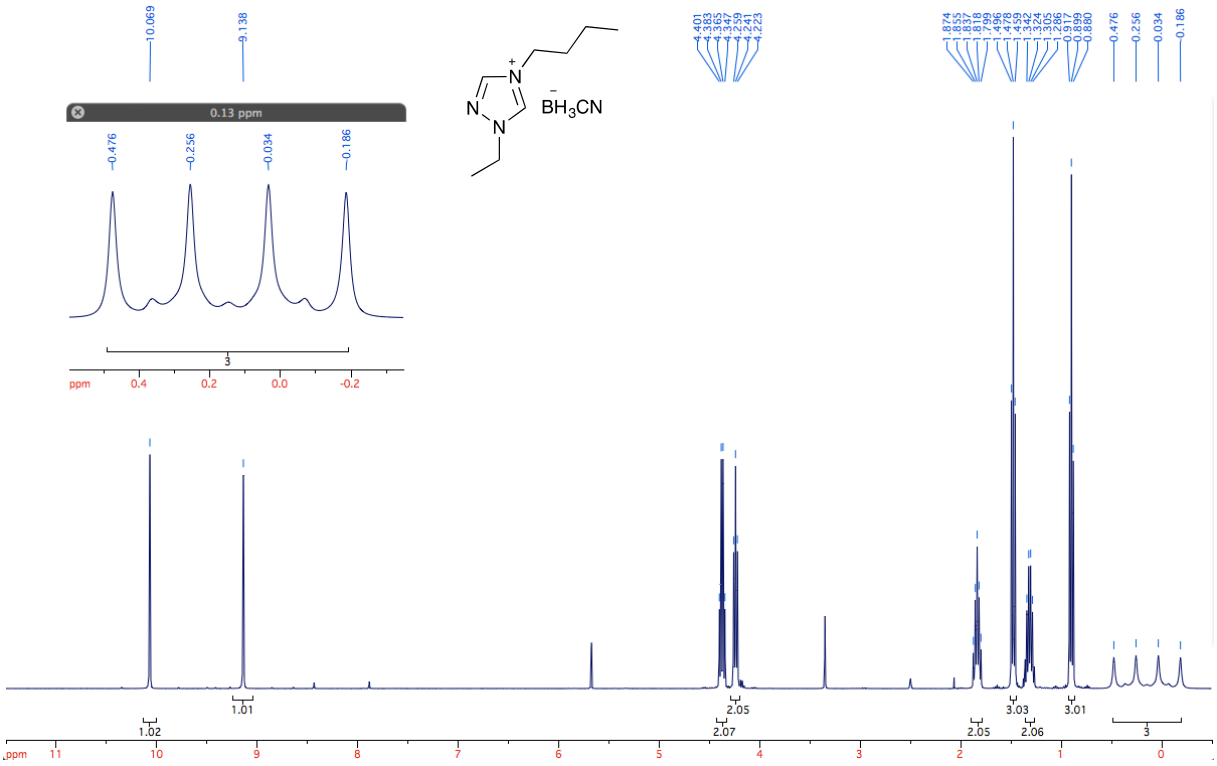

Fig. S41. ^{1}H NMR of 4-Butyl-1-ethyl-1*H*-1,2,4-triazol-4-ium cyanotrihydroborate (**14**).

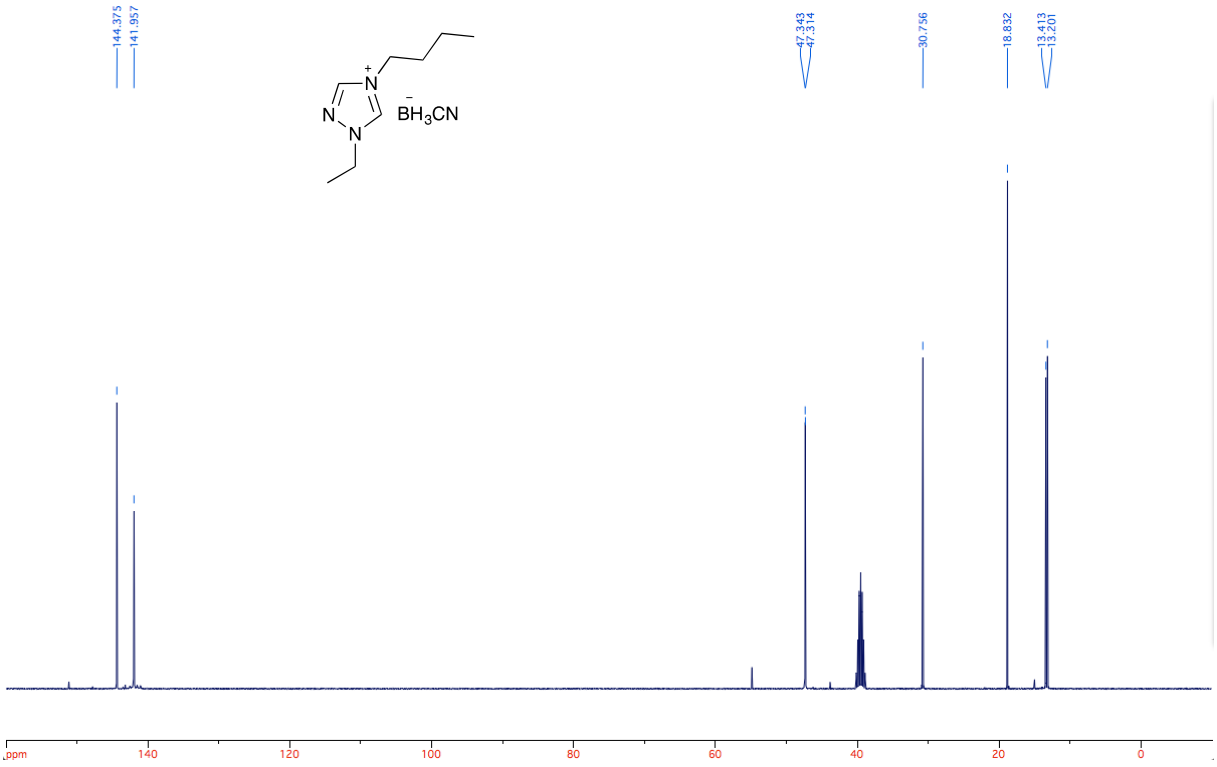

Fig. S42. ^{13}C NMR of 4-Butyl-1-ethyl-1*H*-1,2,4-triazol-4-ium cyanotrihydroborate (**14**).

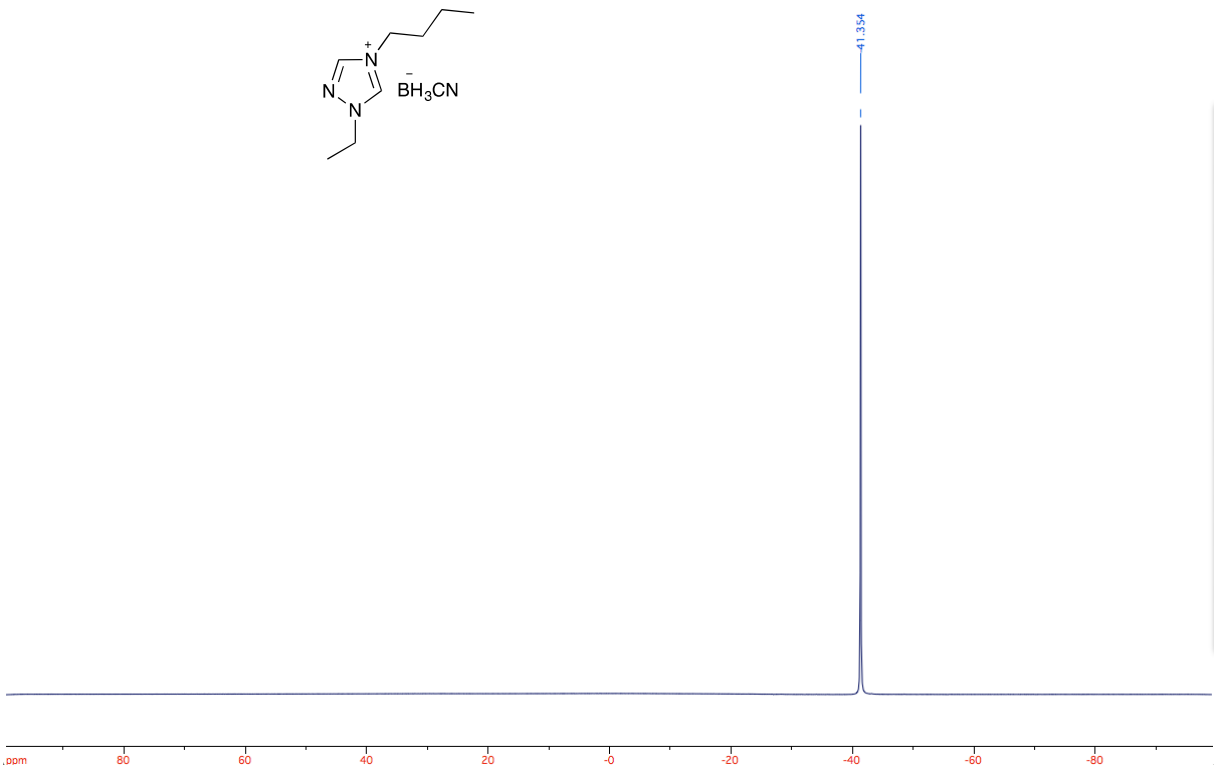

Fig. S43. ^{11}B NMR of 4-Butyl-1-ethyl-1*H*-1,2,4-triazol-4-ium cyanotrihydroborate (**14**).

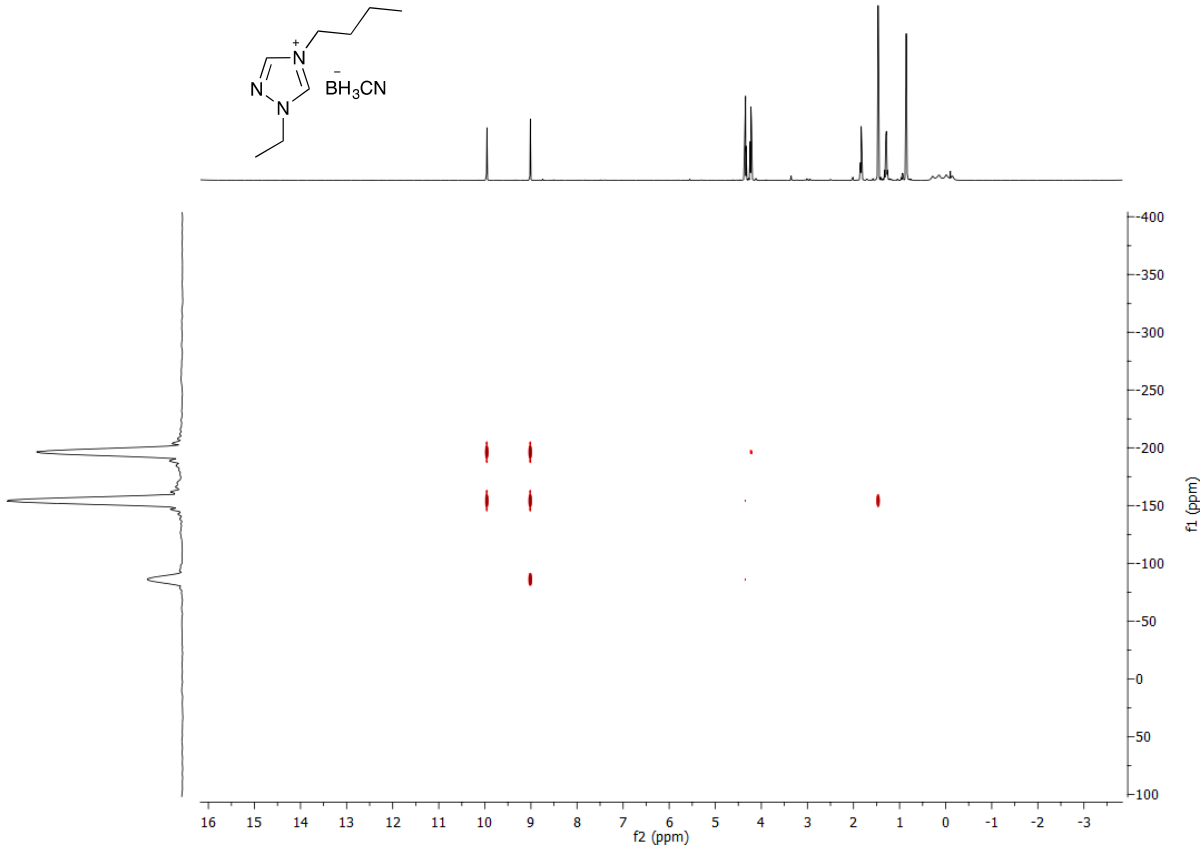

Fig. S44. ^{1}H-^{15}N HSQC of 4-Butyl-1-ethyl-1*H*-1,2,4-triazol-4-ium cyanotrihydroborate (**14**).

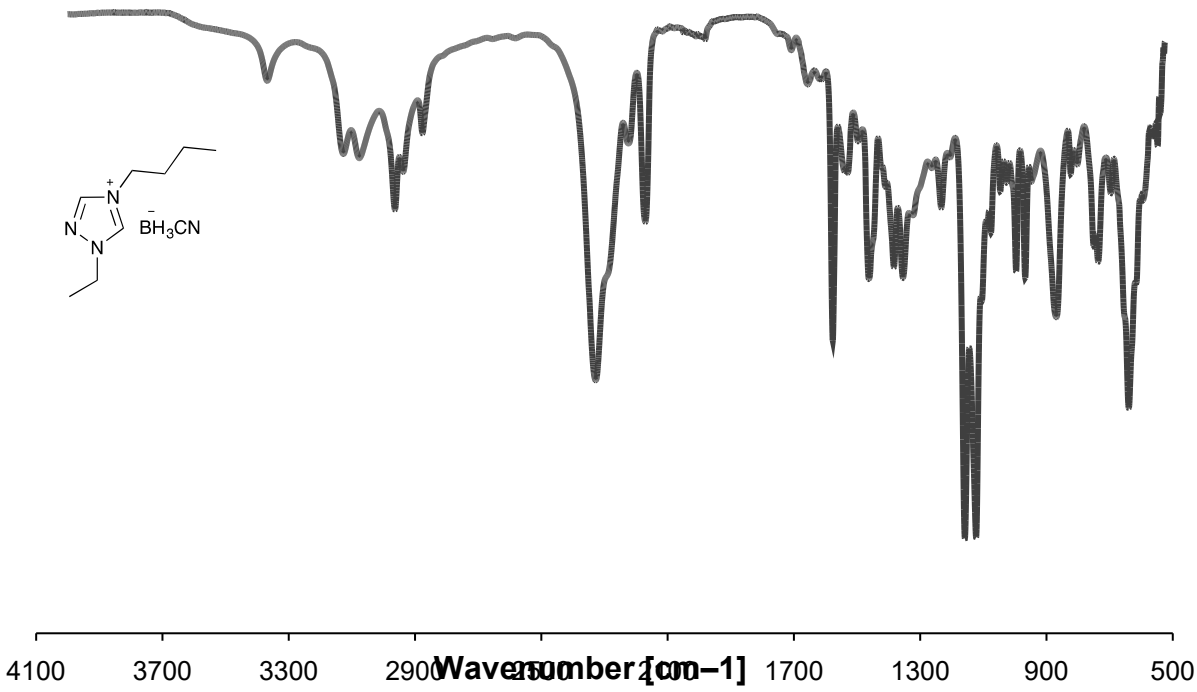

Fig. S45. IR spectrum of 4-Butyl-1-ethyl-1*H*-1,2,4-triazol-4-ium cyanotrihydroborate (**14**).

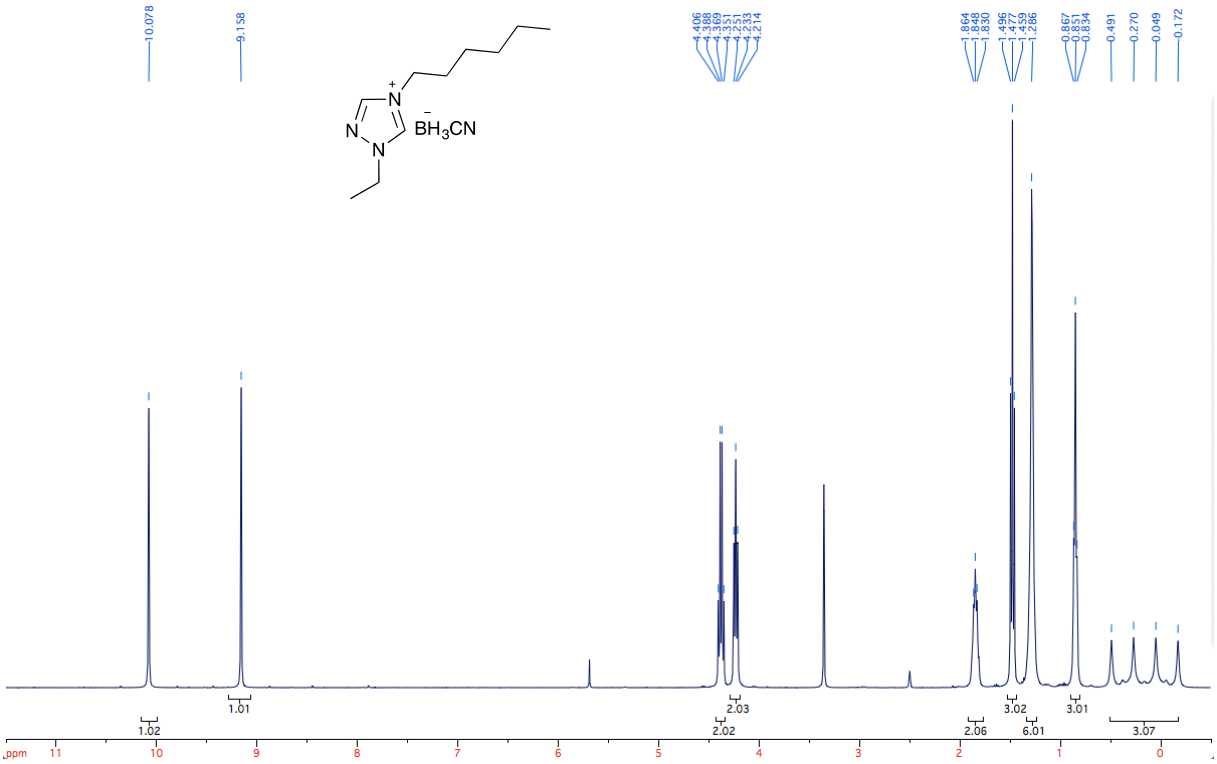

Fig. S46. ^{1}H NMR of 1-Ethyl-4-hexyl-1*H*-1,2,4-triazol-4-ium cyanotrihydroborate (**15**).

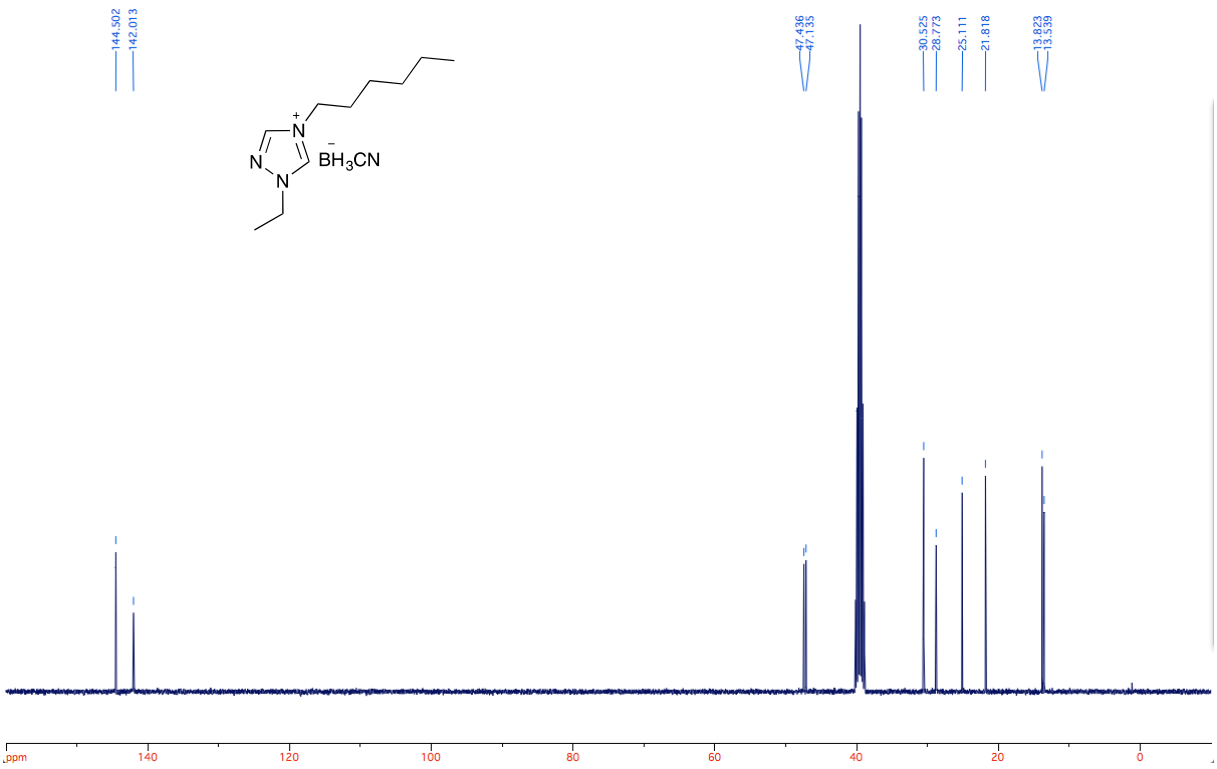

Fig. S47. ^{13}C NMR of 1-Ethyl-4-hexyl-1*H*-1,2,4-triazol-4-ium cyanotrihydroborate (**15**).

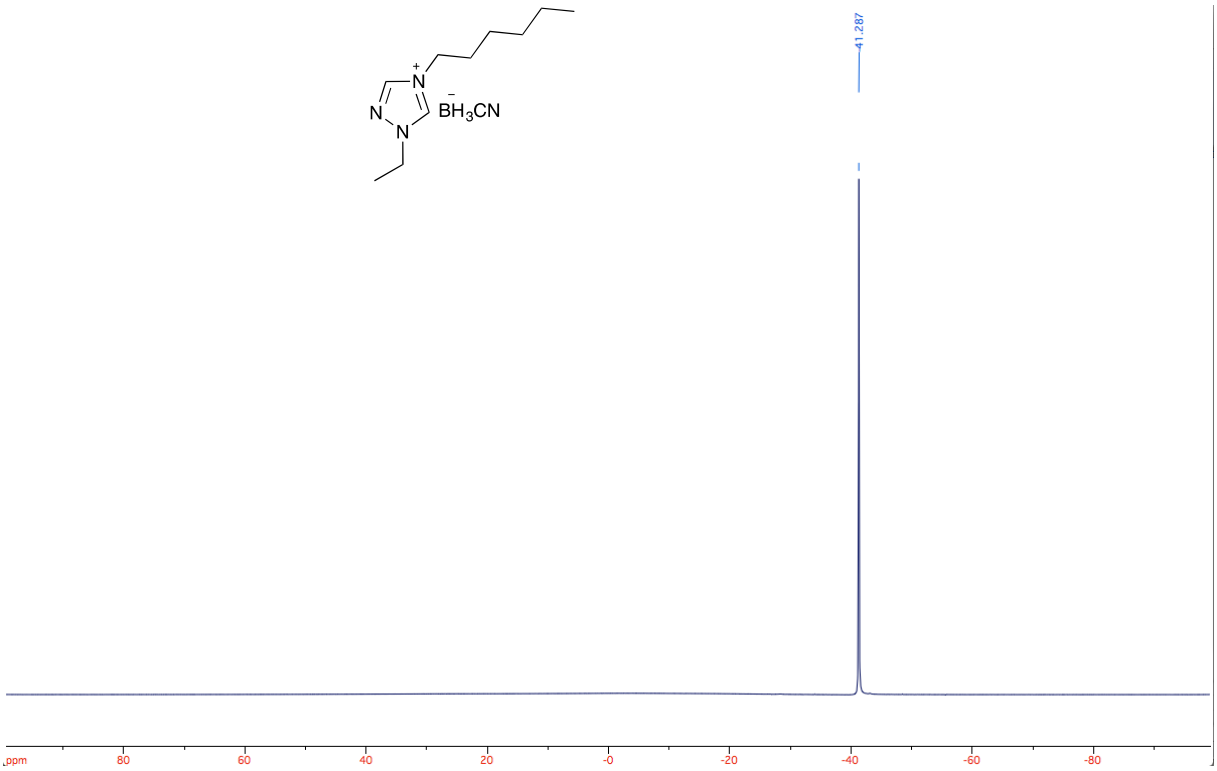

Fig. S48. ^{11}B NMR of 1-Ethyl-4-hexyl-1*H*-1,2,4-triazol-4-ium cyanotrihydroborate (**15**).

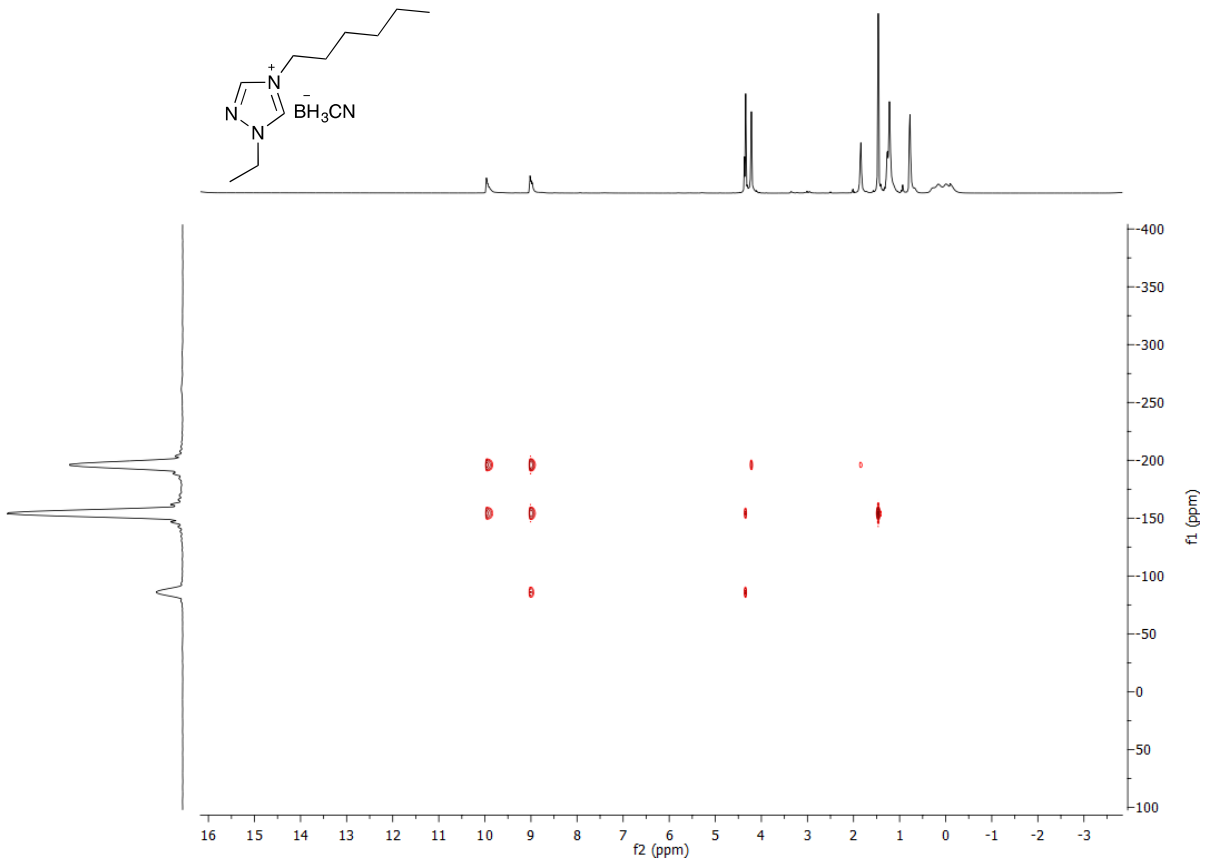

Fig. S49. ^{1}H-^{15}N HSQC of 1-Ethyl-4-hexyl-1*H*-1,2,4-triazol-4-ium cyanotrihydroborate (**15**).

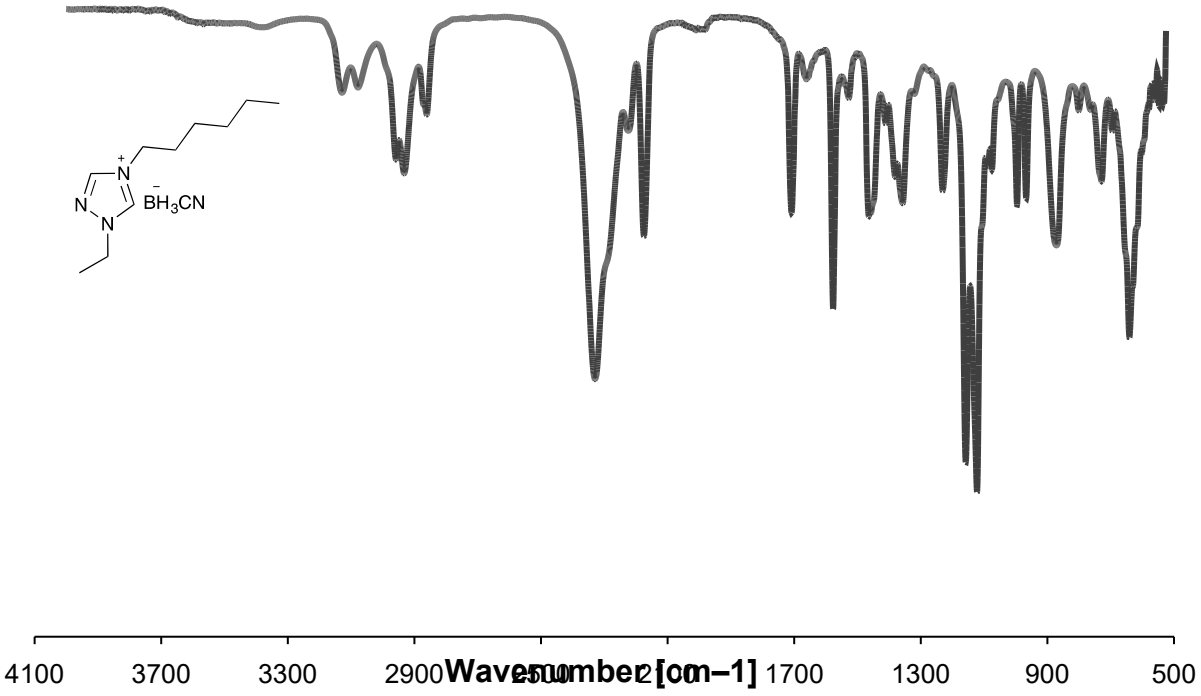

Fig. S50. IR spectrum of 1-Ethyl-4-hexyl-1*H*-1,2,4-triazol-4-ium cyanotrihydroborate (**15**).

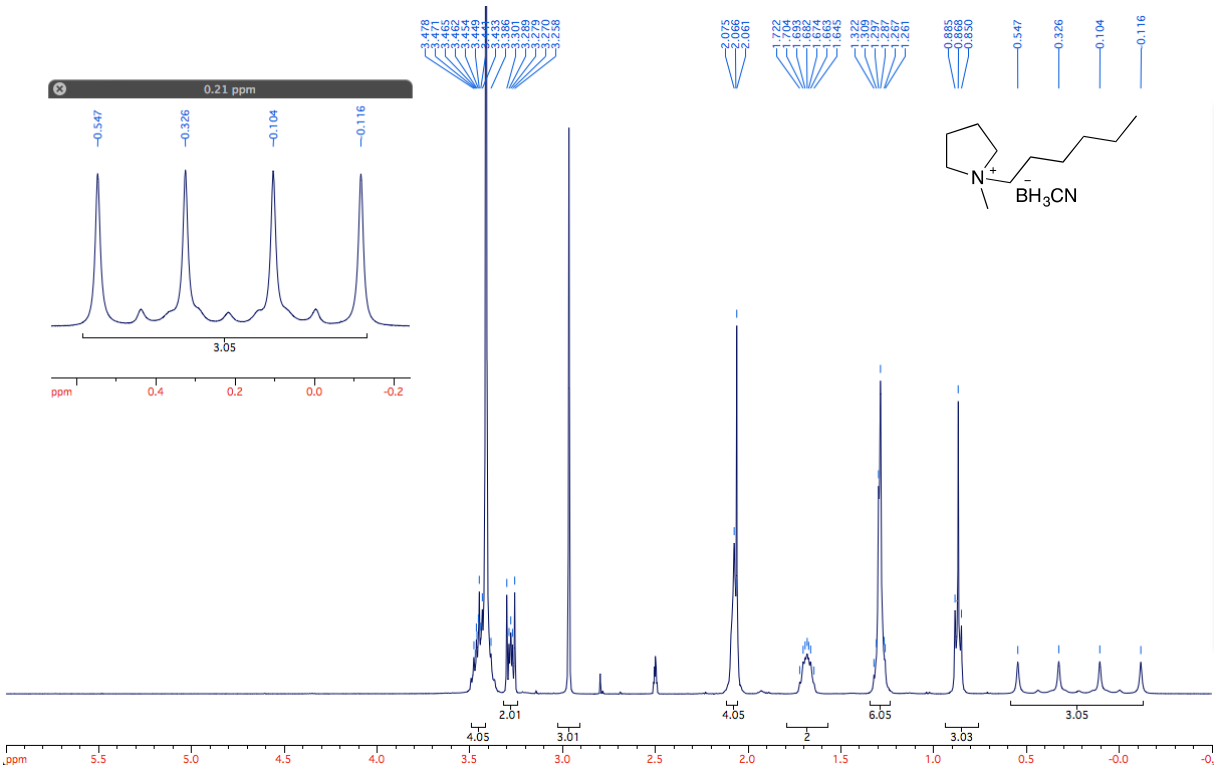

Fig. S51. ^{1}H NMR of 1-Hexyl-1-methylpyrrolidin-1-ium cyanotrihydroborate (**17**).

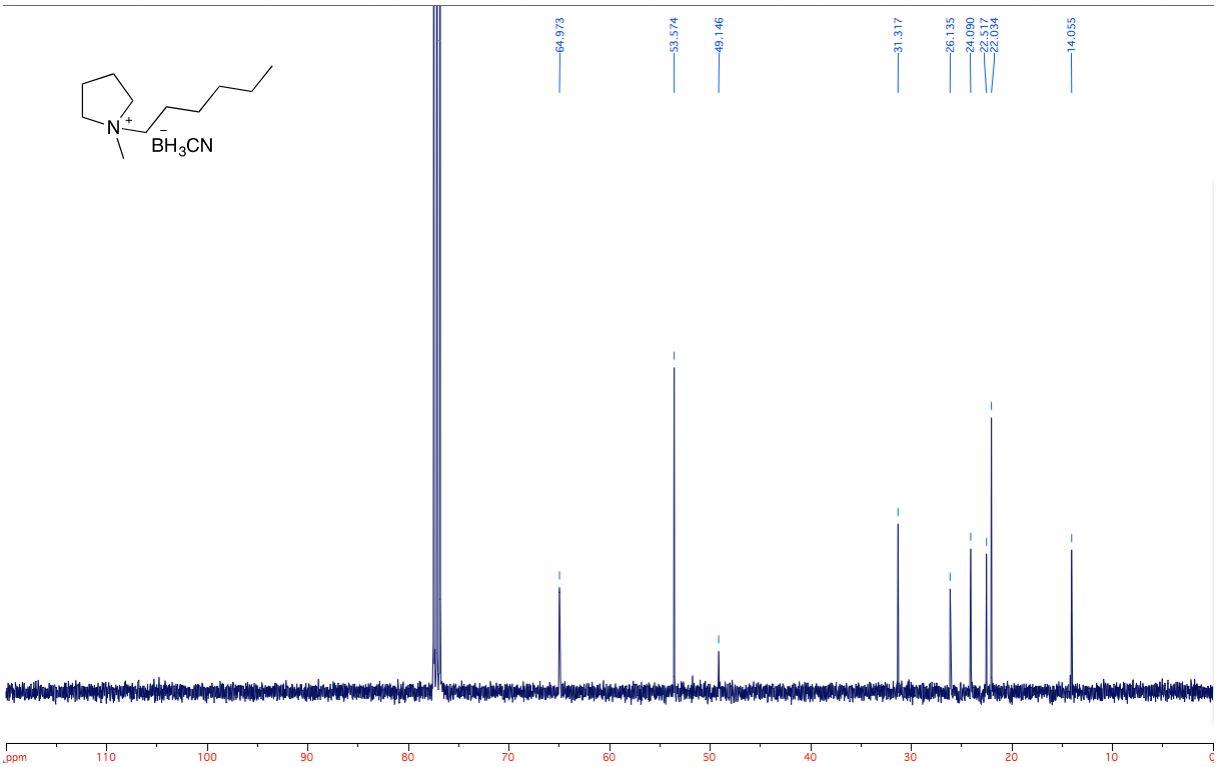

Fig. S52. ^{13}C NMR of 1-Hexyl-1-methylpyrrolidin-1-ium cyanotrihydroborate (**17**).

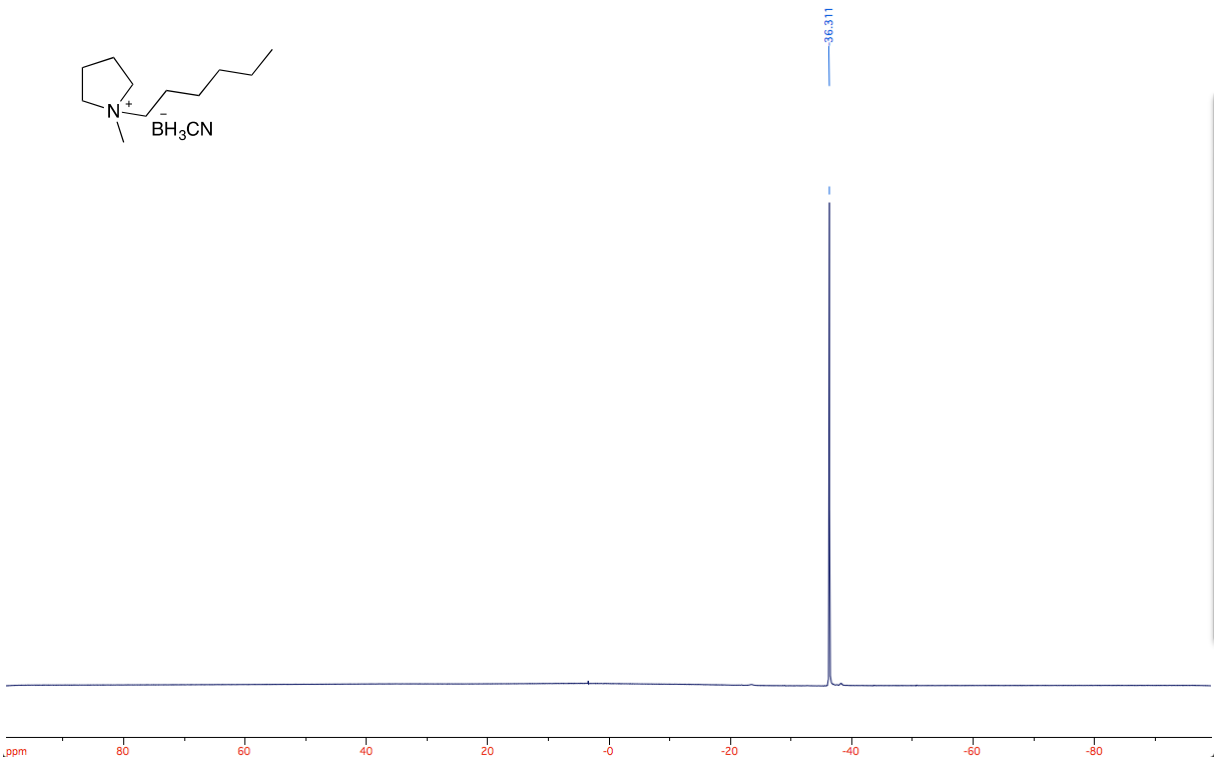

Fig. S53. ^{11}B NMR of 1-Hexyl-1-methylpyrrolidin-1-ium cyanotrihydroborate (**17**).

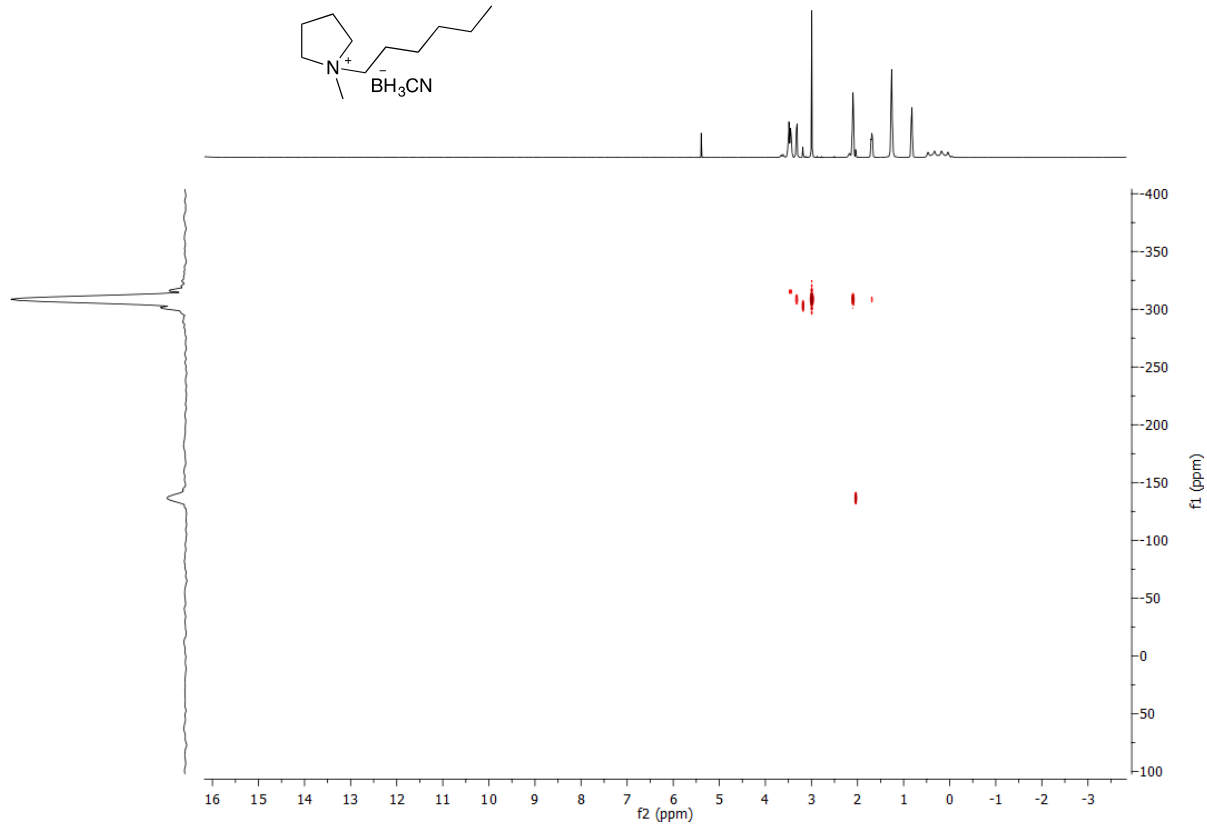

Fig. S54. ^{1}H-^{15}N HSQC of 1-Hexyl-1-methylpyrrolidin-1-ium cyanotrihydroborate (**17**).

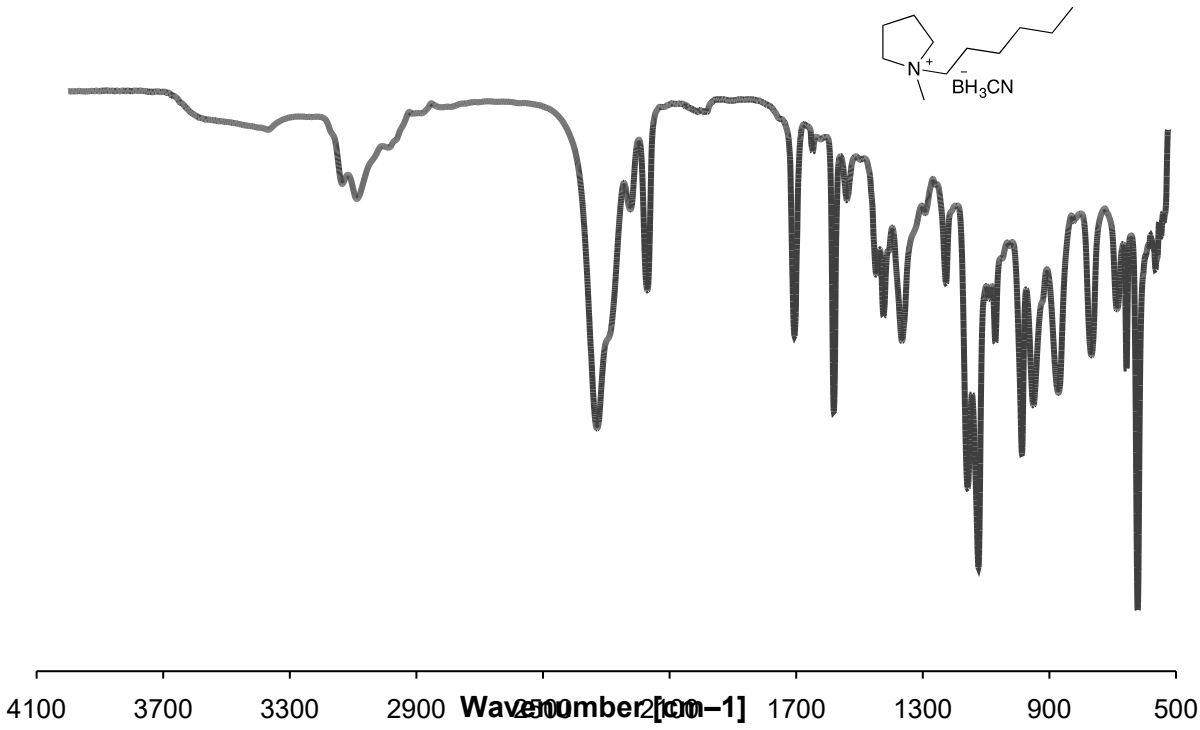

Fig. S55. IR spectrum of 1-Hexyl-1-methylpyrrolidin-1-ium cyanotrihydroborate (**17**).

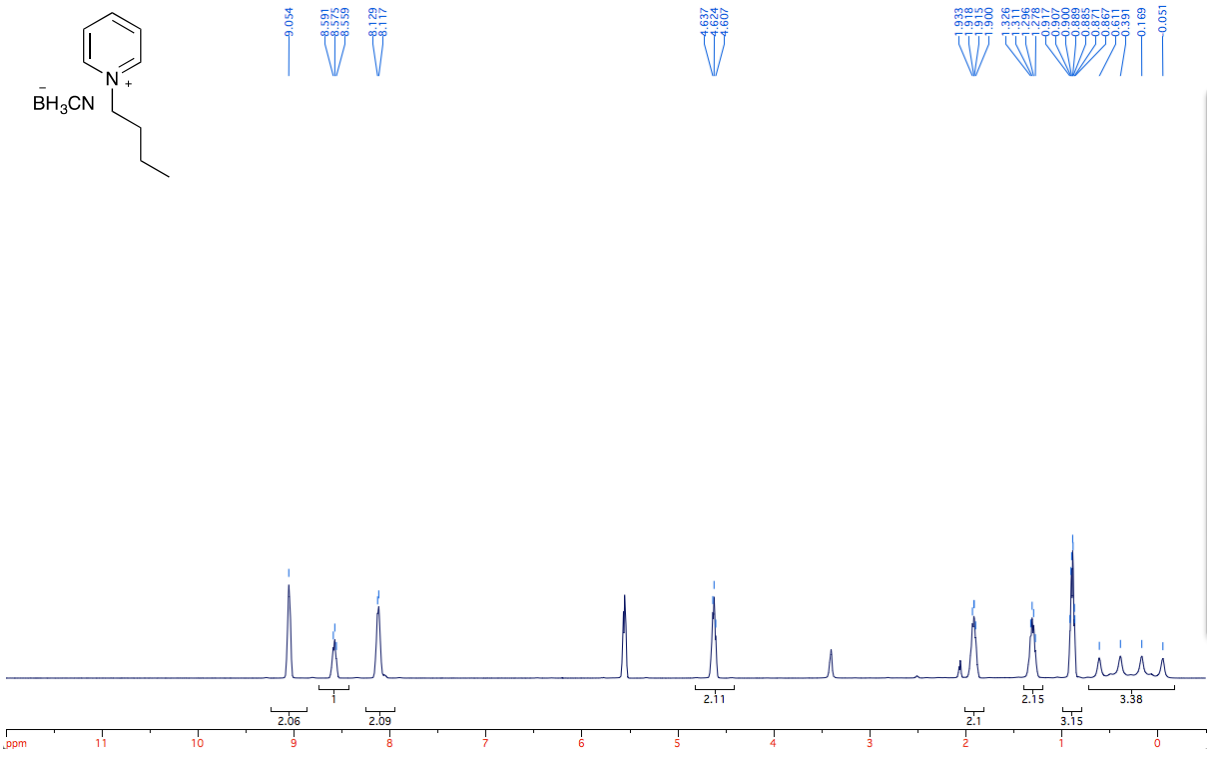

Fig. S56. ^{1}H NMR of 1-Butylpyridin-1-ium cyanotrihydroborate (**19**).

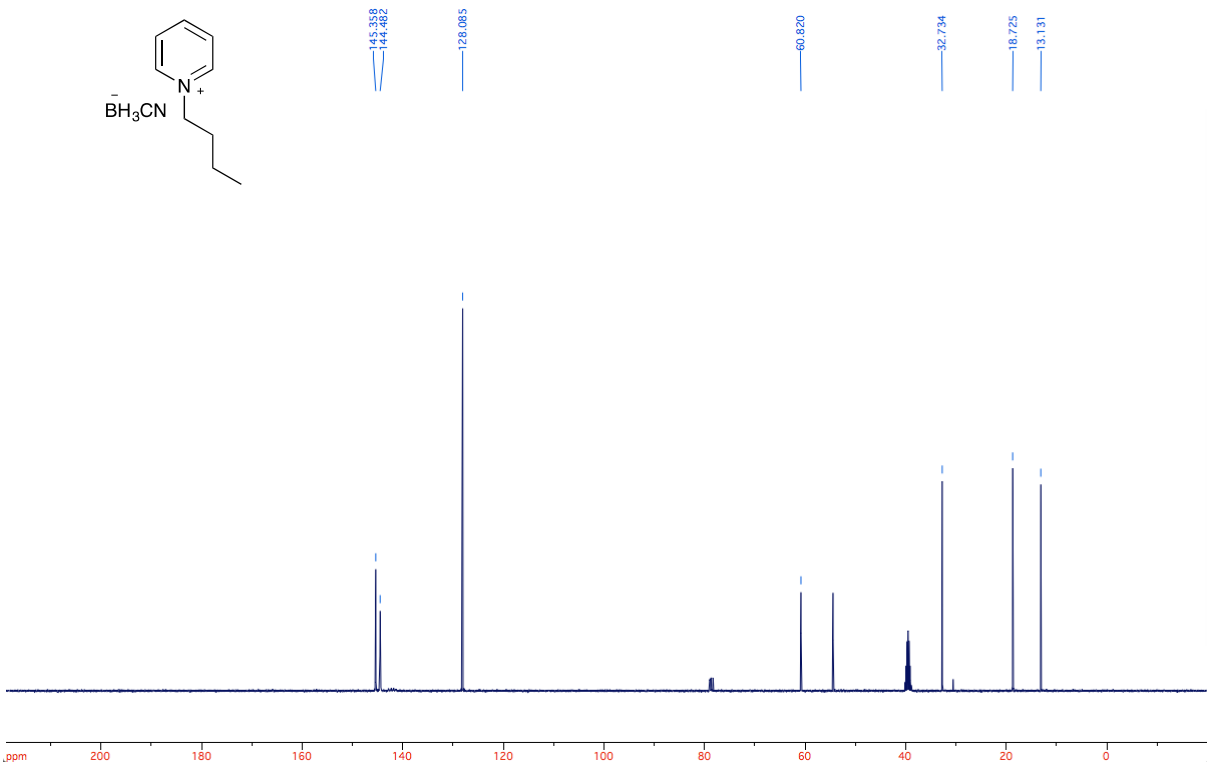

Fig. S57. ^{13}C NMR of 1-Butylpyridin-1-ium cyanotrihydroborate (**19**).

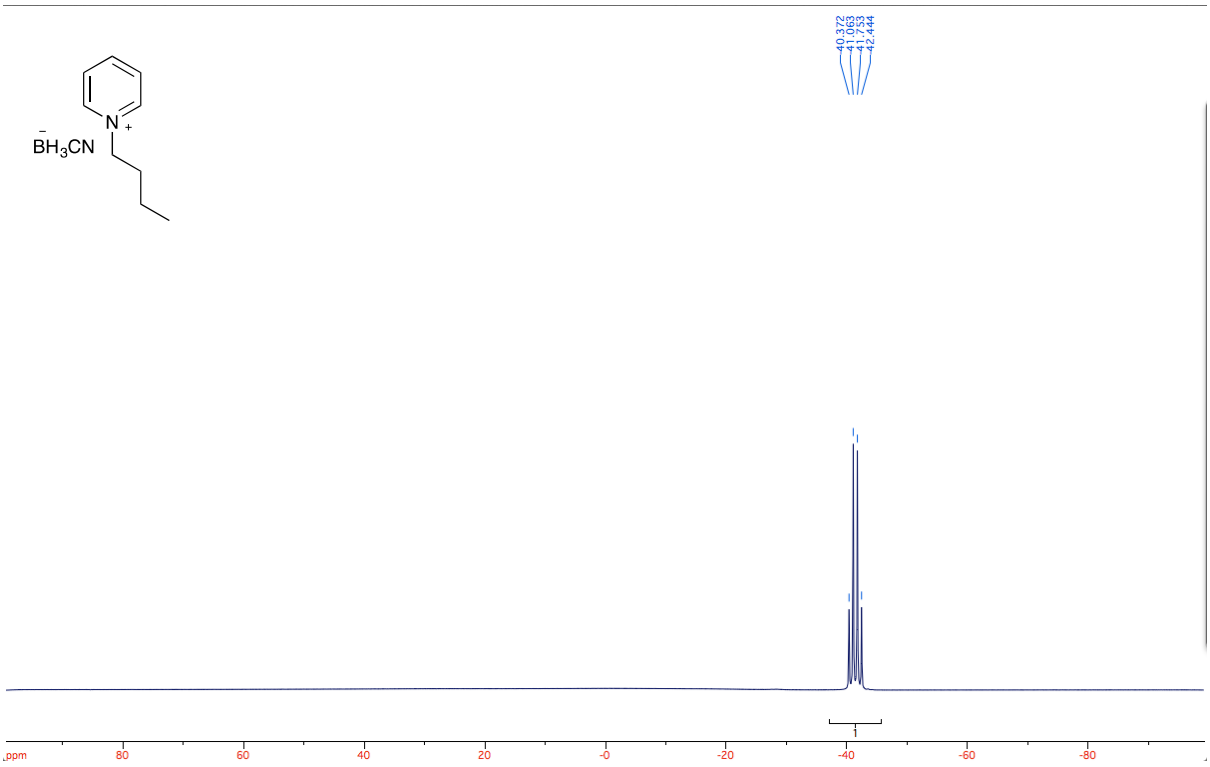

Fig. S58. ^{11}B NMR of 1-Butylpyridin-1-ium cyanotrihydroborate (**19**).

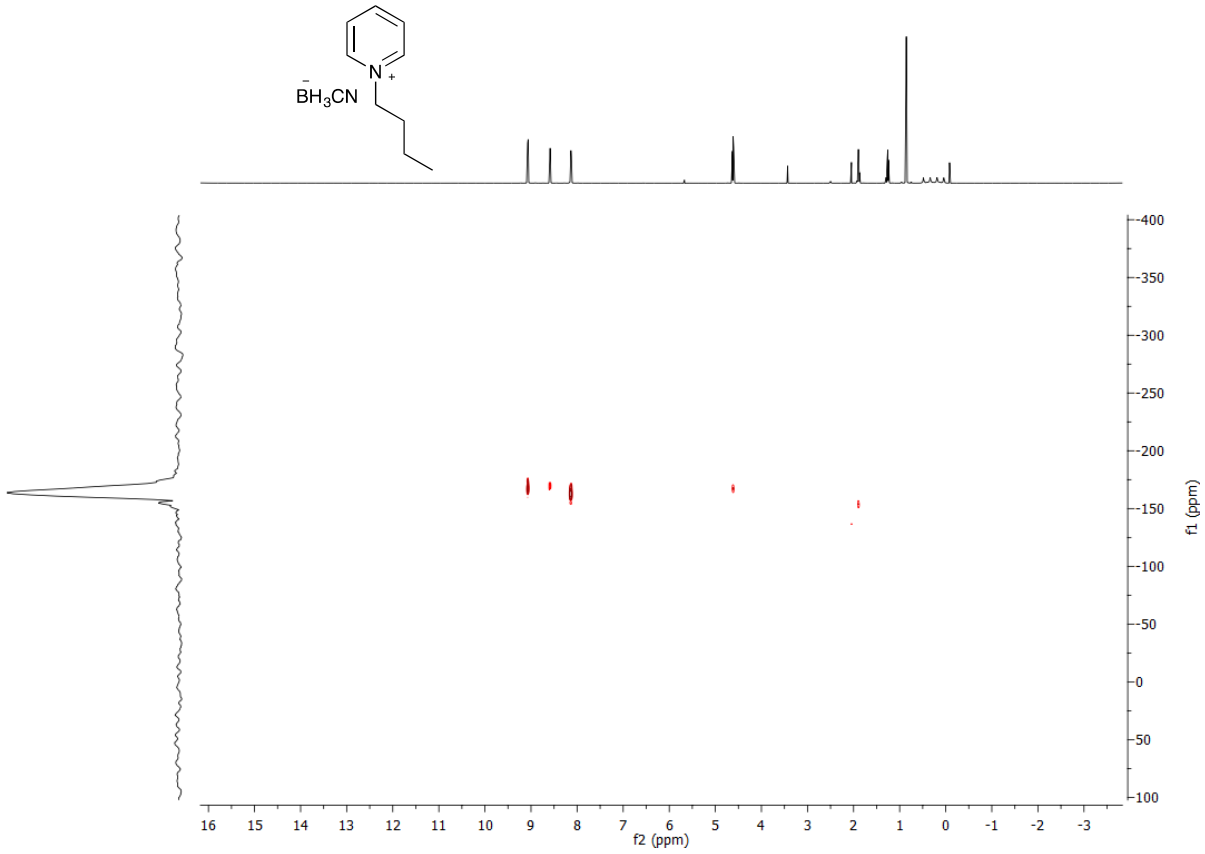

Fig. S59. ^{1}H-^{15}N HSQC of 1-Butylpyridin-1-ium cyanotrihydroborate (**19**).

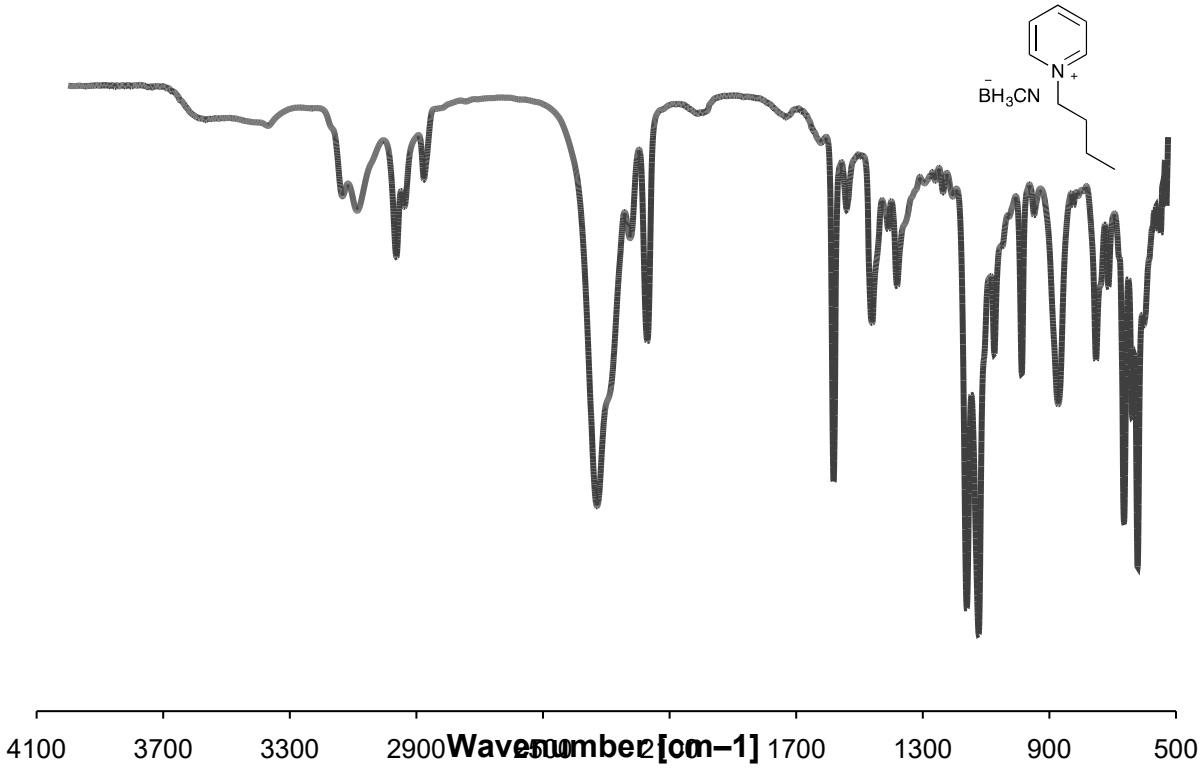

Fig. S60. IR spectrum of 1-Butylpyridin-1-ium cyanotrihydroborate (**19**).

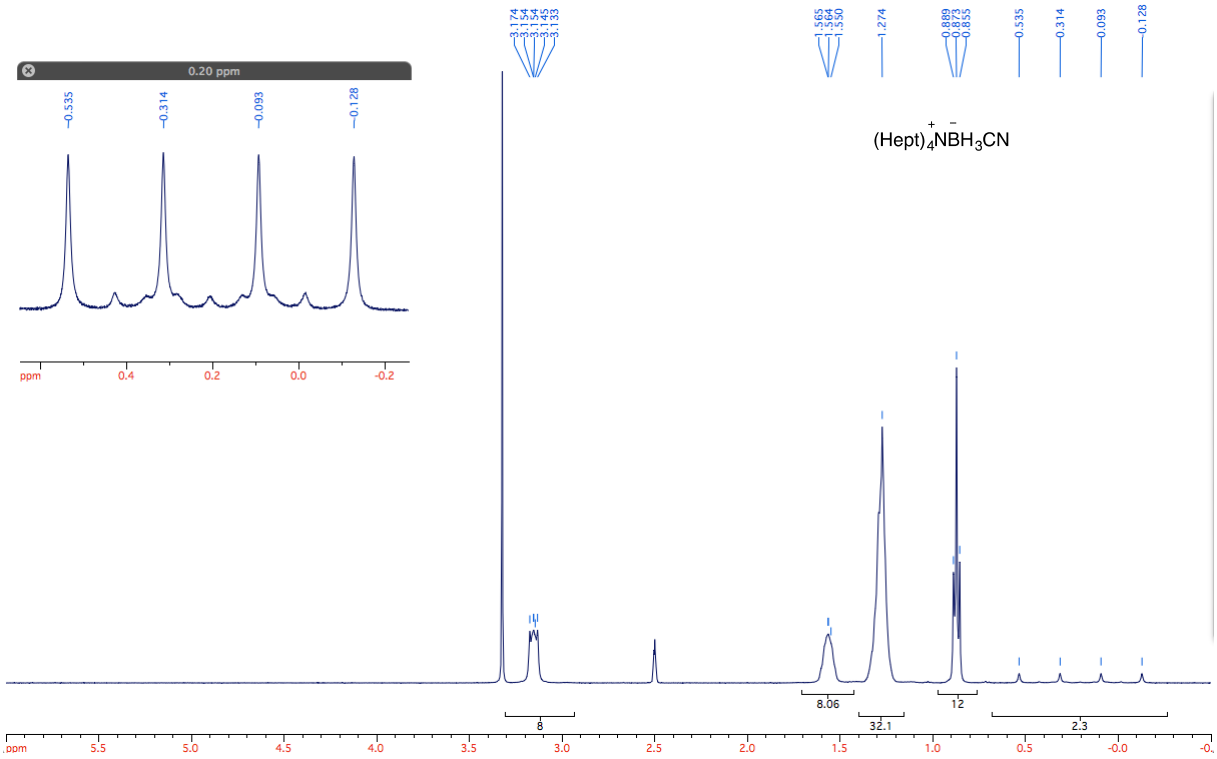

Fig. S61. ^{1}H NMR Tetraheptylammonium cyanotrihydroborate (**20**).

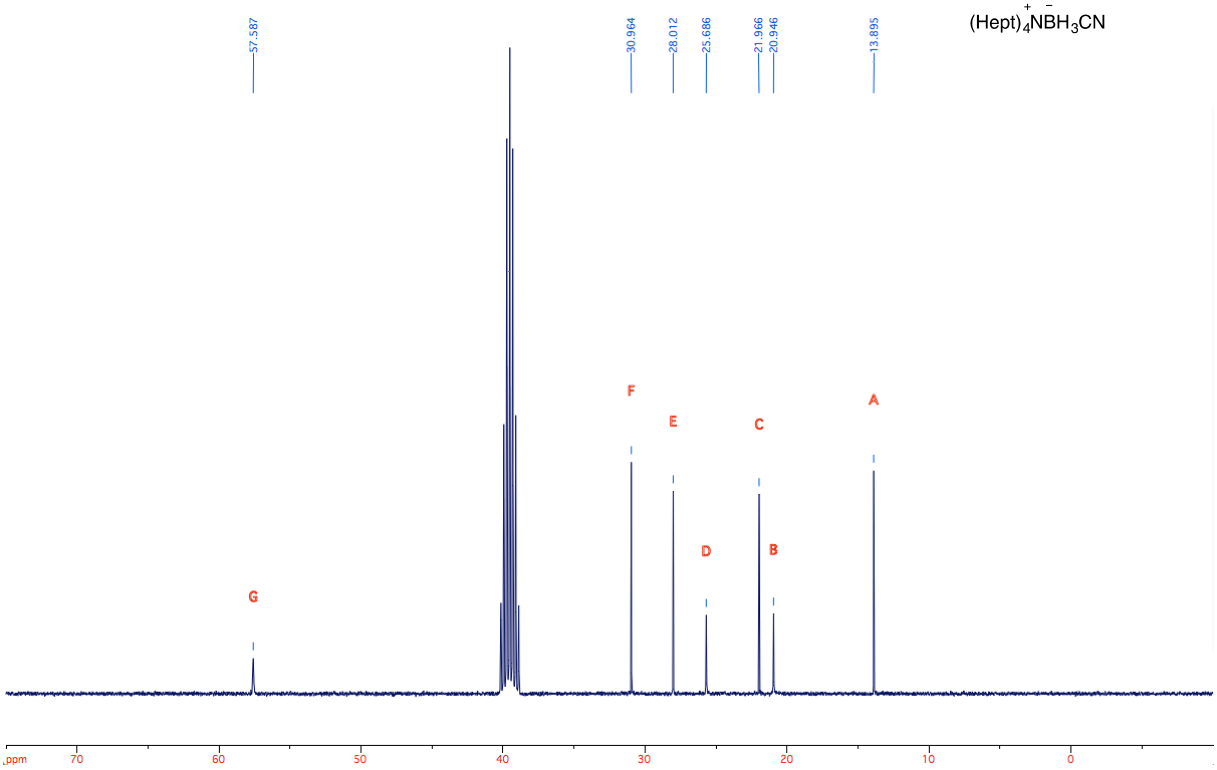

Fig. S62. ^{13}C NMR of Tetraheptylammonium cyanotrihydroborate (**20**).

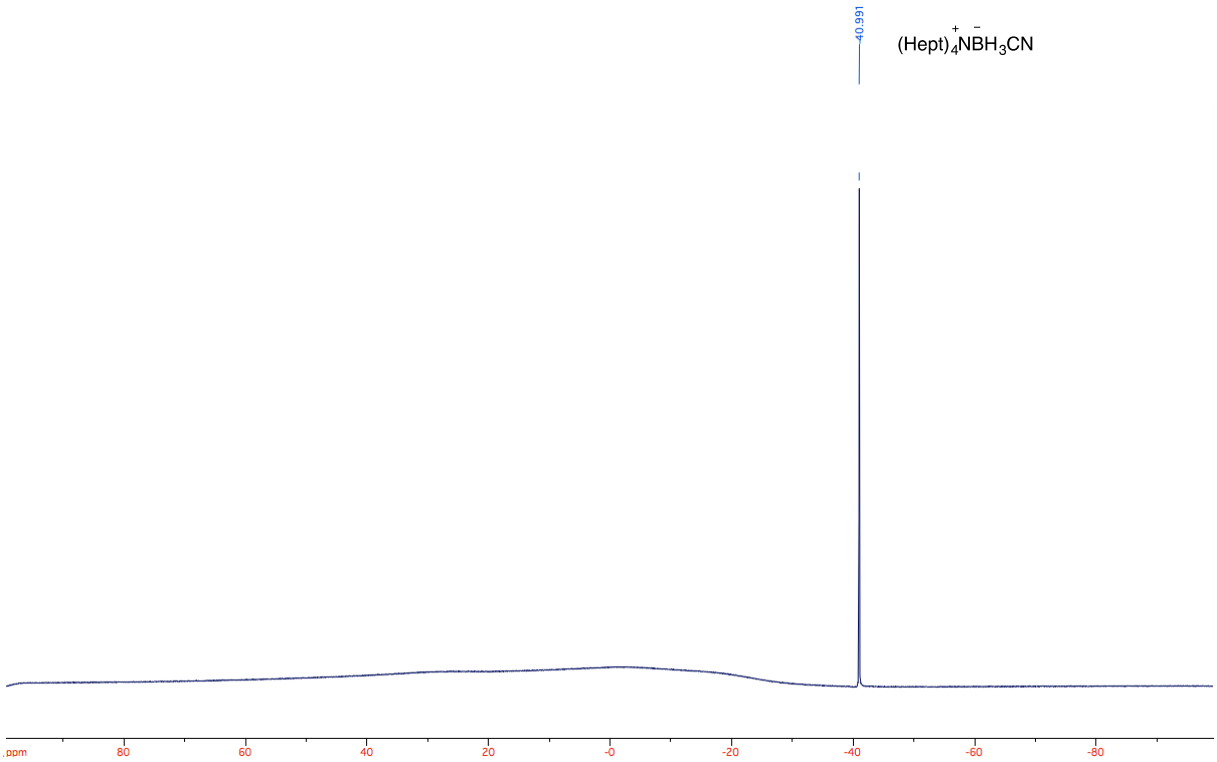

Fig. S63. ^{11}B NMR of Tetraheptylammonium cyanotrihydroborate (**20**).

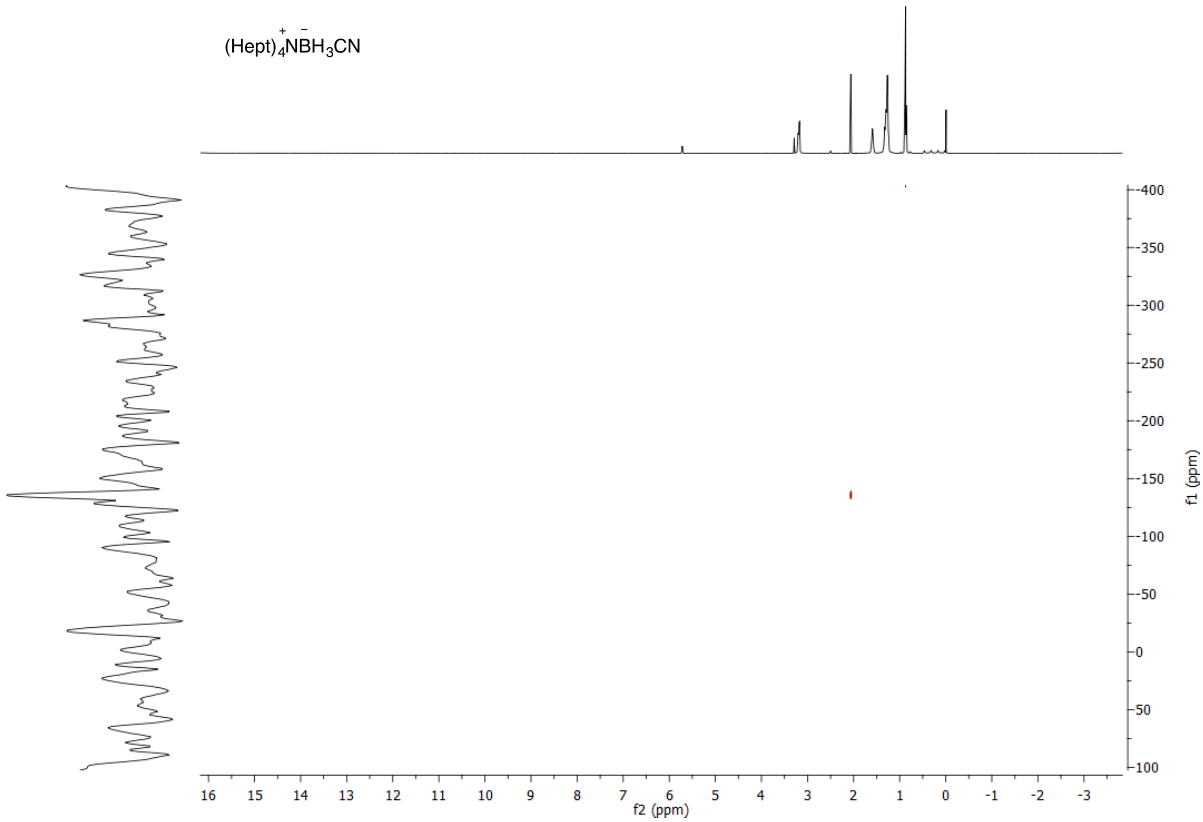

Fig. S64. ^{1}H-^{15}N HSQC of Tetraheptylammonium cyanotrihydroborate (**20**).

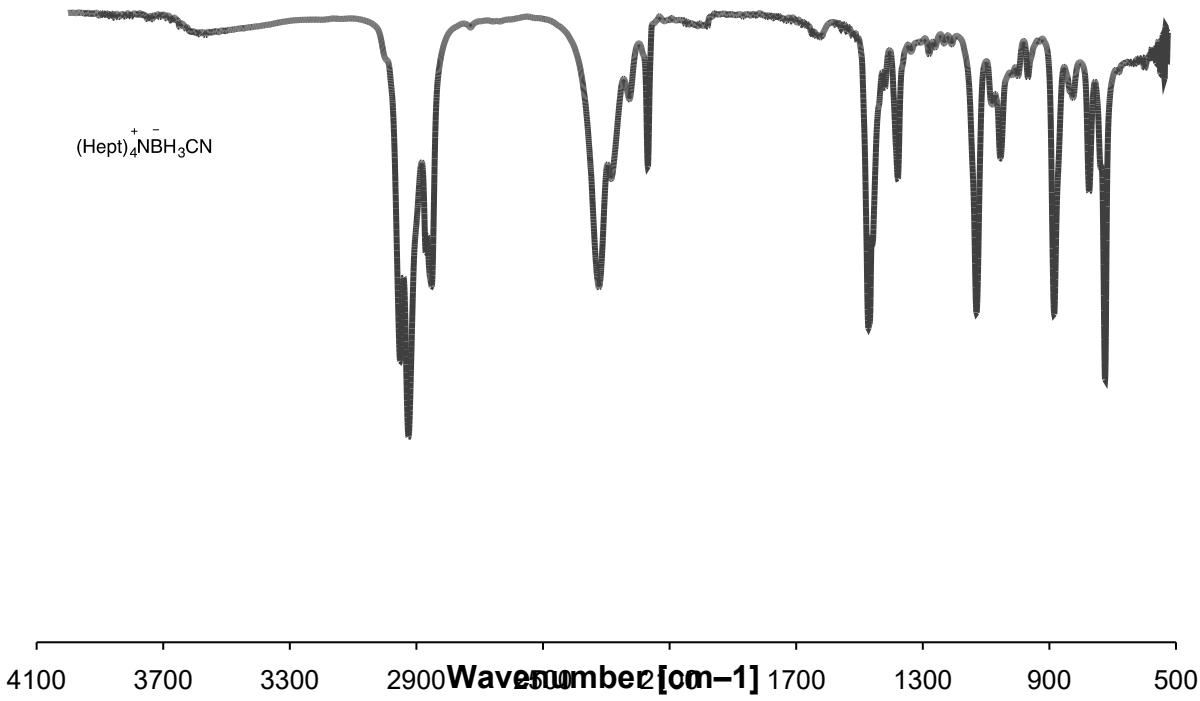

Fig. S65. IR spectrum of Tetraheptylammonium cyanotrihydroborate (**20**).

Computational Methods

All calculations on structural properties of these molecules were performed at the levels of B3LYP/6-311+G(3df,2p) using G03 quantum chemistry package.[1] About the accuracy for the prediction of various properties of energetic molecules, there is a review paper available in the literature.[2] Since we also focus on energies of isodesmic reactions for heats of formation in these molecules, the B3LYP/6-311+G(3df,2p) calculation has been used as our results on heats of formation. Harmonic vibrational frequencies were also calculated at the same theory level as that are used to fully optimize molecular structures, which enable us to confirm the real minima. For heats of combustion, the general reaction equation is given by:

$$C_aH_bBN_c+(O_2)_{a+\frac{b}{2}+\frac{3}{2}} \rightarrow (CO_2)_a+\frac{1}{2}(H_2O)_{\frac{b}{2}}+\frac{1}{2}(B_2O_3)+\frac{1}{2}(N_2)_c$$

The experimental heats of formation for CO_2, H_2O and B_2O_3 in gas phases are -393.51, -241.826 and -835.96 kJ/mol, respectively, which are given from NIST-JANAF thermochemical tables.[3] The Fig. S66 shows the calculated IR spectrum of **6** while the Fig. S67 gives the optimized structures of IL studied herein.

Table S4. Experimental heats of formation for reference molecules.[3]

Name	Formula	ΔH^f_{gas} (kJ/mol)
1*H*-1,2,4-Triazole	$C_2H_3N_3$	192.7
Ammonia	NH_3	106.69
Methane	CH_4	-74.87
Propene	C_3H_6	20.41
Butane	C_4H_{10}	-125.6
n-Hexane	C_6H_{14}	-167.1
Ethane	C_2H_6	-84.0
Heptane	C_7H_{14}	-187.8
Pyridine	C_5H_5N	140.2
Pyrrolidine	C_4H_9N	-3.4
Borone	BH_3	106.69
Hydrogen cyanide	CHN	135.14

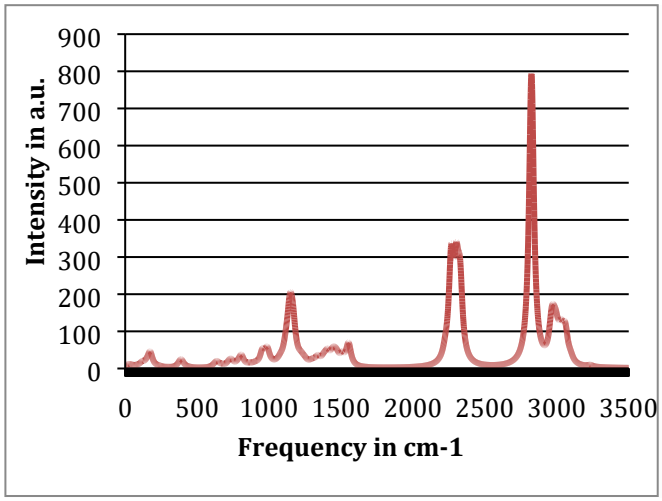

Fig. S66. The calculated IR spectrum of **15** in which there is no negative frequency, showing the real minimum with respect to the total energy.

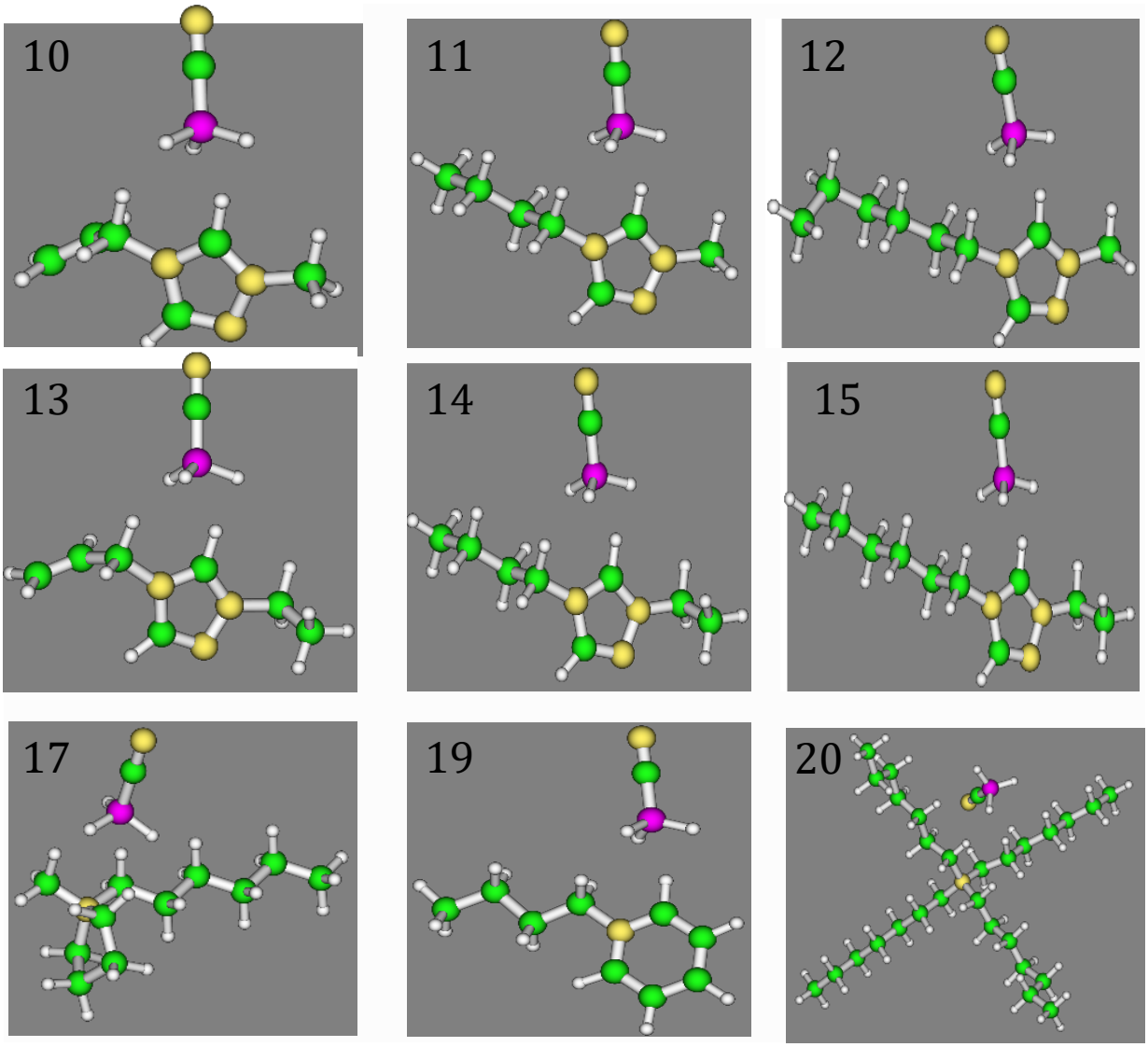

Fig. S67. The optimized structures of all ILs.

Theoretical studies

Calculations of heats of formation for all ILs were based on the following set of hypothetical isodesmic (or nearly isodesmic) reactions from eqn. (1) to eqn. (9), respectively. In these isodesmic reactions, 1H-1,2,4-triazole ($C_2H_3N_3$), ammonia (NH_3), methane (CH_4), propene (C_3H_6), butane (C_4H_{10}), n-hexane (C_6H_{14}), ethane (C_2H_6), heptane (C_7H_{14}), pyridine (C_5H_5N), pyrrolidine (C_4H_9N), borone (BH_3), and hydrogen cyanide (CHN) are taken as reference molecules. Their experimental heats of formation are available and listed in Table S4.[3] The calculated heats of formation and combustion for these IL compounds are listed in Table 1.

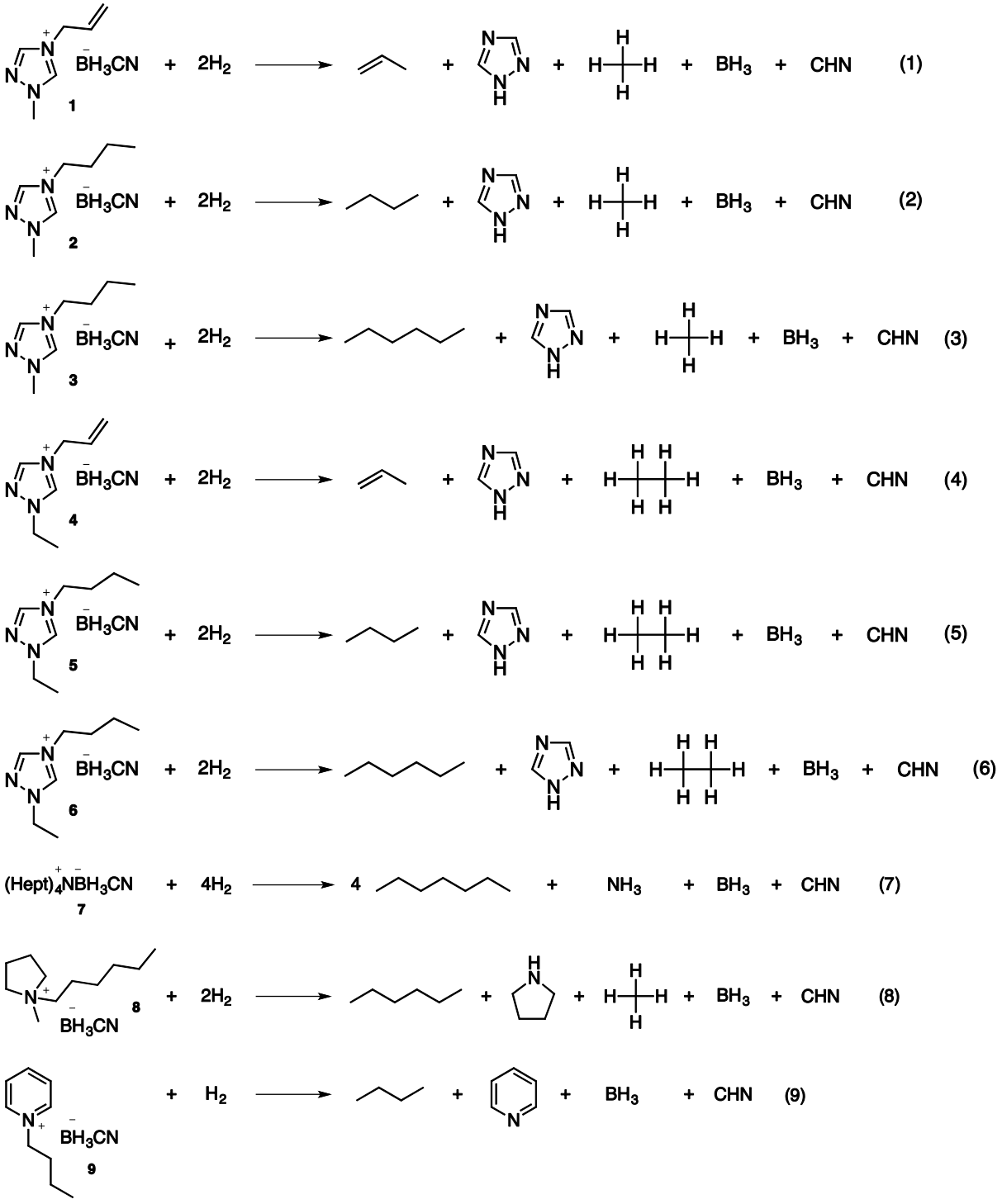

Differential scanning calorimetry (DSC) curves

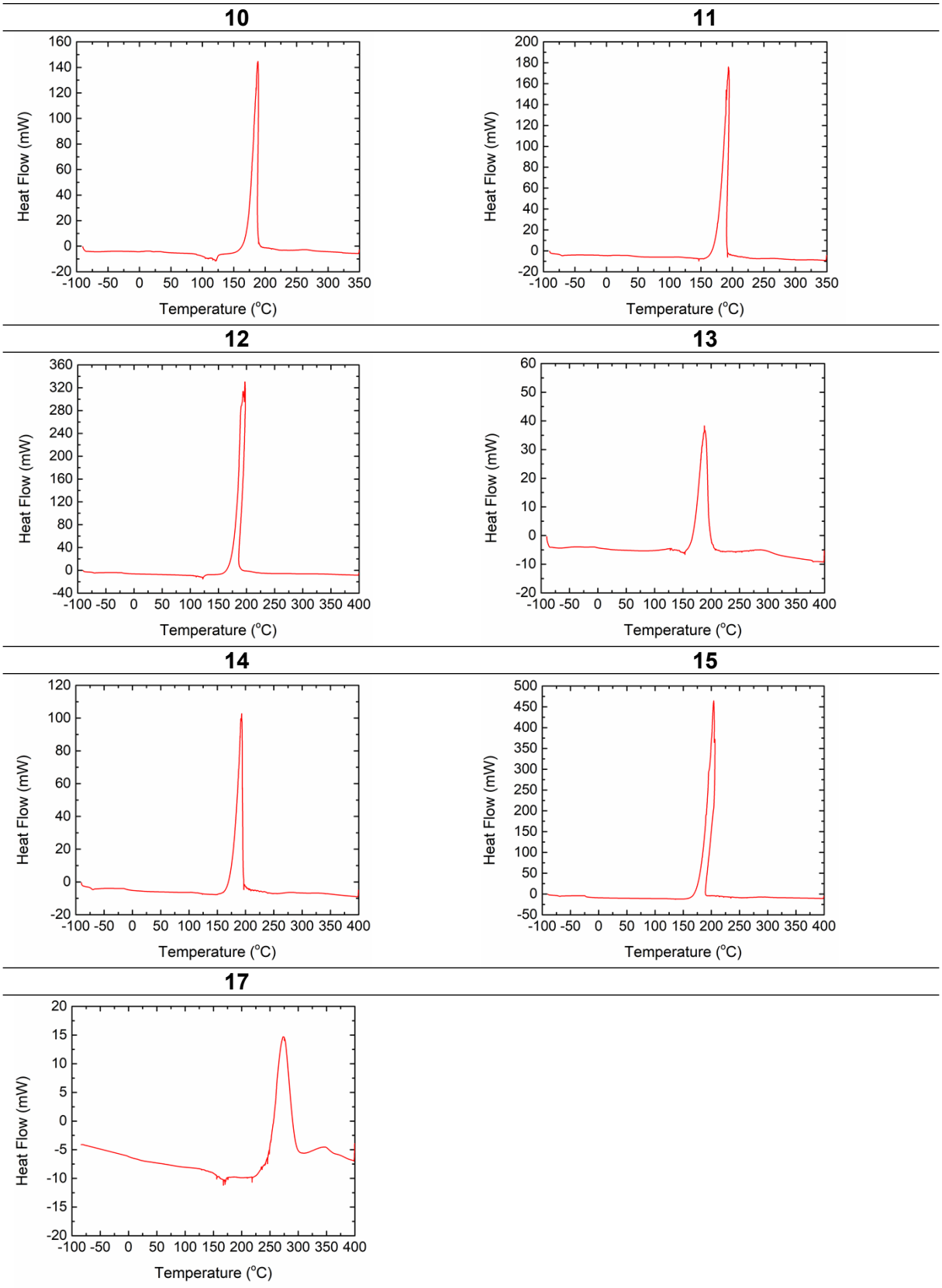

Fig. S68. DSC curves of selected ILs.

^{23}Na-NMR of 17

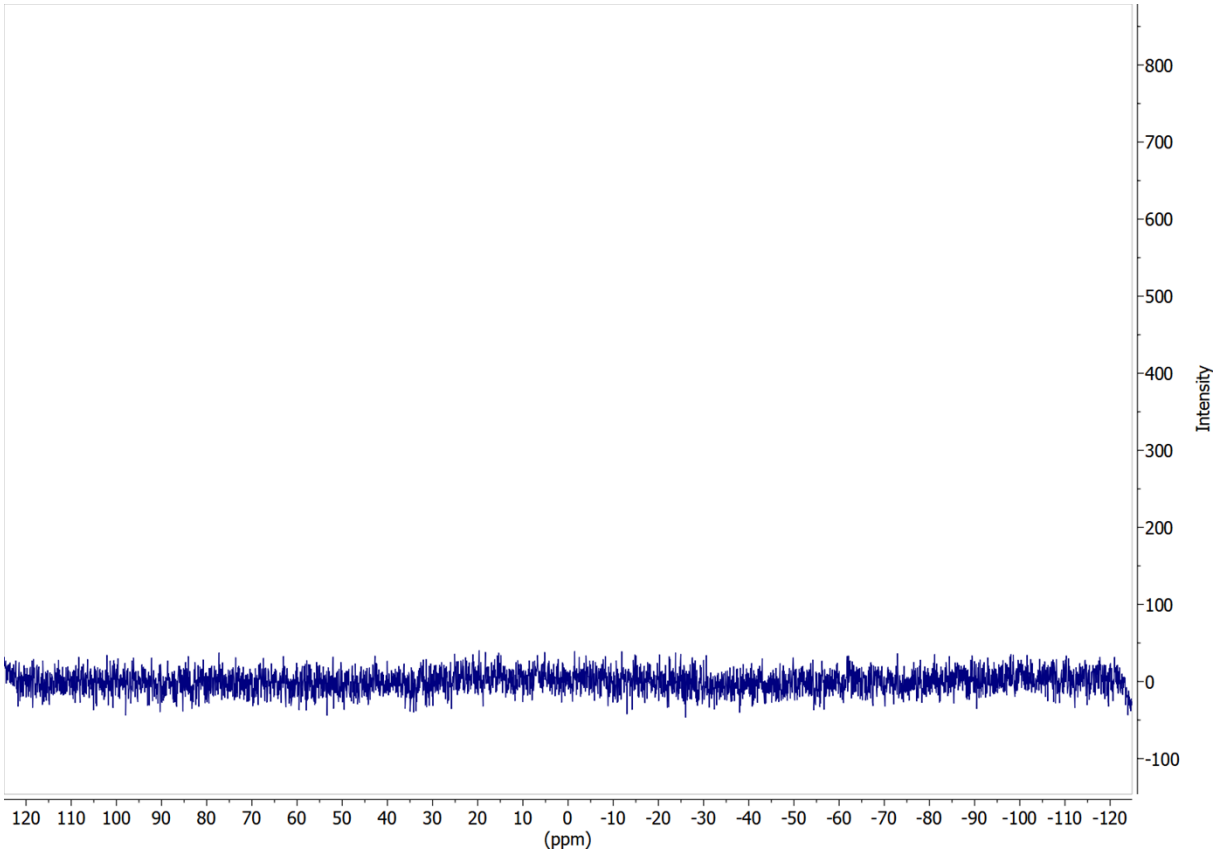

Fig. S69. ^{23}Na-NMR (79 MHz, $CDCl_3$) of 1-Hexyl-1-methylpyrrolidin-1-ium cyanotrihydroborate (**17**).

References

[1]. Gaussian 03, Revision C.02, M. J. Frisch, G. W. Trucks, H. B. Schlegel, G. E. Scuseria, M. A. Robb, J. R. Cheeseman, J. A. Montgomery, Jr., T. Vreven, K. N. Kudin, J. C. Burant, J. M. Millam, S. S. Iyengar, J. Tomasi, V. Barone, B. Mennucci, M. Cossi, G. Scalmani, N. Rega, G. A. Petersson, H. Nakatsuji, M. Hada, M. Ehara, K. Toyota, R. Fukuda, J. Hasegawa, M. Ishida, T. Nakajima, Y. Honda, O. Kitao, H. Nakai, M. Klene, X. Li, J. E. Knox, H. P. Hratchian, J. B. Cross, V. Bakken, C. Adamo, J. Jaramillo, R. Gomperts, R. E. Stratmann, O. Yazyev, A. J. Austin, R. Cammi, C. Pomelli, J. W. Ochterski, P. Y. Ayala, K. Morokuma, G. A. Voth, P. Salvador, J. J. Dannenberg, V. G. Zakrzewski, S. Dapprich, A. D. Daniels, M. C. Strain, O. Farkas, D. K. Malick, A. D. Rabuck, K. Raghavachari, J. B. Foresman, J. V. Ortiz, Q. Cui, A. G. Baboul, S. Clifford, J. Cioslowski, B. B. Stefanov, G. Liu, A. Liashenko, P. Piskorz, I. Komaromi, R. L. Martin, D. J. Fox, T. Keith, M. A. Al-Laham, C. Y. Peng, A. Nanayakkara, M. Challacombe, P. M. W. Gill, B. Johnson, W. Chen, M. W. Wong, C. Gonzalez, and J. A. Pople, Gaussian, Inc., Wallingford CT, 2004.

[2]. Betsy M, Rice, Edward F. C. Byrd, William D. Mattson, Computational Aspects of Nitrogen-Rich HEDMs, *Struc. Bond.,* 2007, **125**, 153-194

[3] M. W. Chase, Jr., NIST-JANAF Thermochemical Tables, Fourth Edition, *J. Phys. Chem. Ref. Data, Monograph*, **9** (1998) 1–1951.